

Pavement Recycling: Shrinkage Crack Mitigation in Cement-Treated Pavement Layers — Phase 1 Laboratory Testing

Authors:
S. Louw, D. Jones, and J. Hammack

Partnered Pavement Research Center (PPRC) Project Number 4.52a (DRISI Task 2708):
Microcracking of Cement-Treated Pavement Layers

PREPARED FOR:

California Department of Transportation
Division of Research, Innovation, and System Information
Office of Materials and Infrastructure

PREPARED BY:

University of California
Pavement Research Center
UC Davis, UC Berkeley




TECHNICAL REPORT DOCUMENTATION PAGE

1. REPORT NUMBER UCPRC-RR-2016-07	2. GOVERNMENT ASSOCIATION NUMBER	3. RECIPIENT'S CATALOG NUMBER
4. TITLE AND SUBTITLE Pavement Recycling: Shrinkage Crack Mitigation in Cement-Treated Pavement Layers — Phase 1 Laboratory Testing		5. REPORT PUBLICATION DATE 09/21/2018
		6. PERFORMING ORGANIZATION CODE
7. AUTHOR(S) S. Louw (ORCID 0000-0002-1021-7110), D. Jones (ORCID 0000-0002-2938-076X), and J. Hammack		8. PERFORMING ORGANIZATION REPORT NO. UCPRC-RR-2016-07
9. PERFORMING ORGANIZATION NAME AND ADDRESS University of California Pavement Research Center Department of Civil and Environmental Engineering, UC Davis 1 Shields Avenue Davis, CA 95616		10. WORK UNIT NUMBER
		11. CONTRACT OR GRANT NUMBER
12. SPONSORING AGENCY AND ADDRESS California Department of Transportation Division of Research, Innovation, and System Information P.O. Box 942873 Sacramento, CA 94273-0001		13. TYPE OF REPORT AND PERIOD COVERED Research Report 01/2015 – 06/2016
		14. SPONSORING AGENCY CODE
15. SUPPLEMENTAL NOTES		
16. ABSTRACT <p>The California Department of Transportation (Caltrans) has been using full-depth reclamation (FDR) as a rehabilitation strategy since 2001. Most projects to date have used a combination of foamed asphalt and portland cement as the stabilizing agent. Recently though, the fluctuating and at times high cost of asphalt binder coupled with the relatively complex mix-design procedure for mixes that include foamed asphalt has generated interest in the use of portland cement alone as an alternative stabilizing agent. However, shrinkage cracking associated with the hydration and curing of the cement-treated layers remains a concern, especially with regard to crack reflection through asphalt concrete surfacings and the related problems caused by water ingress.</p> <p>Considerable research has been undertaken on crack mitigation, and a range of measures related to improved mix designs and construction practices have been implemented by road agencies. One of the most promising measures, used in conjunction with appropriate mix designs, is that of microcracking the cement-treated layer between 24 and 72 hours after construction. In theory, this action creates a fine network of cracks in the layer that limit or prevent the wider and more severe block cracks typical of cement-treated layers. Limited research to assess microcracking as a crack mitigation measure has been completed on a number of projects in Texas, Utah, and New Hampshire. Recommendations from these studies were first implemented by the Texas Department of Transportation and then later by other state departments of transportation. However, longer-term monitoring on a range of projects in Texas and other states has revealed that microcracking has not always been successful in preventing cracking, with some projects showing reflected transverse and block cracks in a relatively short time period, attributable to a number of factors including but not limited to cement spreading, the method of curing, and the interval between base construction and placement of surfacing.</p> <p>Discussions with researchers in Texas indicated that additional research was necessary to better understand the microcracking mechanism, and to identify the key factors influencing performance, including but not limited to aggregate properties, cement content, the time period before microcracking starts, layer moisture contents, roller weights and vibration settings, the number of roller passes, the field test methods and criteria used to assess the degree of microcracking, and the effects of early opening to traffic. A multi-phase project was therefore initiated at the University of California Pavement Research Center (UCPRC) to investigate these outstanding issues. The first phase of this study is discussed in this report, which covers the literature review, preliminary laboratory testing to investigate simulation of the microcracking process in the laboratory, and early results from field testing on four projects where microcracking was implemented.</p>		
17. KEY WORDS Full-depth reclamation; cement stabilization, crack mitigation, microcracking		18. DISTRIBUTION STATEMENT No restrictions. This document is available to the public through the National Technical Information Service, Springfield, VA 22161
19. SECURITY CLASSIFICATION (of this report) Unclassified	20. NUMBER OF PAGES 118	21. PRICE None

Reproduction of completed page authorized

UCPRC ADDITIONAL INFORMATION

1. DRAFT STAGE Final	2. PARTNERED PAVEMENT RESEARCH CENTER STRATEGIC PLAN ELEMENT NUMBER 4.52a				
3. FHWA NUMBER CA192708A	4. VERSION NUMBER 1				
5. CALTRANS TECHNICAL LEAD AND REVIEWER(S) D. Maskey					
6. PROPOSALS FOR IMPLEMENTATION Continue with Phase 2 test road and associated laboratory study					
7. RELATED DOCUMENTS UCPRC-TM-2015-02					
8. LABORATORY ACCREDITATION The UCPRC laboratory is accredited by AASHTO re:source for the tests listed in this report					
9. SIGNATURES					
S. Louw FIRST AUTHOR	J.T. Harvey TECHNICAL REVIEW	D. Spinner EDITOR	J.T. Harvey PRINCIPAL INVESTIGATOR	D. Maskey CALTRANS TECH. LEADS	T. Joseph Holland CALTRANS CONTRACT MANAGER

Reproduction of completed page authorized

DISCLAIMER STATEMENT

This document is disseminated in the interest of information exchange. The contents of this report reflect the views of the authors who are responsible for the facts and accuracy of the data presented herein. The contents do not necessarily reflect the official views or policies of the State of California or the Federal Highway Administration. This publication does not constitute a standard, specification or regulation. This report does not constitute an endorsement by the Department of any product described herein.

For individuals with sensory disabilities, this document is available in alternate formats. For information, call (916) 654-8899, TTY 711, or write to California Department of Transportation, Division of Research, Innovation and System Information, MS-83, P.O. Box 942873, Sacramento, CA 94273-0001.

PROJECT OBJECTIVES

This study is a continuation of PPRC Project 4.36 (“Guidelines for Full-Depth Reclamation of Pavements”) and addresses the project titled “Microcracking of Cement-Treated Layers.” The objective of this project is to develop guidelines for mitigation measures to limit/prevent shrinkage cracking in cement-treated layers.

This will be achieved in two phases through the following tasks:

- Phase 1: Literature review, laboratory testing, and modeling.
 - 1.1 A literature review on research related to crack mitigation in cement-treated materials
 - 1.2 Preliminary laboratory testing to understand crack mitigation mechanisms and identify criteria for modeling the effects of crack mitigation on long-term pavement performance
 - 1.3 Modeling of the effects of crack mitigation on long-term pavement performance
 - 1.4 A summary report with recommendations for Phase 2 testing if appropriate
- Phase 2: Accelerated wheel-load testing and field testing (depending on the results of Phase 1 and under the direction of the Caltrans project steering committee)
 - 2.1 Monitoring of field projects where crack mitigation measures have been used
 - 2.2 Design and construction of a test track to compare different crack mitigation techniques
 - 2.3 Accelerated wheel-load testing to compare performance of the different crack mitigation techniques
 - 2.4 Laboratory testing of specimens sampled from the test track and from field projects to compare laboratory test results with accelerated wheel-load test results and to identify suitable criteria for refining mechanistic-empirical design procedures and performance models for pavements with cement-treated layers
 - 2.5 Preparation of a project research report and guidelines for crack mitigation in cement-treated layers

The report covers Phase 1.

EXECUTIVE SUMMARY

The California Department of Transportation (Caltrans) has been using full-depth reclamation (FDR) as a rehabilitation strategy since 2001. Most projects to date have used a combination of foamed asphalt and portland cement as a stabilizing agent. Recently though, the increasing cost of asphalt binder coupled with the relatively complex mix-design procedure for foamed asphalt has generated interest in the use of portland cement (FDR-PC) alone as an alternative stabilizing agent, where appropriate. However, the high initial stiffness and shrinkage cracking associated with the hydration and curing of the cement-treated layers remains a concern, especially with regard to crack reflection through asphalt concrete surfacings and the related problems caused by water ingress.

Considerable research has been undertaken on crack mitigation on FDR-PC projects, and a range of measures related to improved mix designs and construction practices have been implemented by road agencies. One of the most promising measures, used in conjunction with appropriate mix designs, is that of microcracking the cement-treated layer between 24 and 72 hours after construction. In theory, this action creates a fine network of cracks in the layer that limits or prevents the wider and more severe block cracks typical of cement-treated layers. Limited research to assess microcracking as a crack mitigation measure has been completed on a number of projects in Texas, Utah, and New Hampshire. Recommendations from these studies were first implemented by the Texas Department of Transportation and later by other state departments of transportation. However, longer-term monitoring on a range of projects in Texas and other states has revealed that microcracking has not always been successful in preventing cracking, with some projects showing reflected transverse and block cracks in a relatively short time period.

Discussions with researchers in Texas indicated that additional research was necessary to better understand the microcracking mechanism, and to identify the key factors influencing performance, including but not limited to aggregate properties, cement content, the time period before microcracking starts, layer moisture contents, roller weights and vibration settings, the number of roller passes applied, the field test methods and criteria used to assess the degree of microcracking, the time period before opening the road to traffic, and the time period before placing the surfacing. A project was therefore initiated at the University of California Pavement Research Center (UCPRC) to investigate these outstanding issues. The first phase of this study is discussed in this report, which covers the literature review, preliminary laboratory testing, and early results from field testing on four projects where microcracking was implemented.

A review of the literature on shrinkage crack mitigation revealed that microcracking in combination with appropriate cement-content determination is likely the most appropriate approach to be implemented in

California at this time given the research already conducted. However, other approaches, especially the investigation of hybrid stabilizers (e.g., cement with asphalt emulsion) deserve further investigation for possible future application. The literature review also identified a range of devices that could be used for measuring the effect of microcracking on the stiffness of cement-treated layers. Each device has limitations that have not been fully quantified in terms of either their suitability for verifying whether microcracking has resulted in satisfactory stiffness reduction and/or their applicability as a microcracking quality control procedure on construction projects.

Four field projects on road sections recycled in place using portland cement as the stabilizer were monitored. Visual assessments and soil stiffness gauge measurements (SSG), followed by falling weight deflectometer (FWD) measurements after paving were all undertaken as part of the investigation. The following conclusions were drawn after the first 12 months of observation:

- There was a wide variation in pavement materials and in pavement construction quality across the four projects. On the county road projects, where minimal sampling and testing appears to have been carried out in the project assessment phase, the mix designs did not necessarily accommodate the variation in materials and pavement conditions.
- Specifications are not always being followed to the fullest extent by contractors and they are not being fully enforced by agency engineers.
- In addition to being useful for assessing unbound layer thicknesses and the subgrade conditions of the existing road prior to FDR, DCP tests can also provide a quick indication of weak areas on the project after final compaction.
- The SSG can provide repeatable and reproducible results provided that the testing method is strictly adhered to and that operators are suitably trained and experienced. The variability between consecutive measurements by an experienced operator on the four projects were discussed with the SSG manufacturer.
- The SSG is useful for measuring/checking stiffness gain over time on the days between final compaction and microcracking, for dictating the number of roller passes used to achieve a satisfactory level of stiffness reduction by microcracking, and for checking that a satisfactory drop in stiffness was achieved after microcracking. It can also be used to check areas suspected of having too little or too much cement, especially those areas at the beginning and end of construction sections, and in lane overlap areas. However, the rate at which SSG testing can be conducted is slower than the pace of construction activities and more than one SSG may be required on site on the day of microcracking to keep up with the equipment.
- FWD testing provided useful insights into the stiffness change in FDR-PC layers over time and how this change is affected by material variability, the distribution of cement during construction, and the effectiveness of the microcracking process.
- FWD and SSG results both indicate that microcracking does result in an immediate and notable drop in stiffness in the FDR-PC layer after the procedure has been completed. However, much of the stiffness is recovered by recementation in the days after microcracking, after which stiffness appears to plateau. Stiffness change over time appears to be influenced by temperature; however, insufficient data has been collected to date to draw any firm conclusions about longer-term performance.

Preliminary laboratory testing was undertaken to identify methods that can be used to simulate microcracking of laboratory-prepared specimens. Three laboratory-scale microcracking methods were considered. Based on observations of the specimens before and after microcracking, the method that uses a dual steel wheel vibrating roller to microcrack specimens in a specially constructed pit appeared to provide the best results of the three approaches. The results from laboratory testing on specimens prepared using these techniques were, however, considered to be inconclusive and generally too low compared to backcalculated FWD stiffnesses on the same material. Factors contributing to this include the following:

- The sensitivity to confining stress of the resilient modulus of FDR-PC materials determined using the conventional AASHTO T 307 setup suggested that the material behaves more like an unbound material, which is unlikely given the cemented nature of the material.
- Testing with the conventional AASHTO T 307 setup could not effectively differentiate between the different cement contents of different curing intervals.
- The resilient modulus test results did not accurately reflect the expected effects of microcracking (i.e., they were not similar to those measured on field projects with a stiffness gauge), cement content, and curing time of the laboratory-compacted specimens. The primary reason for this was attributed to the laboratory microcracking procedures developed in Phase 1a not being representative of actual microcracking procedures on FDR-PC construction projects. The approach did not appear to reduce the stiffness of the samples in a repeatable and consistent manner, and in many instances it resulted in cracking and disintegration of the specimens.
- The large variability in the resilient modulus results from tests on both the control and microcracked specimens points to the compaction method that was followed. Based on previous findings from earlier UCPRC research on FDR with foamed asphalt, the sample preparation (quartering and batching) and mixing method were considered to be consistent and unlikely to have contributed much to the variability. However, the compaction method used, although consistent with the AASHTO T 307 method, was considered to be too operator dependent and probably a significant contributor to the variability.
- The brittleness of the laboratory-compacted FDR-PC samples caused the edges of the specimens to chip during handling and testing, which in turn led to tears in the latex membrane used for confining the specimen during testing. These tears led to a loss of confinement, which might also have contributed to the wide variation in the test results.

Based on the above observations, the following recommendations are made for Phase 2 research:

- Develop a more consistent method of laboratory specimen compaction that reduces or eliminates operator bias. The vibrating hammer compaction frame developed by *Wirtgen* is proposed for further evaluation.
- Develop a more appropriate method to induce microcracking in compacted specimens. The method must simulate microcracking on FDR projects. Two approaches are proposed for further study in Phase 2:
 - + Use the *Wirtgen* compaction frame to induce microcracking in the previously compacted specimens. Specimens will need to be placed back into the compaction mold after preliminary curing and subjected to a controlled period of vibration under load. Testing will need to determine

whether microcracking can be satisfactorily induced throughout the specimen or whether only the surface of the specimen is damaged.

- + Use a universal testing machine to simulate the vibration and stress of a steel wheel vibrating roller. The method should be cyclic and stress controlled to reduce the stiffness of the confined specimen to a set percentage.
- Use a revised test setup for resilient modulus testing. Preliminary testing with this setup produced results that matched backcalculated FWD stiffness closely and showed that the cement-stabilized material is not sensitive to confining pressure.
- Consider construction and monitoring of a test road to assess outstanding construction and microcracking issues that cannot be assessed on typical FDR-PC projects on state and county roads. Key factors that need to be investigated include the effect of design strength (i.e., cement content), the time between final compaction and microcracking, roller type, roller settings, and stiffness change over time. Control sections that are not microcracked should be included for performance comparison purposes.

Blank page

TABLE OF CONTENTS

EXECUTIVE SUMMARY	iv
LIST OF TABLES	xii
LIST OF FIGURES	xiii
LIST OF ABBREVIATIONS.....	xvii
TEST METHODS CITED IN THE TEXT	xviii
CONVERSION FACTORS.....	xix
1. INTRODUCTION	1
1.1 Background	1
1.2 Problem Statement	3
1.3 Project Objective/Goal	4
1.4 Report Layout	5
1.5 Measurement Units	5
2. LITERATURE REVIEW	7
2.1 Flexible Pavement Distresses Related to Base Failure	7
2.1.1 Transverse and Longitudinal Cracking	7
2.1.2 Block Cracking	8
2.1.3 Fatigue Cracking	9
2.1.4 Rutting.....	10
2.2 Shrinkage Crack Mitigation.....	10
2.2.1 Design and Construction Considerations	10
2.2.2 Microcracking	11
2.2.3 Effect of Early Trafficking.....	19
2.2.4 Other Mitigation Measures	19
2.3 Measuring Stiffness Change on the Road	19
2.3.1 Falling Weight Deflectometer (FWD)	20
2.3.2 Light Weight Deflectometer (LWD).....	20
2.3.3 Soil Stiffness Gauge (SSG).....	21
2.3.4 Device Comparison.....	22
2.3.5 Conclusions about Stiffness Measurements on Cement-Treated Bases	24
2.4 Resilient Modulus Triaxial Testing.....	24
2.4.1 Test Methods	24
2.4.2 Example Reported Resilient Moduli for Cement Stabilized Materials	27
2.4.3 Stress Dependency of Unbound and Bound Materials.....	27
2.5 Literature Review Summary	28
3. FIELD STUDIES	31
3.1 Introduction.....	31
3.2 Project Details	31
3.3 Testing Plan	32
3.3.1 Test Section Terminology	32
3.3.2 Density and Dynamic Cone Penetrometer Measurements	33
3.3.3 Stiffness Measurement Approach	33
3.4 Test Section Construction	34
3.4.1 Yolo County Road CR32B	34
3.4.2 Yolo County Road CR27	38
3.4.3 Yolo County Road CR99	41
3.4.4 California Road PLU147	43
3.4.5 General Observations from All Construction Projects.....	45
3.5 Density Test Results	47
3.6 Dynamic Cone Penetrometer Results	47

3.6.1	Yolo County Road CR27	48
3.6.2	California Road PLU147	48
3.7	Soil Stiffness Gauge (SSG) Results	49
3.7.1	Effect of Roller Type and Number of Roller Passes on Stiffness Reduction.....	49
3.7.2	Effect of Microcracking on Road CR32B.....	51
3.7.3	Effect of Microcracking on Road CR27	51
3.7.4	Effect of Microcracking on CR99.....	53
3.7.5	Effect of Microcracking on PLU147.....	54
3.8	Falling Weight Deflectometer (FWD) Testing	55
3.8.1	FDR Layer Stiffness Change on CR32B	55
3.8.2	FDR Layer Stiffness Change on CR27	56
3.8.3	FDR Layer Stiffness Change on CR99	57
3.8.4	FDR Layer Stiffness Change on PLU147	57
3.9	Field Testing Conclusions.....	65
4.	PHASE 1: LABORATORY EXPERIMENT DESIGN.....	67
4.1	Introduction.....	67
4.2	Experiment Plan Factors	67
4.3	Materials Used for Testing.....	67
5.	PHASE 1a: LABORATORY MICROCRACKING METHODS	69
5.1	Introduction.....	69
5.2	Vibrating Hammer	69
5.3	Vibrating Table	70
5.4	Steel Wheel Vibrating Roller.....	71
5.5	Summary of Laboratory Microcracking Methods	73
6.	PHASE 1b: LABORATORY TESTING	75
6.1	Introduction.....	75
6.2	Mix Design	75
6.3	Test Method	76
6.4	Test Factorial	76
6.5	Specimen Preparation and Conditioning.....	76
6.6	Microcracking.....	78
6.7	Assessment of Stiffness	78
6.7.1	Resilient Modulus	79
6.7.2	Effect of Bulk Stress	79
6.7.3	Effect of Shear Stress	79
6.7.4	Effect of Cement Content	79
6.7.5	Stiffness Before and After Microcracking	82
6.7.6	Effect of Curing Age.....	82
6.7.7	Discussion	82
6.8	Resilient Modulus Test Method Revision.....	85
6.8.1	Specimen Setup Procedure.....	85
6.8.2	Test Setup Evaluation Parameters.....	87
6.8.3	Resilient Modulus Test Results.....	89
6.8.4	Monotonic Test Results	92
6.8.5	Signal-to-Noise Ratio	92
6.8.6	Discussion	95
6.9	Phase 1b Conclusions and Recommendations	95
7.	CONCLUSIONS AND RECOMMENDATIONS.....	97
7.1	Summary	97
7.2	Conclusions.....	98
7.2.1	Literature Review.....	98
7.2.2	Field Testing	98
7.2.3	Phase 1a: Laboratory Microcracking Methods	99

7.2.4	Phase 1b: Preliminary Laboratory Testing.....	99
7.3	Recommendations.....	100
8.	PROPOSED PHASE 2 TEST ROAD WORKPLAN	101
8.1	Introduction.....	101
8.2	Revised Phase 2 Test Plan	101
8.2.1	Task 7: Test Road Design	101
8.2.2	Task 8: Phase 2 Laboratory Testing.....	105
8.2.3	Task 9: Phase 2 Research Report and Interim Guidelines	106
	REFERENCES	107
	APPENDIX°A: FIELD TESTING LOCATIONS.....	113

LIST OF TABLES

Table 2.1: College Station Project: Stiffness Measurements	13
Table 2.2: San Antonio District Project: Stiffness Measurements	14
Table 2.3: Texas A&M Riverside Project: Stiffness Measurements.....	16
Table 2.4: Texas A&M Riverside Project: Crack Measurements	16
Table 3.1: Project Details	31
Table 3.2: Summary of Mix Designs	32
Table 3.3: Day Section Lengths	32
Table 3.4: Average Construction Section Lengths.....	33
Table 3.5: CR32B: Pavement Structures, prior to FDR and FDR Design	35
Table 3.6: CR32B: Number of Roller Passes for Microcracking.....	35
Table 3.7: CR27: Pavement Structures, prior to FDR and FDR Design	38
Table 3.8: CR99: Pavement Structure, prior to FDR and FDR Design.....	41
Table 3.9: PLU147: Pavement Structure.....	43
Table 3.10: DCP Test Plan	48
Table 3.11: CR32B: Summary of SSG Data	51
Table 3.12: CR27: Summary of SSG Data.....	52
Table 3.13: CR99: Summary of SSG Data.....	54
Table 3.14: PLU147: Summary of SSG Data	54
Table 3.15: PLU147: Normalization Temperature for Each Day	58
Table 6.1: Phase 1b Testing Factorial	76
Table 6.2: Load Sequence for AASHTO T 307	77
Table 6.3: Signal-to-Noise Ratio and Potential Error for TS-1 and TS-2.	94
Table 8.1: Factors Considered in Test Road Design	103
Table 8.2: Proposed Test Road Factorial	104

LIST OF FIGURES

Figure 2.1: Transverse crack.....	7
Figure 2.2: Longitudinal crack.....	8
Figure 2.3: Block cracking.....	9
Figure 2.4: Block crack progression.....	9
Figure 2.5: Fatigue cracking.....	9
Figure 2.6: Pumping through fatigue cracking.....	9
Figure 2.7: Rutting caused by water ingress through cracks into the base.....	10
Figure 2.8: San Antonio District Project: average modulus results (17).....	15
Figure 2.9: Texas A&M Riverside Project: stiffness measurements.....	17
Figure 2.10: Texas A&M Riverside Project: crack length.....	17
Figure 2.11: Falling weight deflectometer.....	20
Figure 2.12: Light weight deflectometer.....	21
Figure 2.13: Soil stiffness gauge.....	22
Figure 2.14: SSG footprint in sand patch.....	22
Figure 2.15: Relationship between FWD and SSG measured stiffness (11).....	23
Figure 2.16: Measured stiffness reduction with FWD and SSG during microcracking (11).....	23
Figure 2.17: AASHTO T 307 resilient modulus test setup.....	24
Figure 2.18: Shear failure of FDR-PC and FDR-FA specimens after UCS testing.....	26
Figure 2.19: Resilient modulus of unstabilized and stabilized materials (29).....	27
Figure 2.20: Resilient modulus of cement stabilized materials tested under repeated loading (30).....	28
Figure 3.1: Testing pattern for soil stiffness gauge and FWD.....	34
Figure 3.2: CR32B: Transverse cracking after microcracking.....	36
Figure 3.3: CR32B: Block cracking on FDR-PC prior to surfacing.....	36
Figure 3.4: CR32B: Water hose dragging on the spread cement.....	36
Figure 3.5: CR32B: Surface raveling.....	37
Figure 3.6: CR32B: Wet, soft location after final compaction.....	37
Figure 3.7: CR32B: Wet and adjacent dry locations tested with SSG.....	37
Figure 3.8: CR32B: Wet section after repair.....	37
Figure 3.9: CR27: Incomplete compaction prior to start of next day construction.....	39
Figure 3.10: CR27: Fine graded material near start of project.....	40
Figure 3.11: CR27: Coarser material throughout majority of the project.....	40
Figure 3.12: CR27: Distressed surface of FDR-PC layer after microcracking near start of project.....	40
Figure 3.13: CR99: Delamination after microcracking.....	42
Figure 3.14: CR99: Depth of delaminated material (50 mm [2 in.]).....	42
Figure 3.15: CR99: Block cracking after microcracking.....	42
Figure 3.16: PLU147: Prime coat stripped from FDR-PC layer after traffic.....	44
Figure 3.17: PLU147: Prime coat stripping from FDR-PC layer during microcracking.....	44
Figure 3.18: PLU147: Water pipe dragging on cement.....	44
Figure 3.19: PLU147: Accumulation of displaced cement in pulverizer wheel track.....	44
Figure 3.20: PLU147: Depth of 4% cement after spreading (\pm 50 mm).....	45
Figure 3.21: PLU147: Depth of cement mound due to dragging of hose (\pm 200 mm).....	45
Figure 3.22: Wave of cement in front of pulverizer skirt on mixing chamber.....	46
Figure 3.23: End of pulverizer pass with no accumulated cement visible.....	46
Figure 3.24: Cement spreader spreading cement on already mixed section.....	46
Figure 3.25: CR27: Number of DCP blows to target depths.....	50
Figure 3.26: CR27: Seating blow penetration depth.....	50
Figure 3.27: PLU147: Number of DCP blows to target depths.....	50
Figure 3.28: PLU147: Seating blow penetration depth.....	50
Figure 3.29: Effect of number of roller passes on stiffness change.....	51

Figure 3.30: CR32B: Average SSG stiffness results after microcracking.	52
Figure 3.31: CR27: Average SSG stiffness results after microcracking.	52
Figure 3.32: CR27: Photographs showing wet surface.	53
Figure 3.33: CR99: Average SSG stiffness results after microcracking.	54
Figure 3.34: PLU147: Average SSG stiffness results after microcracking.	55
Figure 3.35: FWD testing schedule on each project.....	56
Figure 3.36: CR32B: Change in FDR-PC base moduli over time.....	59
Figure 3.37: CR32B: Average base moduli for selected construction sections over time.	59
Figure 3.38: CR32B: FDR-PC base moduli at two temperatures (350 days after microcracking).	59
Figure 3.39: CR27: Mean FDR-PC base moduli 62 days after compaction.	60
Figure 3.40: CR27: Mean FDR-PC base moduli for each construction section over time.	60
Figure 3.41: CR27: Standard deviation of FDR-PC base moduli for each construction section.	60
Figure 3.42: CR27: FDR-PC base moduli in the wheelpath and between wheelpaths after 62 days.....	60
Figure 3.43: CR99: Mean FDR-PC base moduli per construction section over time.	61
Figure 3.44: CR99: FDR-PC base moduli results for 36 days and 48 days after compaction.	61
Figure 3.45: CR99: Ambient temperature variation over time of FWD measurements.....	61
Figure 3.46: PLU147: Average backcalculated stiffnesses for each section.....	62
Figure 3.47: PLU147: Standard deviation of backcalculated stiffnesses for each section.	62
Figure 3.48: PLU147: Surface temperatures in each wheelpath during testing.	62
Figure 3.49: PLU147: Air temperatures during FWD testing.....	62
Figure 3.50: PLU147: Normalized FDR-PC base moduli comparison between test locations.....	63
Figure 3.51: PLU147: Stiffness reduction in the wheelpath compared to between the wheelpaths.....	63
Figure 3.52: PLU147: Mean FDR-PC base moduli for different cement contents over time.	64
Figure 3.53: PLU147: Construction section interface variability due to high cement contents.....	65
Figure 4.1: Sieve analysis of SR88 material.	68
Figure 5.1: Using the vibrating hammer to microcrack a compacted specimen.	70
Figure 5.2: Result of microcracking effort with vibrating hammer.	70
Figure 5.3: Vibrating table.	71
Figure 5.4: Steel wheel vibrating roller.....	72
Figure 5.5: Test pit preparation.	72
Figure 5.6: Final setup before microcracking.....	72
Figure 6.1: FDR-PC mix design.....	75
Figure 6.2: Pug mill mixer.	76
Figure 6.3: Load sequence for AASHTO T 307.	77
Figure 6.4: Vibrating compaction hammer with 148 mm compaction attachment.	78
Figure 6.5: Scouring tool: general view and bottom view.	78
Figure 6.6: Resilient modulus vs. curing time (3% and 4% cement, no microcracking).	80
Figure 6.7: Resilient modulus vs. bulk stress (3% and 4% cement, no microcracking).	80
Figure 6.8: Resilient modulus vs. deviatoric shear stress (3% and 4% cement, no microcracking).	81
Figure 6.9: Difference in resilient modulus between 3% and 4% cement content.....	81
Figure 6.10: Resilient modulus before and after microcracking after 24 hours.	83
Figure 6.11: Resilient modulus before and after microcracking after 48 hours.	83
Figure 6.12: Resilient modulus before and after microcracking after 72 hours.	84
Figure 6.13: Average resilient modulus vs. curing age before and after microcracking.....	84
Figure 6.14: Broken edges caused by brittle nature of stabilized material.....	85
Figure 6.15: Irregular specimen ends leading to poor contact.	85
Figure 6.16: Modified jig for mounting LVDTs on 200 mm × 100 mm specimens.....	86
Figure 6.17: Fabricated jig for mounting LVDTs on 300 mm × 150 mm specimens.....	86
Figure 6.18: LVDT configurations for the different test setups.	88
Figure 6.19: Average resilient modulus test results for FDR-PC and FDR-FA specimens.	90
Figure 6.20: Resilient modulus test results at each cyclic stress for FDR-PC specimens.....	91
Figure 6.21: Monotonic test results.....	93
Figure 6.22: Schematic of signal-to-noise ratio.	93

Figure 6.23: LVDT responses measured using TS-1. 94

Figure 8.1: Proposed test road location. 102

Figure 8.2: Test section planning. 104

Blank page

LIST OF ABBREVIATIONS

AASHTO	American Association of State Highway and Transportation Officials
AC	Asphalt concrete
ANOVA	Analysis of variance
ASTM	American Society for Testing and Materials
Caltrans	California Department of Transportation
CTB	Cement-treated base
DCP	Dynamic cone penetrometer
FDR	Full-depth reclamation
FDR-EE	Full-depth reclamation with engineered asphalt emulsion
FDR-FA	Full-depth reclamation with foamed asphalt
FDR-FA-PC	Full-depth reclamation with foamed asphalt and portland cement
FDR-NS	Full-depth reclamation with no stabilizer
FDR-PC	Full-depth reclamation with portland cement
FWD	Falling weight deflectometer
HMA	Hot mix asphalt
IDT	Indirect tensile
ITS	Indirect tensile strength
LWD	Light weight deflectometer
MC	Microcracking
MDD	Maximum dry density
OMC	Optimum moisture content
NCHRP	National Cooperative Highway Research Program
PCA	Portland Cement Association
PM	Postmile
RAP	Reclaimed asphalt pavement
SSG	Soil stiffness gauge
TxDOT	Texas Department of Transportation
UCPRC	University of California Pavement Research Center
UCS	Unconfined compressive strength

TEST METHODS CITED IN THE TEXT

AASHTO T 11	Standard Method of Test for Materials Finer Than 75- μm (No. 200) Sieve in Mineral Aggregates by Washing
AASHTO T 27	Standard Method of Test for Sieve Analysis of Fine and Coarse Aggregates
AASHTO T 89	Standard Method of Test for Determining the Liquid Limit of Soils
AASHTO T 90	Standard Method of Test for Determining the Plastic Limit and Plasticity Index of Soils
AASHTO T 180	Standard Method of Test for Moisture-Density Relations of Soils Using a 4.54-kg (10-lb) Rammer and a 457-mm (18-in.) Drop
AASHTO T 307	Standard Method of Test for Determining the Resilient Modulus of Soils and Aggregate Materials
AASHTO TP9	Standard Test Method for Indirect Tensile (IDT) Strength of Bituminous Mixtures
ASTM D1557	Standard Test Methods for Laboratory Compaction Characteristics of Soil Using Modified Effort (56,000 ft-lbf/ft ³ (2,700 kN-m/m ³))
ASTM D1633	Standard Test Methods for Compressive Strength of Molded Soil-Cement Cylinders
ASTM D6951	Standard Test Method for Use of the Dynamic Cone Penetrometer in Shallow Pavement Applications

CONVERSION FACTORS

SI* (MODERN METRIC) CONVERSION FACTORS				
APPROXIMATE CONVERSIONS TO SI UNITS				
Symbol	When You Know	Multiply By	To Find	Symbol
LENGTH				
in	in.	25.4	Millimeters	mm
ft	feet	0.305	Meters	m
yd	yards	0.914	Meters	m
mi	miles	1.61	Kilometers	Km
AREA				
in ²	square in.	645.2	Square millimeters	mm ²
ft ²	square feet	0.093	Square meters	m ²
yd ²	square yard	0.836	Square meters	m ²
ac	acres	0.405	Hectares	ha
mi ²	square miles	2.59	Square kilometers	km ²
VOLUME				
fl oz	fluid ounces	29.57	Milliliters	mL
gal	gallons	3.785	Liters	L
ft ³	cubic feet	0.028	cubic meters	m ³
yd ³	cubic yards	0.765	cubic meters	m ³
NOTE: volumes greater than 1000 L shall be shown in m ³				
MASS				
oz	ounces	28.35	Grams	g
lb	pounds	0.454	Kilograms	kg
T	short tons (2000 lb)	0.907	megagrams (or "metric ton")	Mg (or "t")
TEMPERATURE (exact degrees)				
°F	Fahrenheit	5 (F-32)/9 or (F-32)/1.8	Celsius	°C
ILLUMINATION				
fc	foot-candles	10.76	Lux	lx
fl	foot-Lamberts	3.426	candela/m ²	cd/m ²
FORCE and PRESSURE or STRESS				
lbf	poundforce	4.45	Newtons	N
lbf/in ²	poundforce per square inch	6.89	Kilopascals	kPa
APPROXIMATE CONVERSIONS FROM SI UNITS				
Symbol	When You Know	Multiply By	To Find	Symbol
LENGTH				
mm	millimeters	0.039	In.	in
m	meters	3.28	Feet	ft
m	meters	1.09	Yards	yd
km	kilometers	0.621	Miles	mi
AREA				
mm ²	square millimeters	0.0016	square in.	in ²
m ²	square meters	10.764	square feet	ft ²
m ²	square meters	1.195	square yards	yd ²
ha	Hectares	2.47	Acres	ac
km ²	square kilometers	0.386	square miles	mi ²
VOLUME				
mL	Milliliters	0.034	fluid ounces	fl oz
L	liters	0.264	Gallons	gal
m ³	cubic meters	35.314	cubic feet	ft ³
m ³	cubic meters	1.307	cubic yards	yd ³
MASS				
g	grams	0.035	Ounces	oz
kg	kilograms	2.202	Pounds	lb
Mg (or "t")	megagrams (or "metric ton")	1.103	short tons (2000 lb)	T
TEMPERATURE (exact degrees)				
°C	Celsius	1.8C+32	Fahrenheit	°F
ILLUMINATION				
lx	lux	0.0929	foot-candles	fc
cd/m ²	candela/m ²	0.2919	foot-Lamberts	fl
FORCE and PRESSURE or STRESS				
N	Newtons	0.225	Poundforce	lbf
kPa	Kilopascals	0.145	poundforce per square inch	lbf/in ²

*SI is the symbol for the International System of Units. Appropriate rounding should be made to comply with Section 4 of ASTM E380 (Revised March 2003)

Blank page

1. INTRODUCTION

1.1 Background

The California Department of Transportation (Caltrans) has been using full-depth reclamation (FDR) as a rehabilitation strategy since 2001. Most projects to date have used a combination of foamed asphalt and portland cement as the stabilizing agent. However, the fluctuating and at times high cost of asphalt binder coupled with the relatively complex mix-design procedure for mixes that include foamed asphalt has generated interest in the use of portland cement alone (FDR-PC) as an alternative stabilizing agent where appropriate.

Cement-treated (or stabilized) materials in FDR projects are mixtures of soil, aggregate, and/or reclaimed asphalt pavement materials, together with measured amounts of portland cement and water, that are shaped and compacted to form new subbase or base layers in pavement structures. In situ subgrade soils can also be treated to improve the properties of the pavement foundation. Cement-treated bases (CTBs) have been widely used as pavement bases for highways, roads, streets, parking areas, airports, and materials-handling and storage areas. Because CTBs typically have better bearing capacity and durability than bases constructed with unstabilized materials they allow for thinner and usually more cost-effective pavement structures. They have been widely used in the past in California, nationally, and internationally, and considerable research has been undertaken and experience gained on their design, construction, and long-term performance. This report does not document this past research on CTBs.

A well-documented concern about cement-treated bases is the shrinkage cracking associated with the hydration and curing of the stabilized layers. Observations of this cracking date back to ancient Roman times, when horsehair was added to concrete roadways and the structural members in buildings in an attempt to reduce the risk of cracking while the concrete set (1). As hydration and curing progress, the drying shrinkage of the concrete and cement-treated materials is known to contribute the most to shrinkage cracking (2,3). In pavements, shrinkage cracks from underlying cement-treated bases can reflect through the asphalt concrete surfacing, allowing water to infiltrate into the base. Frequent cracks coupled with water infiltration leads to a loss in stiffness in the base layer, resulting in a faster rate of overall deterioration compared to pavements that are not cracked.

Although no costs for shrinkage crack repair are readily available for California highways, the Texas Department of Transportation estimated savings of between \$3.3 million and \$8.6 million in annual net

present value maintenance costs if shrinkage cracking could be prevented on projects where CTB layers are placed (4).

A variety of crack mitigation approaches have been investigated in recent years, including but not necessarily limited to the following:

- Optimizing pavement designs with a specific focus on cement content and design strengths. Caltrans currently specifies a relatively low design strength envelope for cement-treated base (CTB) layers (unconfined compressive strength [UCS] of between 300 and 600 psi [\approx 2 and 4 MPa] after a seven-day cure). Caltrans currently does specify design strengths for full-depth reclamation projects using portland cement as the stabilizer, but a similar strength range to CTBs is typically targeted.
- Improved construction procedures with a specific focus on curing and microcracking of the treated layers with a vibrating roller to alter shrinkage crack development.

Limited research has also been undertaken to assess the influence of using small quantities of asphalt emulsion or foamed asphalt in combination with the cement to alter the hydration process and resulting shrinkage.

Microcracking is currently the most commonly used approach because of its relative simplicity, low cost, and measurable effect. The technique was originally developed in Austria to limit the amount of shrinkage cracking on cement-treated layers. The process entails driving a vibrating steel drum roller over the layer between 48 and 72 hours after its construction. In theory, this action creates a fine network of cracks in the layer that limits or prevents the wider and more severe block cracks typical of cement-treated layers. Limited testing has been completed on a number of projects in Texas, Utah, and New Hampshire. Recommendations from these studies have been implemented by Caltrans and other state departments of transportation. However, longer-term monitoring on a range of projects in Texas and other states has revealed that microcracking has not always been successful in preventing cracking, with some projects showing reflected transverse and block cracks in a relatively short time period. Discussions with the Texas researchers indicated that additional research is necessary to better understand the microcracking mechanism, and to identify the key factors that influence performance. These include but are not limited to aggregate properties, cement content, the time period before microcracking is initiated, layer moisture contents, curing procedures, roller weights and vibration settings, the number of roller passes applied, the time period before placing the surfacing, the time period before opening the road to traffic, and the field test methods and criteria used to assess the degree of microcracking achieved.

1.2 Problem Statement

Microcracking is a promising technique for limiting or preventing shrinkage cracking in cement-treated layers that could reflect through the asphalt concrete surfacing. However, insufficient research has been conducted to fully understand its mechanism, to develop procedures for microcracking (i.e., time interval between construction and microcracking, vibration settings, the number of microcracking cycles, etc.), and to identify suitable criteria for mechanistic-empirical design procedures and performance models of pavement structures that incorporate a microcracked cement-treated layer (which could theoretically have a different mechanistic behavioral life cycle than structures with cement-treated layers that have not been microcracked). Caltrans specifications (Section 30) currently require microcracking on full-depth reclaimed cement-treated layers, but the instructions state only that:

“During the period from 48 to 72 hours after compaction, microcrack the surface by applying 3 passes of the vibratory steel drum rollers used during final compaction at high amplitude, regardless of whether asphaltic emulsion has been applied.”

No additional information is provided, and no tests are required by the specification to determine whether microcracking was effective in reducing initial stiffness. The results of using this method specification had not been evaluated in California prior to the start of this UCPRC study.

The following problem statements have been identified with regard to microcracking and require additional research or refinement/calibration of existing information for California conditions:

- No comprehensive guidelines exist to guide design engineers, contractors, and project specification writers on how to decide on the optimal microcracking procedure for a specific layer design and how to determine whether the desired result has been achieved.
- The research completed in Texas was limited to a small number of projects with a limited range of materials and cement contents. Subsequent observations have found that cement content can have a significant influence on the effectiveness of microcracking. Additional research is required to determine the key factors that influence the effectiveness of microcracking. These may include but are not limited to the following:
 - + Adjusting the time interval between the end of construction and the start of microcracking
 - + Selecting a specific weight of roller
 - + Selecting specific vibration settings
 - + Selecting multiple microcracking actions
 - + Setting required specific changes in measured stiffness after microcracking
- There is no established procedure for accurately measuring the effectiveness of microcracking actions. Currently, a percentage change in stiffness measured with a falling weight deflectometer (FWD), light weight deflectometer (LWD), or soil stiffness gauge (SSG) is recommended. Implementable guidelines based on actual field performance need to be prepared for this activity. Consideration needs to be given to whether the load applied during FWD testing causes additional microcracking in the drop zone, thereby influencing conclusions regarding the level of stiffness change that has been achieved.

- There is no procedure for simulating microcracking in the laboratory as part of a mix design/pavement design process. Such a procedure needs to be developed.
- There is no documented research linking microcracking with layer curing, opening to traffic, and to the period between construction and paving.
- There is no documented research investigating the use of other additives, such as small quantities of asphalt emulsion, foamed asphalt, or synthetic polymer emulsion to enhance crack mitigation when using microcracking.
- There is limited documented research on using alternative strategies to reduce shrinkage cracking, including the use of fibers or retarders to slow the rate of hydration.

1.3 Project Objective/Goal

This study is a continuation of PPRC Project 4.36 (“Guidelines for Full-Depth Reclamation of Pavements”) and addresses the project titled “Microcracking of Cement-Treated Layers.” The objective of this project is to develop guidelines for mitigation measures to limit/prevent shrinkage cracking in cement-treated layers. It is planned that this will be achieved in two phases through the following tasks:

- Phase 1: Literature review, laboratory testing, and modeling
 - Task 1: Conduct a literature review on research related to crack mitigation in cement-treated materials
 - Task 2: Conduct preliminary laboratory testing to understand crack mitigation mechanisms and identify criteria for modeling the effects of crack mitigation on long-term pavement performance
 - Task 3: Model the effects of crack mitigation on long-term pavement performance
 - Task 4: Prepare a summary report with recommendations for Phase 2 testing if appropriate
- Phase 2: Accelerated wheel-load testing and field testing (depending on the results of Phase 1 and under the direction of the Caltrans project steering committee).
 - Task 1: Monitor construction and performance of field projects where crack mitigation measures have been used
 - Task 2: Design and construct a test track to compare different crack mitigation techniques
 - Task 3: Conduct accelerated wheel-load testing to compare performance of the different crack mitigation techniques
 - Task 4: Conduct laboratory testing of specimens sampled from the test track and from field projects to compare laboratory test results with accelerated wheel-load testing results and to identify suitable criteria for refining mechanistic-empirical design procedures and performance models for pavements with cement-treated layers
 - Task 5: Prepare a project research report and guidelines for crack mitigation in cement-treated layers

This report covers Phase 1.

1.4 Report Layout

This research report presents an overview of the work carried out in meeting the objectives of Phase 1 of the study, and is organized as follows:

- Chapter 2 provides an overview of the literature related to the topic.
- Chapter 3 summarizes initial field testing results from four FDR-PC projects in California.
- Chapter 4 summarizes the experiment design for laboratory testing.
- Chapter 5 describes the approaches considered for microcracking laboratory-prepared specimens.
- Chapter 6 details laboratory testing to assess stiffness change on microcracked specimens prepared using the methods described in Chapter 5.
- Chapter 7 provides a project summary, conclusions, and preliminary recommendations.
- Chapter 8 summarizes the proposed Phase 2 experimental plan.
- Appendix A contains information on the field project locations and FWD testing points.

1.5 Measurement Units

Although Caltrans recently returned to the use of US standard measurement units, metric units have always been used by the UCPRC in the design and layout of test tracks, and for laboratory, accelerated load testing, field measurements, and data storage. In this report, both English and metric units (provided in parentheses after the English units) are provided in general discussion. In keeping with convention, metric units are used in laboratory data analyses and reporting. A conversion table is provided on page xviii at the beginning of this report.

Blank page

2. LITERATURE REVIEW

The literature relevant to shrinkage crack mitigation in cement-treated pavement layers in highway pavements with specific reference to full-depth reclamation is discussed under the following headings:

- Flexible pavement distresses related to base failure
- Shrinkage crack mitigation
- Measuring stiffness change

2.1 Flexible Pavement Distresses Related to Base Failure

Cement-treated base (CTB) failures typically cause one or a combination of distresses on the surface of flexible pavements, including transverse cracking, longitudinal cracking, block cracking, fatigue cracking and/or rutting. The cause of these distresses can be load related, non-load related (e.g., environmental effects such as temperature, moisture, and/or freeze-thaw), or a combination of the two. This UCPRC study only discusses cracks associated with cement-treated base behavior, although the authors acknowledge that distresses in asphalt concrete surfacings can also be caused by factors other than base failure.

2.1.1 Transverse and Longitudinal Cracking

Transverse cracks in asphalt pavements over CTB (Figure 2.1) may be caused by the shrinkage associated with hydration and drying in the CTB after construction (3,5,6). Shrinkage cracking in CTBs begins soon after the completion of compaction as hydration reactions begin and the layer dries back. The rate of reflection of these cracks through the asphalt concrete layer is typically dependent on the thickness of that asphalt layer and the cement content of the base (higher cement contents typically result in wider cracks with higher associated stress fields).



Figure 2.1: Transverse crack.

Zube et al. (7) reported that cracking is prominent in CTBs with high unconfined compressive strengths (UCS). This is caused by the higher cement content requiring more water for hydration, which leads to higher drying shrinkage, which in turn causes more cracking than in pavements with lower cement contents (3,7). The restraints from friction between the base and the subbase or subgrade, and between the base and the asphalt surface layer cause tensile stresses in the material around the crack to exceed the tensile strength of that material, resulting in transverse cracks that reflect through to the surface (2). The rate of crack reflection is again dependent on the cement content in the treated layer and to the asphalt layer thickness. The rate of reflection can also be influenced by the integrity of the bond between the base and the surface, with poor bonding leading to a faster rate of cracking in the asphalt layer (2).

A survey conducted by Wen (8) as part of a National Cooperative Highway Research Program (NCHRP) study revealed that transverse cracking and block cracking were considered to be the most severe distresses associated with CTB.

Longitudinal cracking in flexible pavements with CTB (Figure 2.2) have also been recorded (9,10). This distress, usually in the wheelpaths, is caused by the high shear/tension stress at the surface of the asphalt caused by high wheel loads and/or tire pressures (8). Longitudinal cracking outside the wheelpath is more commonly caused by expansive soils and construction effects (5).



Figure 2.2: Longitudinal crack.

2.1.2 Block Cracking

Block cracking (Figure 2.3) in asphalt concrete surfaces can also be attributed to shrinkage cracks in the CTB that have reflected through the asphalt over time. They are caused by cement hydration and thermal expansion and contraction in the cement-treated base, which leads to a series of longitudinal and transverse cracks that eventually join to form a series of blocks in the base that eventually reflect through the asphalt

concrete surfacing (Figure 2.4) (11). Although block cracks will occur in both trafficked and untrafficked areas of the pavement, their formation is not necessarily dependent on traffic loading.



Figure 2.3: Block cracking.



Figure 2.4: Block crack progression.

2.1.3 Fatigue Cracking

Fatigue cracking in asphalt surface layers over CTB (Figure 2.5) can result from the formation of weak areas at the top of the treated layer, caused by carbonation of the cement prior to the surfacing being placed (i.e., inappropriate curing procedures), laminations (i.e., due to inappropriate final leveling and final compaction procedures), or compaction outside of the specified time limits, which in turn can lead to fatigue and compression failures. These weak areas can lead to delamination in the CTB or to debonding between the top of the CTB and the bottom of the asphalt layer, which creates conditions of minimum friction between the different layers (12). The laminations and loss of friction are susceptible to erosion and loss of fines by pumping (Figure 2.6). The strain levels at the bottom of the asphalt surface layer increase as the surface of the base weakens, leading to the fatigue failure.



Figure 2.5: Fatigue cracking.



Figure 2.6: Pumping through fatigue cracking.

2.1.4 Rutting

Rutting in well-constructed CTB layers is rare given their relatively high strengths and stiffnesses. However, on pavements with severe cracking that allows water to infiltrate into the base, rutting often occurs as a result of deformation of the softer base materials under traffic loading (Figure 2.7).



Figure 2.7: Rutting caused by water ingress through cracks into the base.

2.2 Shrinkage Crack Mitigation

Shrinkage cracks in CTB layers can be mitigated through a number of different approaches. Most research has focused on design, in terms of optimizing cement content and layer thicknesses, and on construction, in terms of better mixing, curing, and quality control. Limited research has been undertaken on precracking or microcracking the layer to alter its cracking behavior and thereby reduce the severity of the shrinkage cracks, or on other mitigation measures such as adding asphalt emulsion, foamed asphalt, or synthetic polymer emulsions to the mixing water to alter the hydration reaction of the cement.

2.2.1 Design and Construction Considerations

From a design standpoint, the Portland Cement Association (PCA) (13) has advocated for the use of seven-day unconfined compressive strength values that are lower than those traditionally sought in the past. A range of strengths between a minimum of 300 psi (2.1 MPa) and a maximum of 400 psi (2.8 MPa) are now recommended. These strengths are considerably lower than the previously recommended strength range of 600 psi to 750 psi (4.2 MPa to 5.2 MPa). The Texas Department of Transportation (TxDOT) has reduced cement contents even further in some districts, moving away from previously specified minimum seven-day strengths of 500 psi (3.5 MPa) to seven-day strength ranges of between 200 psi and 300 psi (1.4 MPa to 2.1 MPa) in an attempt to better mitigate shrinkage crack problems that they are experiencing (11). This reduction was based on UCS tests done on cores sampled from treated roads, which revealed that seven-day laboratory-determined strengths of 500 psi typically translated to strengths in excess of 1,500 psi (3.4 MPa)

in the road. The high cement contents required to achieve these strengths resulted in a layer susceptible to very high shrinkage and to cracking associated with the brittle nature of the compacted material.

The 2010 (and provisional 2015) Caltrans Standard Specifications for cement-treated bases (Section 27) specify a minimum seven-day UCS of 750 psi (5.2 MPa). The minimum specified seven-day UCS for full-depth reclamation with cement (Section 30.4) will depend on the project requirements, but will typically be set to a minimum seven-day strength (with modified curing as specified in Section 30.4) of 300 psi (2.1 MPa) and a maximum of 600 psi (4.1 MPa). Caltrans does not have a durability requirement for cement-treated layers.

From a construction standpoint, the PCA also recommends that thicker layers up to 12 in. (300 mm) be constructed at these lower strengths to create a quality base with a balanced design that can support design loads and be sufficiently durable and impermeable in order to resist volume changes, the effects of freeze-thaw cycles, and the effects of moisture changes. Thinner layers (i.e., 6 in. to 8 in. [150 mm to 200 mm]) tend to be more brittle and susceptible to more severe shrinkage cracking. Recent developments in pulverizing equipment have made it possible to achieve consistent in-place mixing to these recommended depths. Other construction considerations to limit the severity of shrinkage cracking include these (3):

- Using the lowest possible moisture content to compact the layer that will still achieve the target strength and density.
- Using appropriate techniques to maintain a consistent rate of curing of the layer. Techniques include maintaining constant moisture content in the layer with regular water spraying (avoiding wetting and drying cycles), using a curing membrane, and/or applying the surfacing layer as soon as the target moisture content has been achieved.
- Including stress relief layers to decrease the potential for shrinkage cracks to reflect through the surface layer. Interlayers include a bituminous surface treatment, geofabrics or geogrids, or a granular layer between the asphalt concrete surface and the cement-treated base.

2.2.2 Microcracking

The process of microcracking cement-treated layers involves applying several passes of a steel drum vibratory roller, at maximum vibration frequency and amplitude settings, over the CTB within a set time window after construction of the treated layer. The theory of microcracking is that the action creates a fine network of cracks in the treated layer that will relieve initial stresses during early hydration of the cement, and thereby limit or prevent the wider and more severe block cracks typical of cement-treated layers. The use of microcracking was first reported in Austria in the mid-1990s (14,15).

Despite fairly wide use of microcracking, including in California, there appears to be very little documented research on the process, when and how to do it, and how it affects the short- medium-, and long-term

behavior and performance of the treated layer. Caltrans specifications (Section 30) simply specify microcracking on full-depth reclaimed cement-treated layers as follows (there is no microcracking requirement in Section 27 [Cement-treated Bases]):

“During the period from 48 to 72 hours after compaction, microcrack the surface by applying 3 single passes with a 12-ton vibratory steel drum roller at maximum amplitude travelling from 2 to 3 mph, regardless of whether asphaltic emulsion has been applied.”

Litzka and Hasleher (14) summarized the findings of their research in Austria as loading the cement-treated layer with up to five passes of a vibratory roller, 24 to 72 hours after final compaction, thus creating a microcracked structure in the stabilized layer. They concluded that microcracking prevents the development of larger stress cracks, which in turn prevents reflective cracking through the asphalt overlay. Further work in Austria by Brandl (15) concluded that the use of microcracking was effective after 24 hours, but that additional microcracking is required if the compressive strength exceeds 725 psi (5.7 MPa) after two days of curing. A target stiffness reduction of 40 percent of the stiffness measured before microcracking was suggested.

Apart from the early work in Austria, the Texas Department of Transportation appears to have undertaken the most work on the topic, but those researchers acknowledge that the interim recommendations published to date are based on a limited experimental design and limited testing, and that the findings are not necessarily conclusive based on these limitations (16). Research in Texas was conducted between 2000 and 2005, during which five projects with a total of 36 test sections were evaluated (4,9,11,17,18). The interim recommendations proposed that microcracking should be performed between 24 and 48 hours after final compaction of the treated layer. The process recommended three or four single passes of a steel wheel roller, with maximum vibration frequency and amplitude settings (17). No research comparing the effect of roller weight or vibration frequency and amplitude settings appears to have been published.

Summary of Texas Projects: City of College Station (Edelweiss)

The Edelweiss project consisted of four test sections (one control and three microcracked) constructed in the summer of 2000 (11). The pavement structures were comprised of 6 in. (150 mm) of lime-stabilized subgrade, 6 in. (150 mm) of CTB, and a 2 in. (50 mm) HMA surfacing. The base design was based on a seven-day unconfined compressive strength of 500 psi (3.5 MPa), which required a cement content of seven percent by mass of the dry aggregate.

Microcracking was performed after 24 hours on two of the sections and after 48 hours on the third using a 12-ton steel drum roller set at maximum vibration amplitude and moving at 2 mph (3.2 km/h, i.e., walking pace). A web of surface cracks was observed in some areas of the layer after microcracking. The effect of

the microcracking on base stiffness was measured with a Humboldt stiffness gauge and a falling weight deflectometer (FWD) before starting microcracking, after two roller passes, and after four roller passes. A second round of FWD measurements was taken approximately six months after construction. The results are summarized in Table 2.1.

Table 2.1: College Station Project: Stiffness Measurements

Time	No. of Roller Passes	FWD		Stiffness Gauge	
		Stiffness (GPa)	Stiffness Change (% of original)	Stiffness (MN/m) ¹	Stiffness Change (% of original)
Construction	0	8.1	0	55.4	0
	2	2.1	75% reduction	38.0	31% reduction
	4	1.2	85% reduction	29.5	47% reduction
+ 48 hours ²	N/A	Not measured		41.2	26% reduction
+ 6 months ³	N/A	12	48% increase	Not measured	
¹ MN/m = meganewtons per meter ² 48 hours after microcracking ³ Approximately 6 months after microcracking					

The FWD measurements show that the first two roller passes caused a significant (75 percent) reduction in stiffness, while the third and fourth roller passes resulted in only a small (additional 10 percent) reduction. The stiffness gauge results differed from those of the FWD and did not follow the same trend in stiffness reduction after two and four roller passes. It is not clear whether the impact of the falling weight caused an additional reduction in stiffness in the drop zone. Both the FWD and the stiffness gauge results show that the reduction in stiffness was temporary and that it had recovered to that of the control section, which was not microcracked, during the six-month interval between evaluations. Transverse cracks were noted on all sections after six months. Crack lengths were between 2.4 ft. and 5.6 ft. per 100 ft. (0.5 m and 1.2 m per 100 m) of pavement on the three microcracked sections, and 27.3 ft. per 100 ft. (5.8 m per 100 m) of pavement on the control section. The TxDOT researchers concluded that microcracking did not adversely affect the load bearing capacity of the bases, and appeared to significantly reduce shrinkage cracking in the first six months after construction. Further monitoring was recommended to assess longer-term performance over a number of seasonal wetting and drying cycles.

Summary of Texas Projects: Bryan District (Road SH47) (17)

Road SH47 was rehabilitated in 2002 using a full-depth reclamation process. The road was pulverized to a depth of 14 in. (350 mm) after which three percent cement was mixed in and then compacted. The laboratory mix design indicated a seven-day UCS of 384 psi (2.6 MPa). The road was divided into 12 sections, based on the day of construction. The CTB was microcracked with a 25-ton roller 24 hours (eight sections of the project), 48 hours (three sections), and 72 hours (one section) after compaction. Three full passes were applied. A 4 in. asphalt concrete overlay was placed on the CTB as a surfacing 72 hours after microcracking of the last section. The effect of microcracking on stiffness was monitored with an FWD on five of the sections (three of the 24-hour sections and two of the 48-hour sections). Average stiffness reduction after microcracking was 60 percent of the stiffness measured before microcracking, with no significant

differences noted for the different microcracking intervals. FWD measurements were repeated after 12 months and stiffnesses were approximately double the stiffness measured prior to microcracking. No cracking was observed at this time. A statistical analysis indicated that the time interval between compaction and microcracking (i.e., between 24 and 48 hours) did not influence the stiffnesses measured after 12 months.

A visual evaluation in 2004 (i.e., 24 months after construction) revealed two transverse cracks on one of the sections. No cracks were observed on the remainder of the project. A follow up evaluation in 2005 found that additional cracking had occurred on the original section with cracks and that new cracks had formed on four additional sections, all which had been microcracked after 24 hours. Crack lengths on each section varied between 16 ft. and 1,404 ft. (5 m and 428 m). Some of the cracks were attributed to construction problems (e.g., longitudinal joints) and not to shrinkage in the cement-treated layer. The change in stiffness before and after microcracking was not measured on the section with the most cracks, and consequently it was not possible to determine whether the additional cracking on this section could have been attributed to inadequate microcracking. The researchers concluded that measurements of stiffness reduction with an FWD, light weight deflectometer (LWD), or stiffness gauge should be a specified project requirement to ensure that adequate and consistent stiffness reduction is achieved during microcracking.

Summary of Texas Projects: San Antonio District (Road SH16) (17)

Road SH16 was rehabilitated in 2003 using a full-depth reclamation process. The existing road was pulverized to a depth of 8 in. (200 mm), treated with three percent cement, and compacted to form a subbase. A new 5 in.-thick base was imported and treated with two percent cement. The road was divided into four sections, based on the day of construction. Section 1 was not microcracked and served as a control, Section 2 was microcracked with a 12-ton roller 24 hours after compaction, and Section 3 and Section 4 were microcracked with three and two and passes respectively with the same roller 48 hours after compaction. Maximum vibration amplitude was used on all sections. The effect of microcracking on stiffness was monitored with an FWD. Stiffness reductions of 42, 73, and 46 percent were recorded on Sections 2, 3 and 4, respectively (Table 2.2).

Table 2.2: San Antonio District Project: Stiffness Measurements

Section	MC ¹ Process (hours/passes)	Stiffness (ksi [GPa])			% Change of Original	
		Initial	After MC ¹	+ 3 months	After MC	+ 3 months
1	0/0	100 (0.7)	N/A	340 (2.3)	N/A	240% increase
2	24/3	120 (0.8)	70 (0.5)	410 (2.8)	42% reduction	242% increase
3	48/3	390 (2.7)	105 (0.7)	435 (3.0)	73% reduction	12% increase
4	48/2	250 (1.7)	135 (0.9)	255 (1.8)	46% reduction	2% increase

¹ MC = Microcracking

A surface treatment (chip seal) was applied as an initial wearing course, followed by 2 in. of hot mix asphalt. The sections were retested with an FWD after three months (Table 2.2 and Figure 2.8). The reason for the limited stiffness increase on Section 4 could not be explained. No cracks were observed. A second visual assessment of the project was conducted after 13 months. All of the sections had cracks, with crack length on Section 2 slightly less than that on the other sections (77 ft. [23.5 m] compared to 90, 94, and 95 ft. [27.4, 28.7, and 30.0 m] on Sections 1, 3 and 4, respectively).

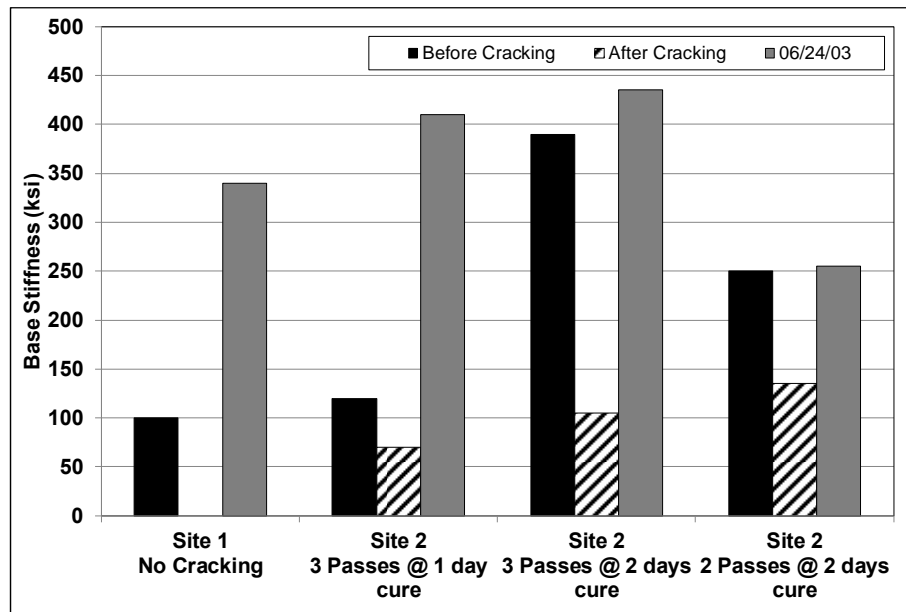


Figure 2.8: San Antonio District Project: average modulus results (17).

Summary of Texas Projects: Texas A&M Riverside Campus (17)

This project was constructed at the Texas A&M Riverside campus in September 2003 to facilitate monitoring of microcracked pavements under controlled conditions. Two roads (Avenue C and Avenue D) were selected for the project. The existing material was pulverized and compacted to form a 6 in.-thick (150 mm) subbase. New aggregate base was placed on the subbase, stabilized with cement, and then compacted. Avenue C was constructed with a cement content of eight percent and Avenue D with four percent. The roads were not surfaced for the duration of the study to allow researchers to monitor the cracking behavior. Each road was divided into six sections with a different crack mitigation treatment, as follows:

- No moist curing, no microcracking (control)
- Moist cure on Day 0, no microcracking, prime coat curing membrane on Day 1
- Moist cure on Days 0 through 3, microcrack on Day 1
- Moist cure on Days 0 through 3, microcrack on Day 2
- Moist cure on Days 0 through 3, microcrack on Day 3
- Moist cure on Days 0 through 3, no microcracking

Stiffness on the sections was measured with an FWD after microcracking and again after 10 and 21 months. Crack lengths were measured after 21 months. The results are summarized in Table 2.3 and Table 2.4 and in Figure 2.9 and Figure 2.10.

Table 2.3: Texas A&M Riverside Project: Stiffness Measurements

Cement Content (%)	Treatment	Stiffness Before Microcracking (ksi, [GPa])		Stiffness After Microcracking (ksi, [GPa])		Stiffness After 10 Months (ksi, [GPa])		Stiffness After 21 Months (ksi, [GPa])	
4	Dry cure, no MC ¹	911	(6.3)	N/A		1,030	(7.2)	681	(4.8)
	Prime Coat Day 1	1,006	(6.9)	N/A		1,200	(8.4)	1,035	(7.2)
	MC Day 1	525	(3.6)	253	(1.7)	1,960	(13.7)	1,175	(8.2)
	MC Day 2	900	(6.2)	262	(1.8)	2,170	(15.2)	1,161	(8.1)
	MC Day 3	860	(5.9)	348	(2.4)	2,495	(17.5)	1,089	(7.6)
	Moist cure, no MC	924	(6.4)	N/A		2,000	(14.0)	1,582	(11.1)
8	Dry cure, no MC	802	(5.5)	N/A		2,300	(16.1)	1,746	(12.2)
	Prime Coat Day 1	1,692	(11.7)	N/A		1,200	(8.4)	1,178	(8.3)
	MC Day 1	1,650	(11.4)	507	(3.5)	4,050	(28.4)	2,401	(16.8)
	MC Day 2	1,450	(5.9)	485	(3.3)	2,500	(17.5)	2,093	(14.7)
	MC Day 3	2,120	(14.7)	890	(6.1)	2,800	(19.6)	1,651	(11.6)
	Moist cure, no MC	2,824	(19.5)	N/A		1,400	(9.8)	1,597	(11.2)

¹ MC = Microcracking

Table 2.4: Texas A&M Riverside Project: Crack Measurements

Treatment	4% Cement		8% Cement	
	Crack Length			
	(ft.)	(m)	(ft.)	(m)
Dry cure, no MC ¹	89	27	277	84
Prime Coat Day 1	78	24	328	100
MC Day 1	76	23	92	28
MC Day 2	34	10	105	32
MC Day 3	81	25	88	27
Moist cure, no MC	50	15	70	21

¹ MC = Microcracking

Summary of Texas Projects: IH 45 Frontage Road (4)

This project was constructed in Huntsville, Texas, on the IH 45 frontage road. Construction took place in December 2004 and May 2005. The design consisted of 10 in. (250 mm) of lime-treated subgrade, 12 in. (300 mm) of pug mill-mixed cement-treated base, and 5 in. (125 mm) of hot mix asphalt. Seven-day UCS strengths and tube suction dielectric values were assessed for a range of cement contents between two and eight percent. A cement content of four percent was selected, giving a UCS of 1,137 psi (7.8 MPa) and dielectric value of 7.3. Although the strength was significantly higher than the 300 psi (2.1 MPa) typically targeted by TxDOT, the decision to go with the higher cement content was based on the dielectric value (4).

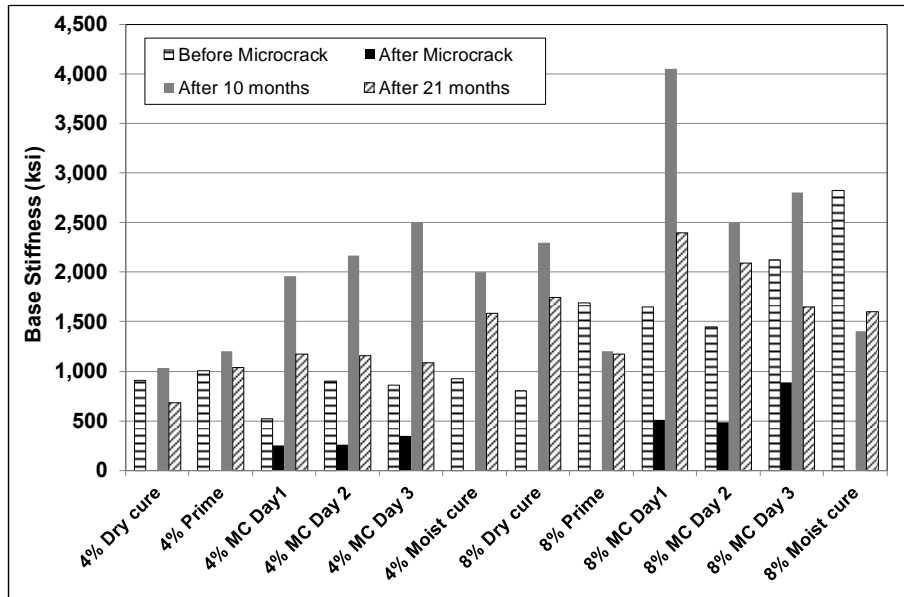


Figure 2.9: Texas A&M Riverside Project: stiffness measurements.

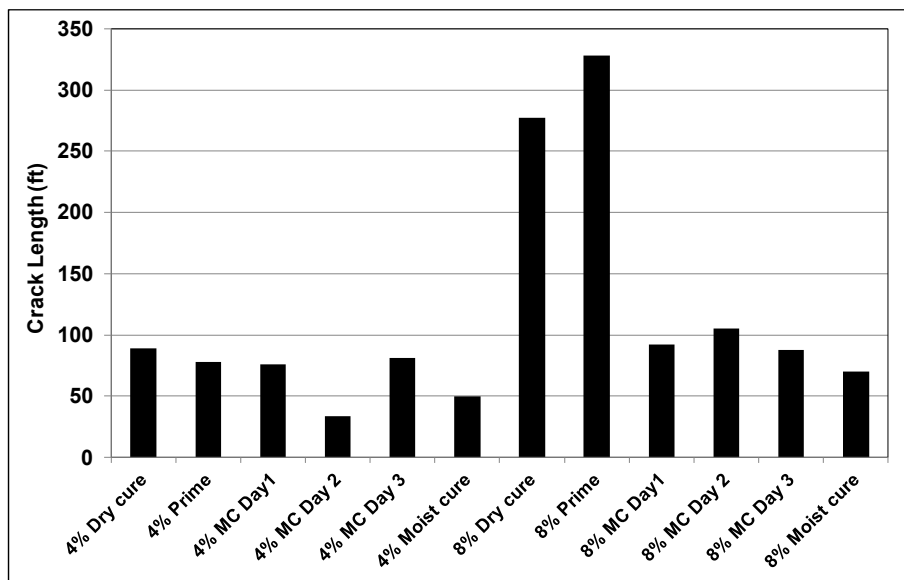


Figure 2.10: Texas A&M Riverside Project: crack length.

All the cement-treated sections were microcracked with the exception of a 200 ft. (60 m) control section. The sections constructed in December 2004 were microcracked after four days due to the slow strength gain attributed to cold weather. The sections constructed in May 2005 were microcracked after two days. A light weight deflectometer (LWD) was used to measure any changes in stiffness. On the December 2004 sections, average stiffnesses before microcracking ranged between 173 ksi and 358 ksi (1.2 GPa and 2.5 GPa). After microcracking, average stiffnesses ranged between 130 ksi and 245 ksi (0.9 GPa and 1.7 GPa), corresponding to stiffness reductions of 24 to 38 percent. On the May 2005 sections, the average stiffnesses before and after microcracking were 476 ksi (3.3 GPa) and 204 ksi (1.4 GPa), respectively, corresponding

to a 57 percent stiffness reduction. A visual evaluation along with FWD measurements was conducted in August 2005. No cracks were observed and there was no difference in the stiffnesses between the microcracked and control sections.

Summary of Texas Projects: Conclusions and Recommendations

Conclusions drawn from the Texas research include the following (17):

- Microcracking, when properly applied, did not result in pavement damage and the base modulus recovered to the same levels as that measured on the control sections that were not microcracked.
- Problematic cracking occurred on pavements with very high base course cement contents if microcracking was not applied. Problematic cracking implies increased crack width, increased total crack length, or both.
- Microcracking reduced the severity of shrinkage cracks in the base regardless of cement content, and in some cases also significantly reduced total crack length.
- Appropriate laboratory design combined with microcracking by three passes of a vibratory roller at high amplitude after two to three days of curing provided a marked reduction in shrinkage cracking problems.
- In cooler temperatures, when cement curing is slower, microcracking had to be delayed. The study recommended that a minimum modulus value of 200 ksi (1.4 GPa) be attained before the layer is microcracked.
- The study recommended a target reduction in average base modulus of 60 percent if an FWD is used to measure stiffness and 40 to 50 percent if a light weight deflectometer or stiffness gauge is used.
- Asphalt curing membranes were minimally effective at reducing cracking problems.
- Moist curing without microcracking resulted in more severe (wider) cracks, compared to moist curing with microcracking, that quickly reflected through the surfacing.
- The use of higher cement contents in general did not provide a significantly increased base modulus, but it did result in more severe cracking problems. Historically, seven-day UCS targets were based upon achieving a high degree of confidence that the material would meet durability criteria—and that it would not be necessary to perform the labor- and time-intensive durability tests. With the recent development of simpler, less time-consuming durability tests (e.g., tube suction), strength requirements should be eased and checked against the new durability requirements. Cement content design should be based on a combination of adequate strength, durability, and moisture resistance.

Based on the research, TxDOT provided the following recommendations for the design and construction of cement-treated bases:

- Design
 - + Seven-day UCS: ≥ 300 psi (2.1 MPa) (according to ASTM D1633, i.e., moist cure)
 - + Dielectric value after tube suction test: ≤ 10
- Construction
 - + After placement and compaction of the CTB to project specifications, moist cure for two days.
 - + Microcrack the section using the same (or equivalent) steel wheel vibrating roller that was used for compaction. If microcracking after two days is not feasible, waiting until the base age reaches

three days is preferable to microcracking after only one day of curing. Layers should not be microcracked until a minimum modulus of 200 ksi (1.4 GPa) has been attained.

- + Continue moist curing to an age of at least 72 hours from the day of placement of the CTB.

2.2.3 Effect of Early Trafficking

Early opening to traffic (i.e., opening to traffic after completion of construction each day) will also result in some degree of microcracking, and it has been observed to reduce the severity of shrinkage cracking in Texas (15) and in New England states (19). In the New England experiments, data suggested that early trafficking adversely affected the initial strength gain and base layer stiffness in the cement-treated sections. After two days of curing, trafficked cement-treated sections exhibited FWD modulus values that were 50 percent lower than those measured on the corresponding untrafficked sections.

One concern of early opening to traffic is the potential for raveling of the surface. This can be addressed by regular watering of the compacted layer, by applying dilute asphalt emulsion to the surface during or immediately after compaction of the treated layer, or by applying a surface treatment to the constructed section each day. The latter approach has been used in Texas with reported success (20,21). Work zone traffic speeds should be enforced on the newly opened sections for the remainder of the construction period and pilot cars should be used when possible.

2.2.4 Other Mitigation Measures

In limited studies, Jones (22) and Jones and Fu (23) observed what appeared to be differences in the shrinkage behavior of stabilized materials when cement and asphalt emulsion or cement and foamed asphalt were combined. In these studies, it was hypothesized that drops of asphalt encapsulated the cement particles, thereby retarding or altering the hydration process and consequently limiting shrinkage. Further research on using this approach to mitigate shrinkage cracking on cement-treated layers is recommended.

2.3 Measuring Stiffness Change on the Road

If microcracking is adopted as a means to reduce the severity of shrinkage cracking on cement-treated layers (in new construction or full-depth reclamation), some method of measuring stiffness change during the microcracking process will be required to determine whether the contractor has met his obligations in terms of the project specifications and whether the desired affect has been achieved. Pavement layer stiffnesses can be measured with a variety of different instruments, including the falling weight deflectometer, the light weight deflectometer, and the soil stiffness gauge, each of which is discussed below. The Clegg Hammer stiffness measuring device has also been assessed for monitoring microcracked layers, and although it proved to be effective in measuring strength gain on cement-treated bases (19,24), it was found to be

insensitive to stiffness changes associated with microcracking after rolling (25). Therefore, the Clegg Hammer is not discussed in this chapter.

2.3.1 Falling Weight Deflectometer (FWD)

The FWD is the most commonly used instrument for measuring deflection on pavements (Figure 2.11). Deflection measurements can be backcalculated to determine layer stiffnesses. Concerns have been raised about using an FWD for measuring the effect of microcracking on base stiffness because the heavier falling weight could induce additional microcracking in the region of the drop zone. For this reason, stiffness gauge manufacturers usually recommend that gauge measurements be taken before FWD measurements (26). If percent of stiffness reduction is being used as a control measure for the number of roller passes applied during microcracking, the use of FWD measurements could be misleading because rolling would be stopped when stiffness had dropped to the required percentage of original stiffness in the FWD drop zone, which might not be representative of the stiffness change in the rest of the pavement.



Figure 2.11: Falling weight deflectometer.

2.3.2 Light Weight Deflectometer (LWD)

The LWD (Figure 2.12) is a portable deflection-measuring device originally developed for measuring in situ stiffnesses on subgrades and newly constructed aggregate bases as an alternative quality control procedure to measuring in situ density. It consists of a load plate, a vertically sliding weight, and up to three deflection sensors connected to a handheld device that stores the data collected. Different size loading plates, different mass weights, and different drop heights are available and are selected based on the expected layer stiffness and thickness. An LWD works on the same principles as a traditional FWD but has fewer sensors and a much lower loading capacity. The maximum measurable layer thickness and measurable layer stiffness are typically in the range of 8 to 12 in. (200 to 300 mm) and 435 ksi (3 GPa), respectively.



Figure 2.12: Light weight deflectometer.

2.3.3 Soil Stiffness Gauge (SSG)

SSGs are offered by a number of different manufacturers and were also originally developed as an alternative to density measurements on compacted, unbound layers. The SSG measures soil stiffness by imparting small deflections to the ground at up to 25 different frequencies, ranging between 100 Hz and 200 Hz. The maximum measurable layer thickness and measurable layer stiffness are similar to those of the light weight deflectometer (i.e., typically in the region of 10 to 12 in. [250 to 300 mm] and 435 ksi [3 GPa], respectively). The devices display the average stiffness, the associated signal-to-noise ratio, which is an indication of the ambient vibrations in the ground, and the standard deviation between the measurements. A Young's modulus can be derived from the user-specified Poisson's ratio and the measured stiffness. The stiffness is calculated according to Equation 2.1 (26).

$$S = P/\delta \quad (2.1)$$

Where: S = Stiffness (MN/m)
 P = force (MN)
 δ = surface displacement (m)

A soil stiffness gauge is portable (Figure 2.13), and typically weighs around 20 lbs (10 kg). It can take measurements with little preparation of the surface. On the hard and rough surfaces typically encountered in the field, a patch of damp sand is used to provide even footing. The device is placed on the sand and twisted to seat the foot (Figure 2.14).



Figure 2.13: Soil stiffness gauge.



Figure 2.14: SSG footprint in sand patch.

2.3.4 Device Comparison

Soil Stiffness Gauge and Light Weight Deflectometer

A soil stiffness gauge and a light weight deflectometer were used side by side on a number of projects in Utah and Wyoming to compare the instruments for monitoring microcracking on cement-treated bases (25). A statistical comparison between the two datasets (more than 300 measurements with each instrument) indicated an R-squared correlation value of 56.4 based on the relationship shown in Equation 2.2. This correlation is relatively weak, and although no reasons were provided by the researchers, it could potentially be attributed to the increasing variability of the measurements as the stiffness of the cement-treated layer increased toward the maximum limits of the instruments.

$$E_{SSG} = 0.675 \times E_{LWD} \quad (2.2)$$

Where: E_{SSG} = Stiffness measured with a soil stiffness gauge
 E_{LWD} = Stiffness measured with a portable falling weight deflectometer

Soil Stiffness Gauge and Falling Weight Deflectometer

The data collected by Scullion on the City of College Station project in Texas (11) was used to compare measurements taken with a soil stiffness gauge to those taken with an FWD at the same location. Figure 2.15 shows the relationship between the stiffness measurements from the two devices. The stiffnesses measured with the FWD were substantially higher than those measured with the stiffness gauge. Similar findings were observed in experiments in New England (19). This was attributed to the much higher loading capacity of the FWD and its ability to measure the stiffness of the entire pavement structure compared to the lighter loading capacity of the stiffness gauge, which generally only measures the stiffness to a depth of 8 to 12 in. (200 to 300 mm). A better correlation (R-squared of 83.81) was achieved between these two instruments compared to the correlation between the stiffness gauge and light weight deflectometer. The FWD measured a two-fold reduction in stiffness compared to the stiffness gauge (Figure 2.16).

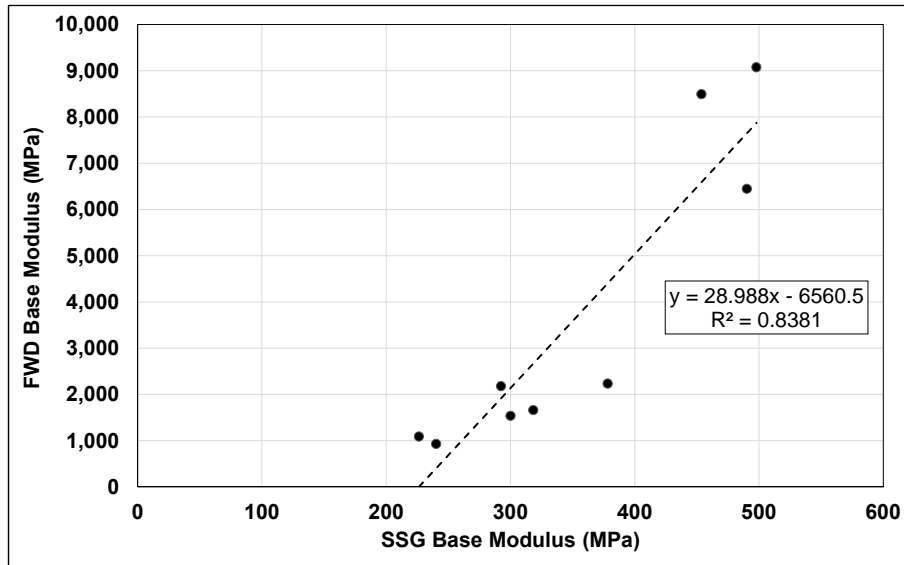


Figure 2.15: Relationship between FWD and SSG measured stiffness (11).

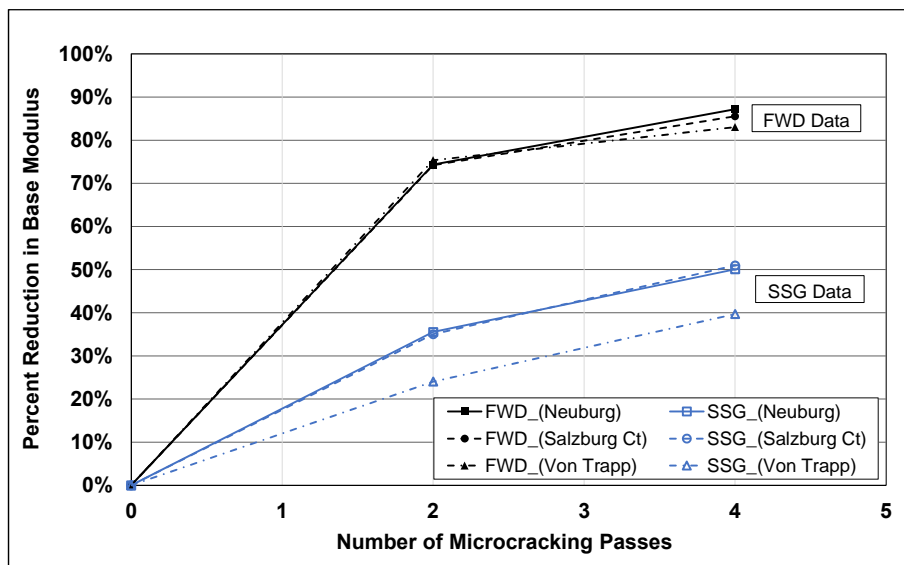


Figure 2.16: Measured stiffness reduction with FWD and SSG during microcracking (11).

This large difference in measurements supports concerns about using an FWD for measuring the effect of microcracking on base stiffness in the first month after construction and/or prior to placing an asphalt concrete surfacing since the heavier falling weight could induce additional microcracking in the stabilized base in the region of the drop zone, giving a result that is unrepresentative of the rest of the stabilized pavement layer.

2.3.5 Conclusions about Stiffness Measurements on Cement-Treated Bases

A range of devices is available for measuring the effect of microcracking on the stiffness of cement-treated layers. Each device has limitations that have not been fully quantified in terms of their suitability for use as a microcracking quality control procedure on construction projects.

2.4 Resilient Modulus Triaxial Testing

2.4.1 Test Methods

Testing the stiffness of stabilized materials in the laboratory is typically achieved by determining the resilient modulus of laboratory compacted specimens or field cores. Although resilient modulus can be measured in a number of different ways, triaxial testing is considered to be one of the most appropriate. The AASHTO T 307 method was designed and is commonly followed for testing the resilient modulus of soils and aggregate base materials and is often used to simulate the stress state of unbound materials in the base layer under traffic. It is a nondestructive test that measures the elastic stiffness of a specimen under different deviatoric stress conditions, from which the resilient modulus can be determined. The standard test setup is shown in Figure 2.17.

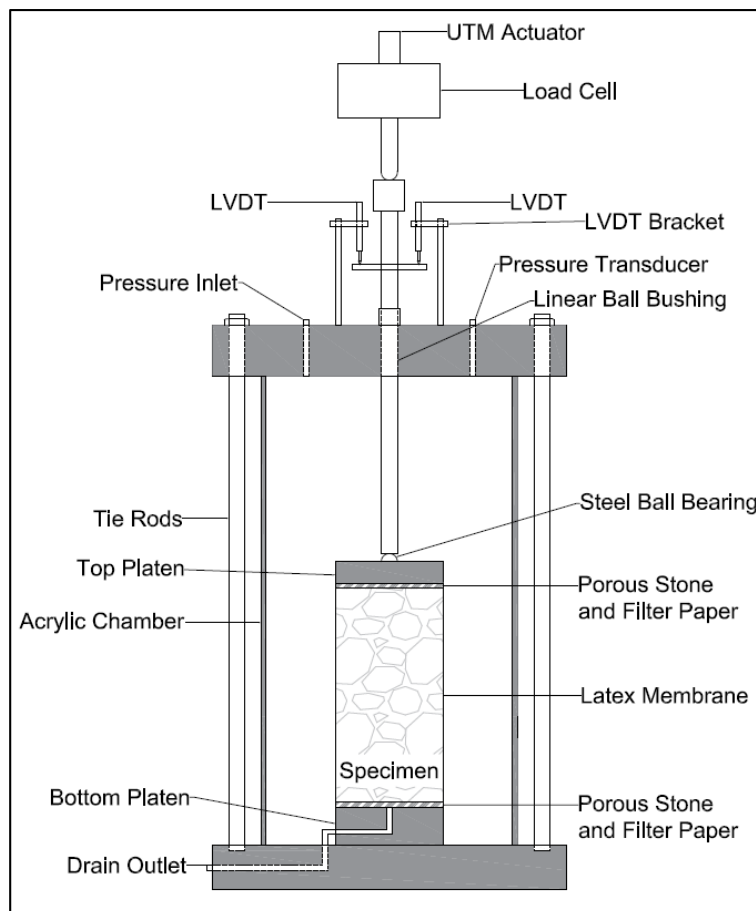


Figure 2.17: AASHTO T 307 resilient modulus test setup.

The equivalent European (EN 13286-7) and Australian (AS 1289.6.8.1) standards are both similar to AASHTO T 307. Each test method prescribes the use of external transducers, mounted on the actuator, to measure deflection (i.e., the linear variable displacement transducers [LVDTs] measure deflection on the top loading platen of the triaxial cell, not on the specimen).

These triaxial testing methods have also been adapted by other researchers for testing bound materials, including Fu (27) who tested FDR-FA materials, and Puppala (28) and Potturi (29) who tested FDR-PC materials. Alabaster (30), Arnold (31,32) and Gonzalez (33) tested aggregate stabilized with foamed asphalt following European Standard EN 13286-7. Arulrajah (34) and Gnanendran (35) tested cement stabilized crushed building demolition waste with AS 1289.6.8.1.

The applied load in the resilient modulus test is small compared to the strength of the material and is applied repeatedly, resulting in close to completely recoverable deformation proportional to the load. Resilient modulus is defined as the recoverable strain at the peak deviatoric stress, with the deviatoric stress being the difference between the axially applied stress and the confining stress. Since the applied load is small compared to the bearing strength of the material, the same sample can be used repeatedly for multiple tests under different loading and environmental conditions.

Various aspects of triaxial setups for testing pavement materials have been documented since the 1960's (36). One of the key issues identified was non-uniform strain and stress distributions in the specimen. Taylor (37) found that the use of porous stone plates in the setup created frictional ends, which led to surface traction and prevented radial deformation at the ends of the specimen when subjected to axial loading. This results in "dead zones" at the specimen ends, leading to the classical hour-glass shape after failure in monotonic tests (Figure 2.18), caused by stress states in the "dead zones" that are different to those in the middle of the specimen. The magnitude and impact of the "dead zones" depend on the material type, degree of stabilization, material stress history, the test procedure, and the purpose of the test (36-38).

Several methods have been developed to counter the effect of the non-uniform stress distribution caused by these end effects. These include the use of lubricated ends (36), frictionless ends (39), or increased height-to-diameter ratio specimens, which provide a larger area of uniform stress distribution across the specimen center (40,41). Chiu (40) showed that the secant modulus and peak deviatoric stress is reasonably constant with specimen size ratios between 2:1 and 2.5:1. Specimens with height-to-diameter ratios above 2.5:1 tend to buckle under load and are not recommended (36). Peng (39) showed that vertical strains decrease from the specimen ends to a more uniform strain distribution over the middle-third of granite and steel specimens with the use of frictional ends. This effect is known as the Saint-Venant's principle. Peng also developed a

test setup for more uniform testing that uses Teflon-lined steel inserts between the specimen and the end platens.



Figure 2.18: Shear failure of FDR-PC and FDR-FA specimens after UCS testing.

Burland and Symes (42) found that small strain measurements can be accurately collected using on-specimen transducers. TRB (43) proposed a method for mounting on-specimen transducers at quarter-points. Hilbrich (44) mounted LVDTs at quarter-points on 300 mm x 150 mm specimens to measure resilient modulus over the center of the specimen during testing on cement stabilized materials and reported satisfactory results. Two LVDTs were mounted at 180° offsets at each quarter-point in these studies. However, Hilbrich reported considerable sensitivity in terms of specimen preparation on measured results, and reported high noise levels in excess of 25 percent. Araya (45) tested unbound granular materials for resilient deformation using European Standard EN 13286-7, but with on-specimen LVDTs at third-points. Louw (46) experimented with mounting gauge-points on laboratory compacted FDR-PC specimens to measure dynamic modulus at different temperatures in an Asphalt Mix Performance Tester (AMPT) on 150 mm x 100 mm specimens (1.5:1 height-to-diameter ratio compared to typical triaxial test specimens which have a 2:1 ratio) and obtained reasonable results compared to field measurements.

Groeger (47) provided a detailed discussion on AASHTO T 307, and listed several aspects for consideration for an updated version of the specification. Issues including load cell location, deformation measurement, and the number of LVDTs were discussed.

2.4.2 Example Reported Resilient Moduli for Cement Stabilized Materials

The resilient modulus of cement stabilized aggregate determined with AASHTO T 307 or similar methods is typically between 200 MPa and 1,000 MPa. Puppala (28) tested RAP stabilized with 2 percent and 4 percent cement. Resilient moduli of between 220 MPa and 450 MPa and between 250 MPa and 500 MPa were recorded for the stabilizer contents, respectively, equating to increases of 32 percent and 50 percent above that of the unstabilized RAP control. Potturi (29) compared unstabilized aggregates to aggregates stabilized with 2 percent and 4 percent cement (Figure 2.19). Cement stabilization increased the resilient modulus on average by 52 MPa (19 percent increase) with 2 percent cement and 74 MPa (28 percent increase) with 4 percent cement when compared to the unbound material.

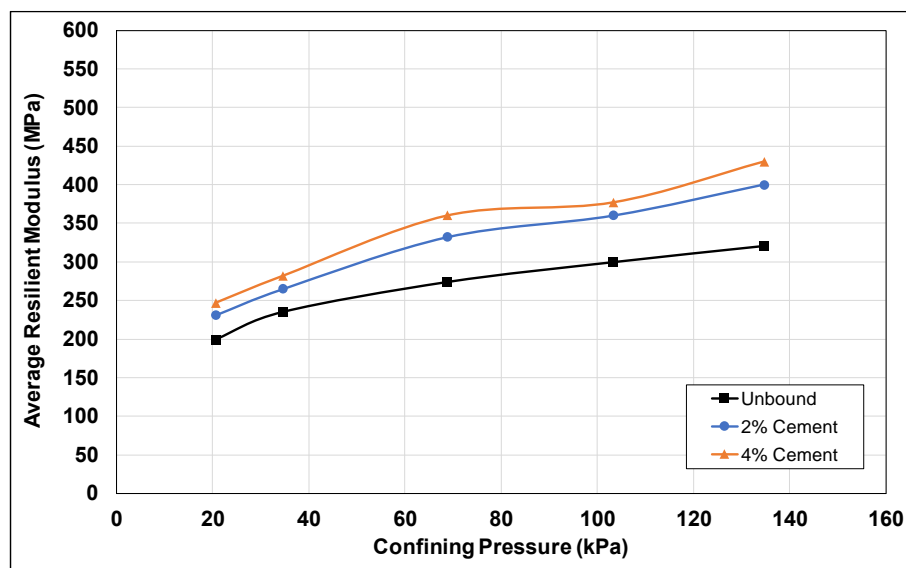


Figure 2.19: Resilient modulus of unstabilized and stabilized materials (29).

Alabaster (30) tested permanent deformation of cement stabilized materials using EN13286-7. The resilient modulus recorded during the repeated load test for specimens stabilized with various cement contents, ranging from 1.5 percent to 6 percent, are provided in Figure 2.20. The results did not distinguish between the different stabilizer contents, indicating that there was a problem with the test setup.

2.4.3 Stress Dependency of Unbound and Bound Materials

Unbound materials typically exhibit a non-linear effect with a change in stress. Resilient moduli typically increase with increases in confining and deviatoric stresses, which in turn leads to stress-hardening effects (48), even at relatively low stress levels. This non-linear behavior can be theoretically explained by two phenomena (49):

- The specimen density increases as particles slide under increasing stresses, resulting in more contact points between the particles, and
- An increase in the interparticle forces results in a stronger bond between particles.

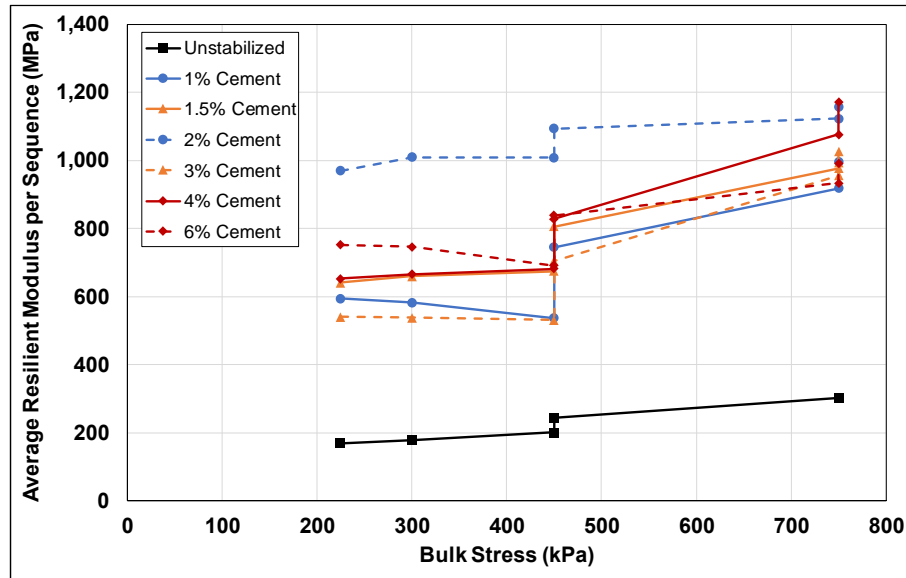


Figure 2.20: Resilient modulus of cement stabilized materials tested under repeated loading (30).

For these phenomena to apply to cemented materials, it would be necessary for the shear forces between contact points to exceed the friction of the cementitious bonds between the aggregate particles. It can thus be expected that confining pressure would have little to no effect until the cementitious bonds have been broken, where after the specimen will behave similar to an unbound material. This has been proven for concrete (50), lightly cemented soil (51), and frozen silts (52) using confining pressures between 90 kPa and 500 kPa.

However, the test results from Puppala (28), Potturi (29), and Alabaster (30) all suggest that cement-stabilized materials behave similar to unbound materials (i.e., are subject to stress hardening) and not according to the phenomena described by Loveday, given that resilient moduli appear to increase with increasing confining pressure and increased shear stress. This behavior is unlikely to be caused by high stresses exceeding the strength of the cementitious bonds since the resilient modulus test is highly repeatable, and the levels of the axial and confining stresses are low enough to not cause permanent damage. None of the authors discussed this discrepancy, and reported that the cement stabilized materials were stress sensitive.

2.5 Literature Review Summary

A review of the literature on shrinkage crack mitigation revealed that microcracking in combination with appropriate cement-content determination is likely the most appropriate approach to be implemented in California at this time given the research already conducted. Based on this finding, the microcracking

approach was selected for further study with the intention of building on the research already completed in other states.

The laboratory testing approach for resilient modulus testing using AASHTO T 307 was selected to measure the stiffness gain over time and loss of stiffness after microcracking.

Blank page

3. FIELD STUDIES

3.1 Introduction

Four FDR-PC projects were monitored during this Phase 1 study. All projects were on two-lane roads. Three of the projects were undertaken by the Yolo County Department of Public Works and one by Caltrans in Plumas County. The Yolo County projects were all done in full-closures with the roads being closed to all traffic except local residents for the duration of the projects. Full-width sections of the road were processed each day on these projects. The Caltrans project was completed under traffic, with one-lane closures during the day (traffic control with pilot car). Processed sections were opened to traffic approximately four hours after final compaction so that both lanes were open to traffic each night.

Additional base material was spread on sections of the Yolo County projects to increase lane/shoulder width and to improve alignment. All projects were pre-pulverized prior to spreading the cement.

Construction activities were monitored on each of the projects and stiffness measurements were taken before and after microcracking with a soil stiffness gauge (SSG) until placement of the asphalt concrete surfacing. Thereafter, visual assessments and falling weight deflectometer (FWD) measurements were carried out at regular intervals. No control sections (i.e., sections with no microcracking) were included in any of the projects given that the responsible road agencies understandably did not want to run the risk of having short sections of pavement with reflected shrinkage cracks.

This chapter summarizes the projects where the evaluations were done, the testing plan, observations, and testing results.

3.2 Project Details

Project details including surfacing thickness and recycled layer thickness are summarized in Table 3.1. Mix design details for the FDR-PC layers are summarized in

Table 3.2.

Table 3.1: Project Details

Road	Construct. Date	Location	10 ⁶ ESALs/year	AC ¹ Thickness (mm [ft.])	FDR-PC Thickness (mm, [ft.])	Average Subgrade R-value
CR32B	9/2014	Yolo	0.288	125 (0.4)	350 (1.2)	5
CR27	9/2015	Yolo	0.798	115 (0.4)	350 (1.2)	23
CR99	9/2015	Yolo	1.980	150 (0.5)	300 (1.0)	9
PLU147	9/2015	Plumas	1.270	90 (0.3)	260 (0.8)	79

¹ AC = Asphalt concrete

Table 3.2: Summary of Mix Designs

Project	Section Length	Mill Depth (mm)	Cement Content (%) ¹	Design Strength ² (MPa [psi])	OMC (%)	MDD (kg/m ³ [pcf])	Mod. Proctor Compaction (% of MDD)
CR32B	2.82 km	350	4.0	3.5 (500)	7.2	2,000 (125) ³	95
CR27	1.40 km	350	3.0	2.8 (400)	6.4	2,185 (136)	95
CR99	0.76 km	300	4.0	2.4 (350)	7.8	2,056 (128)	95
PLU147	PM7.5–8.5	260	2.5	2.4 (350)	4.3	1,860 (116)	95
PLU147	PM8.5–8.9	260	4.0	2.4 (350)	5.2	1,800 (112)	95

¹ Percent by weight of aggregate

² Following AASHTO D1663, with a modified curing technique. Specimens were wrapped in plastic and cured in an oven at 38°C (100°F) for 7 days.

³ Maximum dry density (MDD) was averaged over two samples. The first (1,820 kg/m³ [113.5 pcf]) was sampled from a core hole during field investigations. The second (2,200 kg/m³ [137.3 pcf]) was from a reconstituted sample that included pulverized asphalt concrete, gravel, and silty sand with 4 percent cement.

3.3 Testing Plan

The test plan for visual assessments and stiffness measurements was based on the approach used on the Texas Department of Transportation projects discussed in Chapter 2, with a primary focus on assessing stiffness change in the recycled layer over time.

3.3.1 Test Section Terminology

Day Section

A *day section*, as defined for this project, is the length of construction completed in a single day and includes pre-pulverization (if required), cement spreading, mixing, primary compaction, shaping and final compaction. This term is used to differentiate between parts of the project that were constructed on different days, and to denote the time after compaction before microcracking, since microcracking was typically done on a single day. The length of the section depended on whether the full width of the road was recycled during the day or whether only a single lane was recycled. Day section lengths for the four projects evaluated are summarized in Table 3.3. On the three county projects where the full width was recycled, the average length of a *day section* was 582 m (1,909 ft.). On the Caltrans project, the average length was 2,234 m (7,330 ft.).

Table 3.3: Day Section Lengths

Location	Day	Road			
		CR32B (m [ft.])	CR27 (m [ft.])	CR99 (m [ft.])	PLU147 (m [ft.])
Yolo (Both lanes / day)	1	1,310 (4,300)	588 (1,930)	383 (1,257)	-
	2	838 (2,750)	433 (1,421)	509 (1,670)	-
	3	671 (2,201)	285 (935)	-	-
	4	-	136 (446)	-	-
Plumas (One lane/day)	1	-	-	-	1,961 (6,435)
	2	-	-	-	2,507 (8,225)

Construction Section

Construction section refers to the length of a subsection within a *day section* on which cement was spread and pulverized without interruption (i.e., from where the recycler started to pulverize to where it stopped and returned to where it started, but with a lateral offset). There was typically more than one *construction section* within one *day section*, and their lengths varied depending on a number of factors including the capacity of the cement spreader, wind direction and speed, number of water tankers and distance to the water source, and whether compaction could be completed in the specified time window, typically two hours after water was first added to the cement. Construction section lengths on the four projects that were evaluated are provided in Table 3.4.

Table 3.4: Average Construction Section Lengths

Road	Average Length (m [ft.])	Standard Deviation (m [ft.])
CR32B	150 (492)	43 (142)
CR27	131 (249)	64 (266)
CR99	99 (154)	63 (216)
PLU147	235 (772)	114 (373)

3.3.2 Density and Dynamic Cone Penetrometer Measurements

The contractors, or an appointed consultant, measured density with a nuclear gauge after final compaction according to the specification requirements for quality control. A limited number of these measurements were obtained from the contractors for comparison against stiffness measurements.

UCPRC staff took dynamic cone penetrometer (DCP) measurements on two of the projects (CR27 and PLU147) to supplement the density measurements and to obtain an indication of layer thicknesses. The testing plan targeted at least one DCP test per construction section. Hope (25) and Potturi (29) both compared DCP test results with SSG and FWD, and this UCPRC study did not attempt to replicate these studies.

3.3.3 Stiffness Measurement Approach

The testing plan proposed that initial stiffness measurements should be taken with an SSG after final compaction, before, during (i.e., between each roller pass), and after microcracking, and then daily until base stiffness exceeded 600 MPa (i.e., the limit of the gauge) or until the asphalt concrete surfacing was placed. After placement of the asphalt surfacing, the testing plan proposed that stiffness should be measured with an FWD, with the first FWD test completed as soon as possible after surfacing (typically within one or two days depending on when permission was granted to test by the resident engineer). Thereafter, the plan noted that testing should be carried out on alternating days for the first two weeks after surfacing, then biweekly for the next two months, and then every three months for the remainder of the first year after

construction. After the first year, the plan called for FWD testing to be carried out biannually at the beginning and end of the rain season.

The testing plan was adhered to as closely as possible; however, logistics, availability of road closures, weather conditions, and a number of other factors limited the number of measurements that could be taken, and the time intervals between measurements. FWD tests were carried out in a rolling closure on the Yolo County roads, and in a one-lane closure on PLU147, with a pilot car guiding traffic in the other lane.

SSG Testing Pattern

The SSG testing pattern used on all projects is shown in Figure 3.1. This pattern focused on the areas where construction sections started and ended, with quarter points within the construction section, and offsets to detect any inconsistencies between the roller passes. The number of testing points also depended on the length of the project, with longer spacing on longer projects to ensure that representative data could be collected within the available testing time. The duration of one SSG test was approximately two minutes. Location of testing points did not factor into the actual time of microcracking as this would have complicated the testing program.

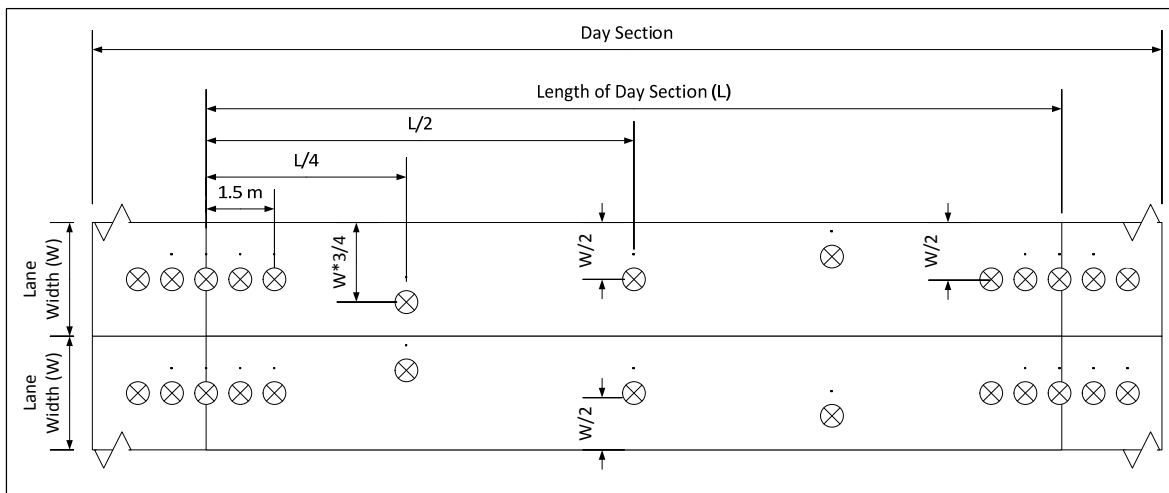


Figure 3.1: Testing pattern for soil stiffness gauge and FWD.

3.4 Test Section Construction

3.4.1 Yolo County Road CR32B

Design

This project is located on Yolo County Road CR32B, extending from the Davis city limit to 2.9 km (1.8 miles) east of the city limit. A map with the project location is provided in Appendix A. Construction started on September 8, 2014. The pavement structure prior to rehabilitation and the rehabilitation design

are summarized in Table 3.5. The specified design strength for the FDR-PC layer was 3.4 MPa (500 psi) after a seven-day cure when testing according to the modified AASHTO D1633 method. A mix design, performed on material collected from test pits along the project, determined that four percent cement would satisfy this strength requirement.

Table 3.5: CR32B: Pavement Structures, prior to FDR and FDR Design

Pavement Layers		Avg. Thickness (mm [ft.])	Std. Deviation (mm [ft.])	Minimum (mm [ft.])	Maximum (mm [ft.])
Existing Structure	AC surface	110 (0.36)	15 (0.05)	89 (0.42)	127 (0.42)
	Aggregate base	140 (0.46)	21 (0.07)	101 (0.33)	165 (0.54)
	Aggregate subbase	142 (0.46)	69 (0.23)	101 (0.33)	292 (0.96)
FDR Design	AC surface	125 (0.42)			
	FDR base	350 (1.16)			
	Aggregate subbase	38 (0.13)			

Construction

The existing road was prepulverized, shaped, and compacted on September 8. Stabilization started on September 9, using full-width stabilization, to a design depth of 350 mm (14 in.). However, a gas line was hit by the recycler, and construction stopped 240 m (800 ft.) from the start. The stabilized material was compacted and graded between the start and 140 m, with the remainder left uncompacted but moisture conditioned. After completion of repairs to the gas line, construction restarted on September 11 at the start of the project. In order to accommodate the delay in compaction on the previously processed section, an additional two percent cement was spread over the entire 240 m of processed material, mixed, shaped, and compacted. Construction continued as per specification from 240 m to the end of the project. Construction stopped at a chainage of 1,310 m on September 11, at 2,148 m on September 12, and at 2,819 m on September 13 (Table 3.3).

Microcracking was performed between 48 and 72 hours after final compaction on each of the day sections, on September 13 and September 15, with a 12-ton vibratory roller at maximum amplitude setting for the vibration. The contractor used an SSG to monitor the decrease in stiffness after each roller pass. The number of passes required to reduce the stiffness by 40 percent are listed in Table 3.6.

Table 3.6: CR32B: Number of Roller Passes for Microcracking

Chainage (m [ft.])	Roller Passes
0 (0) to 833 (254)	4
833 (254) to 4,800 (1,463)	2
4,800 (1,463) to 6,300 (1,920)	4
6,300 (1,920) to 9,400 (2,865)	2

The UCPRC conducted separate SSG tests between September 14 and September 18, when placement of the asphalt concrete surfacing began. Permission to start FWD testing on the paved surface was granted on September 19.

Observations from Construction

The construction process generally followed standard FDR procedures, complying with the specifications. However, a number of distresses observed on the completed FDR-PC layer prior to surfacing were attributed to deviations from standard practice. In addition to the fine transverse cracks typically seen after microcracking (Figure 3.2), some block cracking was also observed on the base prior to surfacing (Figure 3.3). This block cracking was limited to a long, narrow zone along the length of the project and was attributed to shrinkage associated with a windrow of cement formed by dragging of the water pipe connecting the recycler and the water tanker (Figure 3.4).



Figure 3.2: CR32B: Transverse cracking after microcracking.



Figure 3.3: CR32B: Block cracking on FDR-PC prior to surfacing.



Figure 3.4: CR32B: Water hose dragging on the spread cement.

Raveling of the surface was observed in the wheelpaths along most of the project. This was attributed to road users ignoring the closure and driving on the road before and after construction each day (CR32B is a frontage road to Interstate 80 and is used by East Davis residents to access Interstate 80 at the Chiles Road on-ramp). Water sprayed during curing accumulated in the low spots caused by this raveling (Figure 3.5). Wet, soft patches were also observed in a number of locations corresponding to areas where water was spilled onto the section during mixing (Figure 3.6 and Figure 3.7). Spills occurred either during switching of tankers (i.e., draining of water in the pipe) or when the dragged pipe got trapped underneath the recycler wheels, causing it to disconnect from the water truck and spill water until the valve was closed. The resident

engineer required some of these areas to be reworked with an additional two percent cement and then recompacted (Figure 3.8, note the absence of absorbed water in the repaired area. Although the entire road was sprayed with water prior to taking the photograph, the higher cement content in the repaired area absorbed the available moisture faster than the surrounding previously stabilized material.). SSG measurements were taken on one of the wet areas that was not repaired (Figure 3.7), and compared to an adjacent drier area to quantify the effects on stiffness gain of not repairing overly wet areas.



Figure 3.5: CR32B: Surface raveling.



Figure 3.6: CR32B: Wet, soft location after final compaction.



Figure 3.7: CR32B: Wet and adjacent dry locations tested with SSG.



Figure 3.8: CR32B: Wet section after repair.

3.4.2 Yolo County Road CR27

Design

This project is located on Yolo County Road CR27, starting 100 m (328 ft.) east of the intersection of CR98 and CR27 and ending at the intersection of CR99 and CR27. Total length of the project is 1.4 km (4,630 ft.). A map with the project location is provided in Appendix A. Construction started on September 7, 2015, in a full closure. The pavement structure prior to rehabilitation and the rehabilitation design are summarized in Table 3.7.

Table 3.7: CR27: Pavement Structures, prior to FDR and FDR Design

Pavement Layers		Avg. Thickness (mm [ft.])	Std. Deviation (mm [ft.])	Minimum (mm [ft.])	Maximum (mm [ft.])
Existing Structure	AC surface	102 (0.34)	44 (0.15)	25 (0.08)	152 (0.5)
	Aggregate base	181 (0.60)	56 (0.19)	127 (0.42)	305 (1.0)
	Aggregate subbase	350 (1.16)	101 (0.34)	229 (0.75)	508 (1.67)
FDR Design	AC surface	115 (0.38)			
	FDR base	350 (1.16)			
	Aggregate subbase	250 (0.83)			

The specified design strength for the FDR-PC layer was 2.8 MPa (400 psi) after a seven-day cure when tested according to the modified AASHTO D1633 method. A mix design, performed on material collected from a test pit on the project, determined that three percent cement would satisfy this strength requirement. Optimum moisture content was determined to be eight percent by mass of dry aggregate.

Construction

The existing road was prepulverized, shaped, and compacted on September 7. Stabilization started on September 8 with the full width processed in each construction section. Construction activities ended abruptly on the first day, with the last 250 m (820 ft.) of mixed material left uncompacted (Figure 3.9). This section was shaped and compacted the following morning, much later than the specification requirement, which dictates that all compaction should be completed within two hours after mixing has started (i.e., when water contacts the cement). Stabilization and mixing continued on the second day (from chainage 588 m [1,930 ft.] to 738 m [2,424 ft.]), but compaction was only completed on this section after approximately five hours due to the rollers being used to complete the previous day's work. Construction of the remaining 662 m [2,172 ft.] was delayed for 13 days (reason is unknown), before being completed in two days. The initial section of the project was sprayed with water on a daily basis during the delay. The project specifications did not dictate what action needed to be taken if the two-hour compaction limit was achieved and no corrective action or penalties were requested by the resident engineer.

Microcracking was performed between 48 and 72 hours after final compaction on each of the day sections. Three roller passes were applied, with a 12-ton vibratory roller at maximum amplitude setting for the

vibration. The contractor did not take any stiffness measurements during the process to monitor the decrease in stiffness after each roller pass. SSG measurements were taken by the UCPRC, starting after the final compaction on the first day of construction (September 8, 2015), and continuing throughout the construction period. FWD testing was initiated seven days after placement of the asphalt concrete surfacing.



Figure 3.9: CR27: Incomplete compaction prior to start of next day construction.

Observations from Construction

Apart from the delayed compaction noted above, the construction process generally adhered to standard FDR procedures and complied with the specifications. However, a number of problems were observed that might influence the longer-term performance of the road.

The asphalt concrete and base thicknesses on the existing pavement at the start and end of the project were thinner than on the rest of the project, probably because of the need to match existing alignments during the original construction of the road. Asphalt concrete thicknesses were between 25 mm and 50 mm (0.08 ft. and 0.17 ft.) at the start and end, compared to between 100 mm and 125 mm (0.33 ft. and 0.42 ft.) over the remainder of the project, while the base thickness was approximately 150 mm (0.5 ft.) at the start and end compared to 175 mm (0.58 ft.) on the remainder. The reclaimed material in the first 140 m (460 ft.) and the last 90 m (295 ft.) of the project appeared to be much finer than on the remainder of the project (Figure 3.10 and Figure 3.11), and this was attributed to more of the subbase and possibly some of the subgrade having been pulverized to compensate for the thinner asphalt concrete and base in these parts of the project.

The start of the section at the southwest corner had to tie in with the existing roadway and a property entrance after mixing. This required excessive shaping to ensure the final grade was at the desired level. The effect of the raised edges of the existing roadway structures imposed additional limitations on the grader operator. The serrated blade on the grader also tended to screen the material, depositing the fine material on the reworked surface while pushing the coarse material to the edges. This resulted in a layer of fine material

approximately 25 mm (1 in.) thick on top of the underlying coarser material. This fine material layer tended to break up and separate from the underlying material during microcracking (Figure 3.12).



Figure 3.10: CR27: Fine graded material near start of project.



Figure 3.11: CR27: Coarser material throughout majority of the project.



Figure 3.12: CR27: Distressed surface of FDR-PC layer after microcracking near start of project.

3.4.3 Yolo County Road CR99

Design

This project is located on Yolo County Road CR99, starting at West Kentucky Avenue in Woodland and continuing for 760 m (2,500 ft.) northwards toward Interstate 5. A map with the project location is provided in Appendix A. Construction started on September 9, 2015, in a full closure. The pavement structure prior to rehabilitation and the rehabilitation design are summarized in Table 3.8. Asphalt concrete and base layer thicknesses on the existing road varied significantly.

Table 3.8: CR99: Pavement Structure, prior to FDR and FDR Design

Pavement Layers		Avg. Thickness (mm [ft.])	Std. Deviation (mm [ft.])	Minimum (mm [ft.])	Maximum (mm [ft.])
Existing Structure	AC surface	185 (0.62)	60 (0.20)	102 (0.34)	274 (0.91)
	Aggregate base	103 (0.34)	152 (0.51)	0 (0)	356 (1.19)
	Depth to subgrade	286 (0.95)	106 (0.35)	165 (0.55)	457 (1.52)
FDR Design	AC surface	150 (0.50)			
	FDR base	300 (1.00)			

The specified design strength for the FDR-PC layer was UCS of 2.4 MPa (350 psi) after a seven-day cure tested according to the modified AASHTO D 1633 method. A mix design, performed on material collected from a test pit on the project, determined that four percent cement would satisfy this strength requirement. Optimum moisture content was determined to be eight percent by mass of dry aggregate.

Construction

The section was prepulverized, shaped, and compacted on September 21. Stabilization started on September 23 and was completed the following day, with the full width processed in each construction section. Microcracking followed Section 30 of the 2015 Caltrans specifications with three roller passes applied between 48 and 72 hours after final compaction. The contractor did not take any stiffness measurements during the process to monitor the decrease in stiffness after each roller pass. SSG measurements were taken by the UCPRC, starting after final compaction on both days of construction, and during and after microcracking. FWD testing was initiated 21 days after final compaction of the base with the number of tests and number of days between testing visits limited by the high traffic volumes on the road.

Observations from Construction

The construction process generally followed standard FDR procedures and mostly complied with the project specifications. However, a number of construction-related problems attributed to deviations from standard practice were observed on the completed base prior to surfacing. Localized areas of thin, poorly compacted material were exposed after microcracking (Figure 3.13 and Figure 3.14). These areas were about 1.0 m (3 ft.) wide and about 10 m (33 ft.) long, and were attributed to additional trimming with the grader to meet

grade requirements. The thickness of the loose layer was approximately 50 mm (2 in.). These areas were repaired by reworking the material, adding two percent cement, mixing by hand, and recompact with the same 12-ton vibratory roller.



Figure 3.13: CR99: Delamination after microcracking.



Figure 3.14: CR99: Depth of delaminated material (50 mm [2 in.]).

Block cracking (Figure 3.15) similar to that discussed in Section 3.4.1 was observed on sections of the FDR-PC layer prior to surfacing. The cause was attributed primarily to higher-than-design cement contents in these areas caused by accumulations of cement resulting from dragging of the water pipe connecting the recycler and the water tanker.



Figure 3.15: CR99: Block cracking after microcracking.

3.4.4 California Road PLU147

Design

This project is located on State Route 147 in Plumas County, starting at the intersection with Plumas County Road A13 in Hamilton Branch (Postmile [PM] 7.5) and continuing northwards for 1.4 miles (PM8.9). A map with the project location is provided in Appendix A. Construction started on September 15, 2015, using a system of single-lane closures for construction with traffic driving on the open lane behind a pilot car. Traffic was permitted on the finished sections behind a pilot car after final compaction was completed. The pavement structure prior to rehabilitation and the rehabilitation design are summarized in Table 3.9. There was considerable variation in thickness of the surfacing and base along the length of the project. Between PM7.5 and PM8.5, the surface and base layer thicknesses were about 295 mm (1.0 ft.) and 150 mm (0.5 ft.), respectively, compared to about 270 mm (0.9 ft.) and 100 mm (0.33 ft.), respectively, between PM8.5 and PM8.9.

Table 3.9: PLU147: Pavement Structure

Pavement Layers		Avg. Thickness (mm [ft.])	Std. Deviation (mm [ft.])	Minimum (mm [ft.])	Maximum (mm [ft.])
Existing Structure	AC surface	244 (0.81)	151 (0.50)	137 (0.46)	350 (1.17)
	Aggregate base	127 (0.42)	37 (0.12)	100 (0.33)	151 (0.50)
	Depth to subgrade	76 (0.25)	108 (0.36)	0 (0)	152 (0.51)
FDR Design	AC surface	90 (0.30)			
	FDR base	260 (0.87)			

Mix design results, performed on material collected from test pits along the project, indicated that two different cement contents would be required to stabilize the two sections with different layer thicknesses and different material properties. The specified design strength for the FDR-PC layer was 2.4 MPa (350 psi) and the mix designs dictated that 2.5 percent cement would satisfy this strength requirement between PM7.5 and PM8.5, while 4.0 percent would be required between PM8.5 and PM8.9. The design strengths were achieved after a seven-day cure, tested according to the modified AASHTO D 1633 method. Optimum moisture content was determined to be eight percent by mass of dry aggregate.

Construction

Construction started on September 15. The road was prepulverized, shaped, and compacted on the first two days. Stabilization was completed over the following two days, finishing on September 18. A prime coat was applied to the compacted base after final compaction each day, but the emulsion generally did not break before the section was opened to traffic, due to the cool, shady conditions. This resulted in rapid stripping of the prime by the traffic as well some raveling of the surface (Figure 3.16). Both lanes were microcracked in a single roller pass at maximum vibration on September 19. Additional damage to the prime coat occurred during microcracking, with the roller picking up the prime, which adhered to the drum (Figure 3.17). Completing the microcracking in one day meant that the interval between final compaction and the treatment

was 72 hours and 48 hours for the first and second days' construction respectively, but only 24 hours for the third days' construction. This microcracking action did not meet the Caltrans specification requirements, which required three vibratory roller passes at maximum amplitude between 48 and 72 hours after completing final compaction.



Figure 3.16: PLU147: Prime coat stripped from FDR-PC layer after traffic.



Figure 3.17: PLU147: Prime coat stripping from FDR-PC layer during microcracking.

Observations from Construction

The contractor did not use a bar between the water truck and the pulverizer to support the water hose and prevent it from dragging on the surface (Figure 3.18). This resulted in the cement being windrowed by the pipe (Figure 3.19) and accumulated at the end of each construction section. Figure 3.20 and Figure 3.21 show the effect of this accumulated cement. Figure 3.20 shows the depth of the spread cement before the start of mixing (i.e., ± 50 mm [2 in.]). Figure 3.21 shows the depth of cement accumulated at the end of a construction section by the dragging pipe (i.e., ± 200 mm [8 in.]). This practice resulted in some areas of the road being stabilized with much lower cement contents than the specified design, while other areas had significantly higher cement contents than the specified design.



Figure 3.18: PLU147: Water pipe dragging on cement.



Figure 3.19: PLU147: Accumulation of displaced cement in pulverizer wheel track.



Figure 3.20: PLU147: Depth of 4% cement after spreading (± 50 mm).



Figure 3.21: PLU147: Depth of cement mound due to dragging of hose (± 200 mm).

This could lead to localized areas of distress including rutting (too little cement), longitudinal cracking in the zone of differential stress between the low and high cement contents, and/or reflected block cracking in areas with higher cement content.

3.4.5 General Observations from All Construction Projects

In addition to the observations discussed in the previous sections, accumulation of cement in front of the pulverizer mixing chamber as it proceeded along a construction section was observed on all the projects (Figure 3.22). This cement was deposited at the end of the construction section, resulting in a localized area where the cement content was significantly higher than the design cement content and the cement content of the surrounding areas. On some projects, the recycler continued past the end of the section until the excess cement had been mixed in (Figure 3.23). The cement spreader would then start from the beginning of the next construction section, spreading cement over the area where the excess cement had already been mixed (Figure 3.24). On other projects, the accumulated cement was left in place and the spreader would start from the accumulated pile. Regardless of the approach followed, all of the projects had some localized areas of high cement content at the end of one construction section and the beginning of the next. The effect of these localized areas of high cement content on stiffness was measured with an SSG during construction and with an FWD after opening to traffic.

Section 30 of the Caltrans standard specifications does not have any requirements for preventing or dealing with these localized areas of cement accumulation. The specifications do, however, indicate that mixing on the following section should start at least 2 ft. (600 mm) behind the line where the pulverizer stopped mixing on the previous section. Consideration should be given to amending the specifications to require careful setting of the skirt on the pulverizer mixing chamber to prevent this accumulation at the end of the construction section and the resulting lower-than-design cement content along the section that has already been mixed.



Figure 3.22: Wave of cement in front of pulverizer skirt on mixing chamber.



Figure 3.23: End of pulverizer pass with no accumulated cement visible.



Figure 3.24: Cement spreader spreading cement on already mixed section.

Another observation was the problem of potential damage to underground services. On the CR32B project, the prepulverization and stabilization passes were both theoretically done to the same target depth, however during the stabilization pass a gas line was hit. Similar problems were noted on other projects not discussed in this report. These projects had grade-height restriction and shoulder-widening requirements, which are typically addressed by moving excess material from the existing alignment onto the shoulders after prepulverization, followed by shaping and compacting prior to the final level of the base layer so that the new asphalt concrete layer will match the existing grade and tie in to existing intersections and driveways. This effectively reduces the thickness of the prepulverized material. If the recycler is set to the same milling depth for the stabilization pass, the effective milling depth will be deeper because of the change in grade, and this can lead to damage of underground services. Another potential consequence of the deeper milling on the stabilization pass is a change in the ratio of RAP, base, and subgrade materials in the mix. Given that during mix design the stabilizer contents are based on this ratio, altering it may change the strengths of the new layer, which in turn could impact the design life. For example, on the CR32B project, the deeper

milling depth on the stabilization pass reduced the percentage of RAP and aggregate base in the mix by 11 and 14 percent respectively, and increased the subgrade content by 25 percent when compared to the prepulverization pass.

Other general observations relevant to all the field projects include the following:

- The project specifications are not being strictly enforced on some projects.
- Dragging of the water hose connecting the recycler and the water tanker was evident on all projects, leading to the accumulation of cement at the end of construction sections and often along one of the edges of a construction section. The 2015 Caltrans specifications (Section 30-4.03B) require that the water pipe be fastened to a bar connecting the recycler and water tanker. However, this requirement was not adhered to by the contractor or enforced by the resident engineer.
- Traffic speeds on the compacted FDR-PC surface prior to placing of the asphalt concrete surfacing were often equal to or higher than the normal speed limit for the road, and considerably higher than the posted limit in the construction zone, leading to rapid raveling of the surface. Speed limits should be strictly enforced in construction zones, both for safety reasons and to preserve the newly constructed surface.

3.5 Density Test Results

Density measurements were taken by the contractor, or an appointed consultant, with a nuclear gauge on all four projects. However, the readings were only compared with the mix-design density to determine relative compaction, rather than comparing the results with a wet density determined on material sampled at each nuclear gauge testing position. Given that there is usually considerable variation in material properties along the length of any in-place recycling project, and that the variability was apparent on the four projects studied, the density measurements provided were not considered suitable for use in any analysis to determine the effect of compaction on stiffness behavior.

3.6 Dynamic Cone Penetrometer Results

Although the dynamic cone penetrometer (DCP) is not generally used for quality control in the United States, it was used on the CR27 and PLU147 projects, one day after final compaction, to obtain a quick indication of layer thickness and to identify any variability through the recycled layer. It was also used to evaluate the effects of the late compaction on CR27 (discussed in Section 3.4.2). The testing plan is summarized in Table 3.10. Only a limited number of tests were conducted at each project for the following reasons:

- The duration of each test exceeded the time available to perform tests at the same intervals as the SSG and FWD tests.
- DCP testing requires three technicians to perform the test according to the ASTM test method (ASTM D6951). On most days only one technician was available to perform postconstruction tests.

- DCP tests cannot be repeated in the same location, and consequently it is unsuitable for accurately tracking stiffness gain over time at a single location.
- DCP tests are not appropriate for strongly cemented materials.

Table 3.10: DCP Test Plan

Road	Evaluation Section	Station (ft.)	Observation
CR27	1	1,300 to 1,800	Material appeared to have a finer grading
	2	2,500 to 3,300	Check area with late compaction
	3	3,400 to 5,200	Control section, road constructed to specification
PLU147	1	3,670 to 8,250	Check construction uniformity
	2	8,250 to 10,300	

3.6.1 Yolo County Road CR27

The compaction consistency was investigated by counting the number of blows required to reach depths of 50 mm, 100 mm, 200 mm, and 300 mm (2, 4, 8, and 12 in.) in the 300 mm-thick FDR-PC layer. The results are summarized in Figure 3.25. More blows were required to reach depths of 50 mm and 100 mm on Section #1 than on Section #2 or Section #3. There was considerable variation in the number of blows required to reach each depth on Section #2, with an average of 4.5 blows to 50 mm and 18 blows to 100 mm. On one testing location, only one blow was required to reach 50 mm and only three blows to reach 100 mm, indicating a very weak, unstabilized area in the upper zone of the layer. On Section #3, an average of six blows were required to reach 50 mm and 30 blows to reach 100 mm. There was less variation in the number of blows required to reach 200 mm and 300 mm on Section #1 and Section #2. Approximately twice as many blows were required to reach these depths on Section #3.

Figure 3.26 compares the seating blow depths on the three sections. This value is not typically recorded, but observations during the DCP test on Section #2 indicated a significantly higher penetration compared to tests on Section #1 and Section #3 when the seating blow was applied. The highest penetration depth with a single blow on Section #2 was 75 mm and the lowest was 10 mm, with an average of 22 mm. The mean seating blow depths on Section #1 and Section #3 were 13 mm and 16 mm, respectively. The DCP test results therefore provided a rapid indicator of variability and confirmed that the section where the road was compacted later than allowed in the project specification did not have comparable shear strength to the other sections that were compacted within the specification time frame. These weaker areas could lead to localized areas of distress on this section.

3.6.2 California Road PLU147

DCP testing on PLU147 was performed randomly along the project to evaluate construction uniformity, with 10 tests on Section #1 (2.5 percent cement) and four tests on Section #2 (4.0 percent cement). A similar testing approach to that used on CR27 was used, except that the final testing depth was 260 mm to match

the FDR-PC layer thickness on this project. Figure 3.27 compares the number of blows between the two sections. A higher number of blows were required to reach the selected depth on Section #2 compared to that on Section #1 as expected, given the higher cement content.

Figure 3.28 illustrates the penetration depth of the seating blows. Section #2 had a lower seating blow depth, as expected. The results indicate that there were no weak areas in the upper zone of the layer at the locations that were tested. The range of blows required to reach the test depths on PLU147 was less variable compared to the tests on CR27. Mean penetration depths for the seating blow were 12 mm and 10 mm on Section #1 and Section #2 respectively, with differences between the lowest and highest penetration depth of 8 mm and 5 mm, respectively.

The DCP results validate the observations made during the construction of CR27 and PLU147. All the DCP testing was done before microcracking. CR27 had several construction issues, and also adhered loosely to the standard specification. PLU147 on the other hand, adhered more strictly to the standard specification. The DCP results show that weak biscuit layers had a higher presence on CR27 compared to PLU147.

3.7 Soil Stiffness Gauge (SSG) Results

The SSG data were analyzed to determine the following:

- The effect of roller passes on stiffness
- Curing time after compaction, and
- Construction variability.

3.7.1 Effect of Roller Type and Number of Roller Passes on Stiffness Reduction

The effect of roller type and the number of roller passes on stiffness reduction, measured with an SSG during microcracking activities on CR32B, CR27, CR99 and PLU147 can be summarized as follows:

- CR32B was microcracked with two different rollers. The first was a 12-ton single drum vibratory roller and the second was a 9-ton dual steel drum vibratory roller. A 40 percent reduction in stiffness was achieved with two passes of the single drum roller and with four passes of the dual drum roller. Both were set at maximum vibration.
- CR27 was microcracked according to the specification with a single drum roller (three passes at maximum vibration amplitude).
- CR99 was microcracked to 40 percent of the initial stiffness, which required two passes of a single drum roller set at maximum vibration.
- PLU147 was microcracked with a single pass of a single drum roller set at maximum vibration.

A plot of the average stiffnesses measured after each roller pass is shown in Figure 3.29. A clear trend between number of microcracking passes and reduction in stiffness is evident.

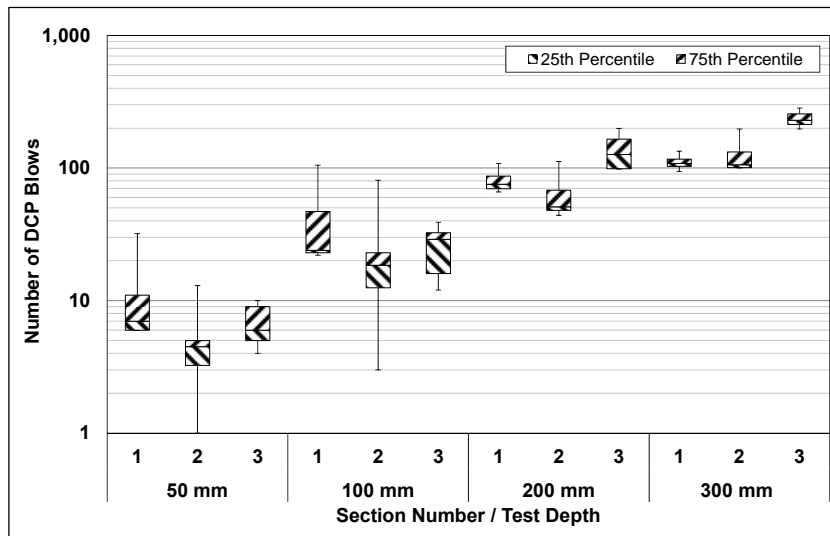


Figure 3.25: CR27: Number of DCP blows to target depths.

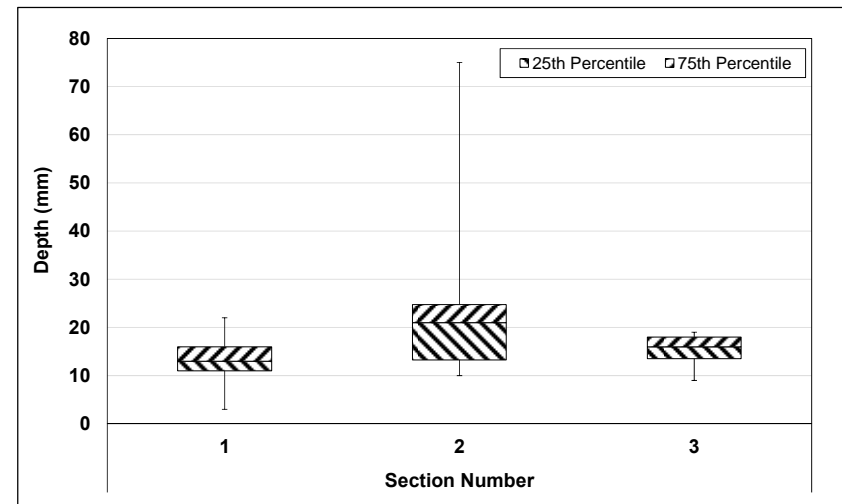


Figure 3.26: CR27: Seating blow penetration depth.

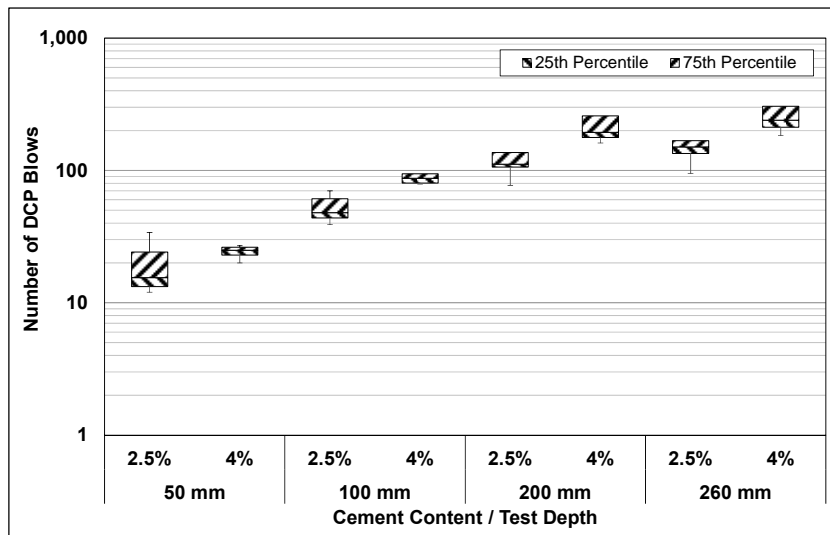


Figure 3.27: PLU147: Number of DCP blows to target depths.

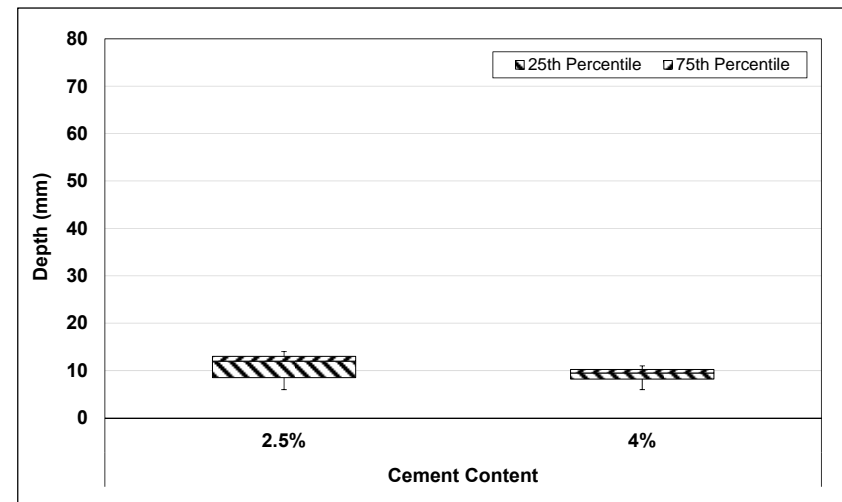


Figure 3.28: PLU147: Seating blow penetration depth.

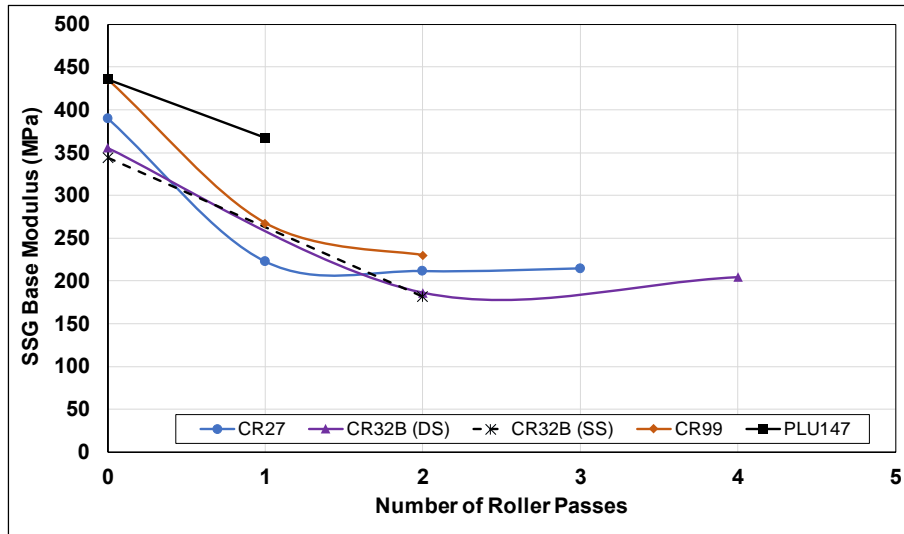


Figure 3.29: Effect of number of roller passes on stiffness change.

3.7.2 Effect of Microcracking on Road CR32B

SSG testing on CR32B started after approximately 25 percent of the project had already been microcracked due to the limited preparation time between the UCPRC being notified of the project and the actual start date of the project. The SSG measurements are summarized in Table 3.11 and Figure 3.30. The results show a considerable drop in stiffness after microcracking, as expected. However, the original stiffness measured before microcracking was reached just one day after microcracking. Stiffness continued to increase, but at a slower rate over the next four days.

Table 3.11: CR32B: Summary of SSG Data

Days Before/After Microcracking	Microcracked?	Number of Points	Mean (MPa)	Std. Dev. (MPa)	Std. Error (MPa)
0	No	127	361	128	11
0	Yes	137	201	71	6
1		85	354	89	10
2		67	407	96	12
3		62	385	99	13
4		70	447	92	11
5		7	471	110	42

3.7.3 Effect of Microcracking on Road CR27

A more complete set of data points spanning three days before microcracking through five days after microcracking was collected on CR27. The results are summarized in Table 3.12 and Figure 3.31, and show that stiffness increased with time in the days between final compaction and microcracking. A significant drop in stiffness was recorded after microcracking, as expected. A large increase in stiffness was recorded one day after microcracking, after which the rate of increase plateaued with no significant increase in stiffness recorded on days two through five after microcracking.

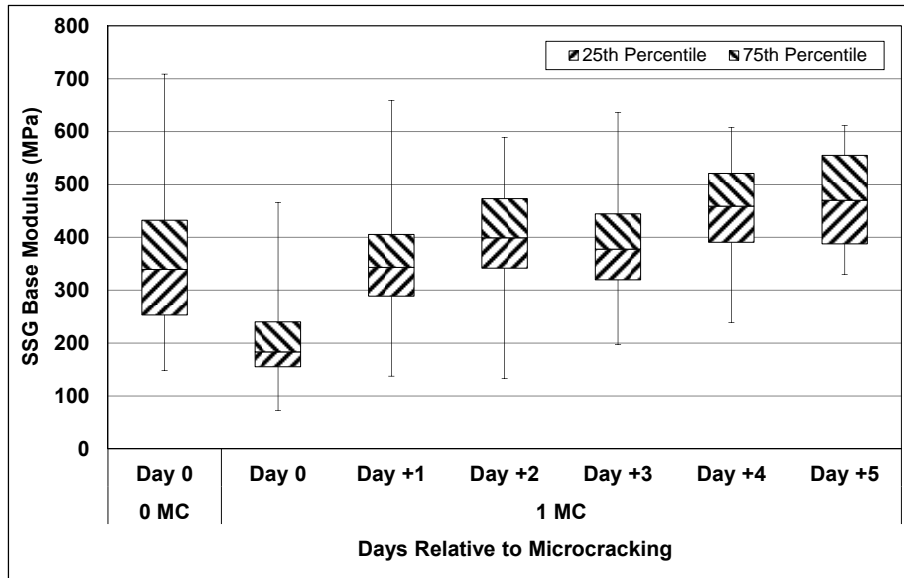


Figure 3.30: CR32B: Average SSG stiffness results after microcracking.

Table 3.12: CR27: Summary of SSG Data

Days Before/After Microcracking	Microcracked?	Number of Points	Mean (MPa)	Std. Dev. (MPa)	Std. Error (MPa)
-3	No	72	272	74	9
-2		174	301	91	7
-1		133	323	100	9
0		35	380	112	19
0	Yes	163	221	65	5
1		26	339	70	14
2		75	294	57	7
3		128	313	85	7
4		29	339	81	15
5		25	318	76	15

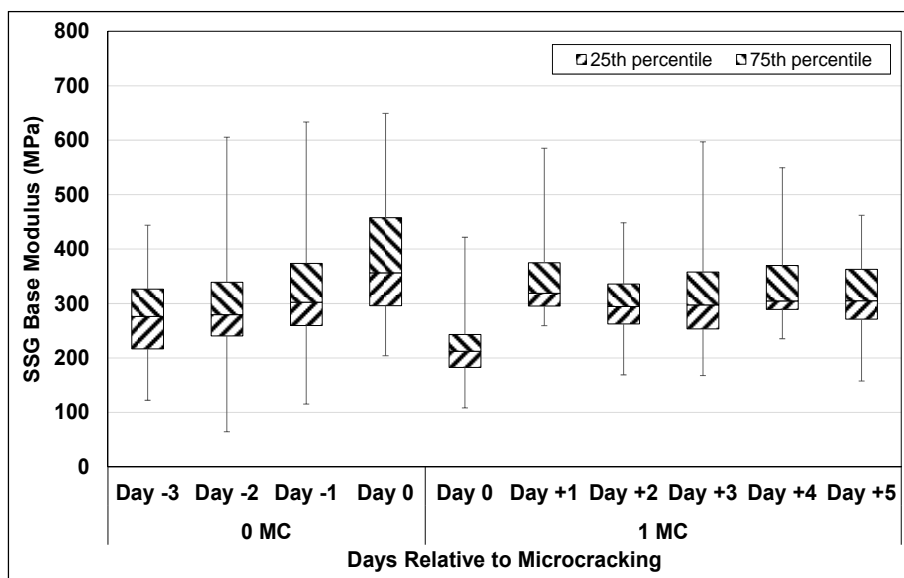


Figure 3.31: CR27: Average SSG stiffness results after microcracking.

Regular water curing until paving was specified for the project, and photographs taken on the day of microcracking (Figure 3.32) indicate that this was carried out in the early stages of the project. Although a water tanker spraying the road was observed by the UCPRC crew during daily stiffness measurements, it is not clear whether sufficient water was sprayed since the UCPRC crew were only on site for a limited period and no records of watering were made available by the contractor or the county. Weather station records for the area show a mean ambient temperature of 27°C (81°F), a maximum temperature of 38°C (100°F), and low relative humidity during daylight hours. It is therefore possible that the amount water and frequency of spraying was unable to maintain sufficient moisture in the layer to sustain hydration and a corresponding stiffness increase.



Figure 3.32: CR27: Photographs showing wet surface.

3.7.4 Effect of Microcracking on CR99

A representative set of data points spanning two days before microcracking through four days after microcracking was collected on CR99. The results are summarized in Table 3.13 and Figure 3.33, which show a clear difference between the rate of stiffness gain prior to and then after microcracking. A large increase in stiffness was recorded one day after microcracking, after which the rate of increase plateaued with no significant increase in stiffness recorded on days two through four—similar to that recorded on CR27. There was a wide variation in stiffness for each day along the length of the section, especially on the day prior to microcracking.

Table 3.13: CR99: Summary of SSG Data

Days Before/After Microcracking	Microcracked?	Number of Points	Mean (MPa)	Std. Dev. (MPa)	Std. Error (MPa)
-2	No	68	356	91	11
-1		64	412	103	13
0		31	436	86	16
0	Yes	66	250	66	8
+2		65	309	74	9
+3		32	305	66	12
+4		31	320	77	14

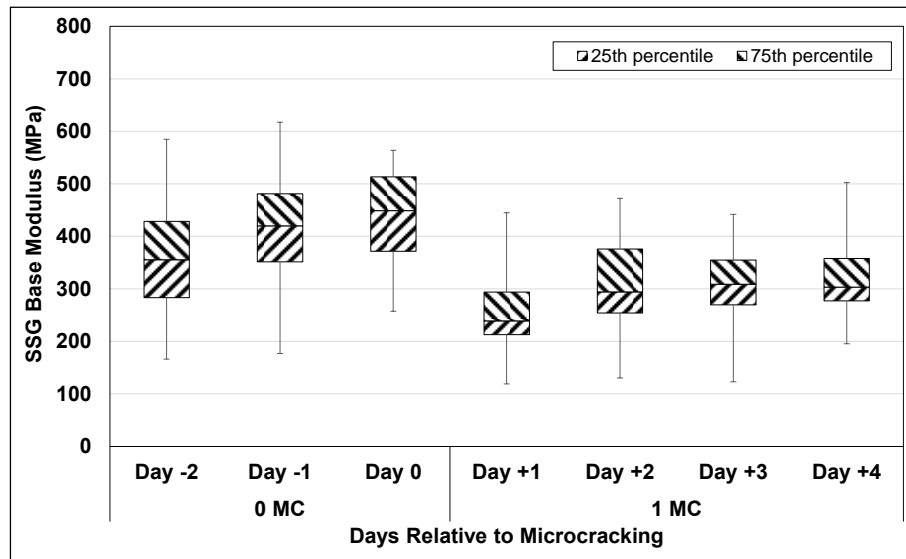


Figure 3.33: CR99: Average SSG stiffness results after microcracking.

3.7.5 Effect of Microcracking on PLU147

A set of data points spanning two days before microcracking and the day of microcracking was collected on PLU147. Additional measurements could not be taken on subsequent days due to limitations with road closures (i.e., the completed lane was being used by traffic) and then paving of the section. The results are summarized in Table 3.14 and Figure 3.34, which show considerable stiffness gain prior to microcracking followed by a sharp decrease after a microcracking. Stiffness measurements along the section appeared less variable than those on the county road projects, however, there were fewer measurement locations on this project compared to the county road projects.

Table 3.14: PLU147: Summary of SSG Data

Cement Content (%)	Days Before/After Microcracking	Microcracked?	Number of Points	Mean (MPa)	Std. Dev. (MPa)	Std. Error (MPa)
2.5	-2	No	20	220	62	14
2.5	-1	No	55	333	69	9
4.0			13	367	61	17
2.5	0	Yes	73	434	92	11
4.0			56	406	99	13
2.5	0	Yes	24	366	73	15
4.0			39	368	71	11

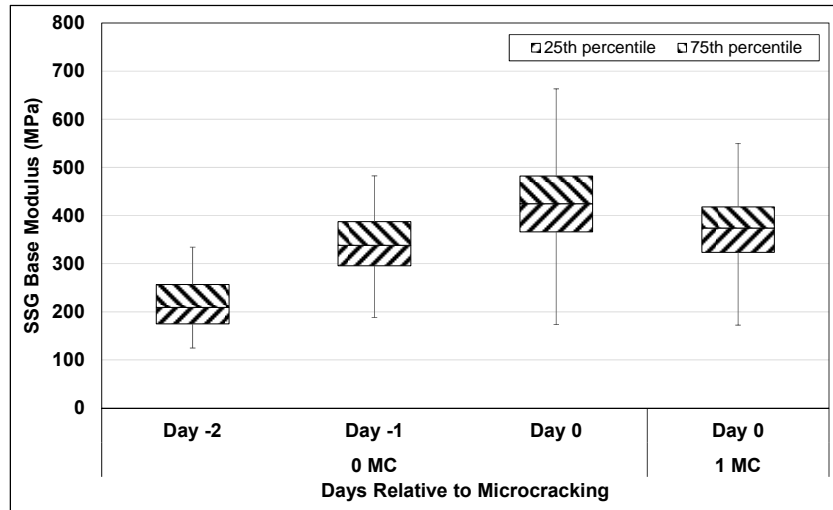


Figure 3.34: PLU147: Average SSG stiffness results after microcracking.

3.8 Falling Weight Deflectometer (FWD) Testing

FWD testing was conducted after the sections were microcracked, paved with asphalt concrete and approved for testing by the project engineer. The frequency of FWD testing, by month, is summarized in Figure 3.35. Testing on CR99 and PLU147 was limited by the availability of road closures and traffic control. Some tests on PLU147 could not be completed in the proposed schedule due to snow and to temperatures lower than the operating limits of the equipment.

The FWD test drop locations on each road are listed in Appendix A. All FWD stiffnesses were backcalculated using *CalBack*, a layer elastic analysis program developed at the UCPRC, based on the pavement structures discussed in Section 3.4. A Poisson's ratio of 0.35 was assumed for each layer in the analyses.

3.8.1 FDR Layer Stiffness Change on CR32B

The FWD testing plan on CR32B focused on capturing the stiffness gain characteristics, long-term stiffness, in-project variability, and the effects of temperature on the FDR-PC base. Testing was performed between the wheelpaths in both the eastbound and westbound lanes (see Table A.1 in Appendix A) at both low and high temperatures (i.e., tests in the morning and afternoon of the same day).

The FDR-PC layer moduli for each day of tests on CR32B is shown in Figure 3.36 and Figure 3.37. Figure 3.36 shows values for the mean, and the mean plus and minus one standard deviation, of the stiffness backcalculated for each day of testing. Figure 3.37 shows average stiffness for selected day-sections. The data show a wide variation in base modulus, with about an order of magnitude difference in modulus

between the section with the lowest stiffness and the section with the highest stiffness. Stiffness increased rapidly in the first 30 days after construction, and then plateaued to a much slower rate up to the last set of measurements taken 350 days after construction. The average moduli for selected construction sections are shown in Figure 3.37 to illustrate the range of measured stiffnesses.

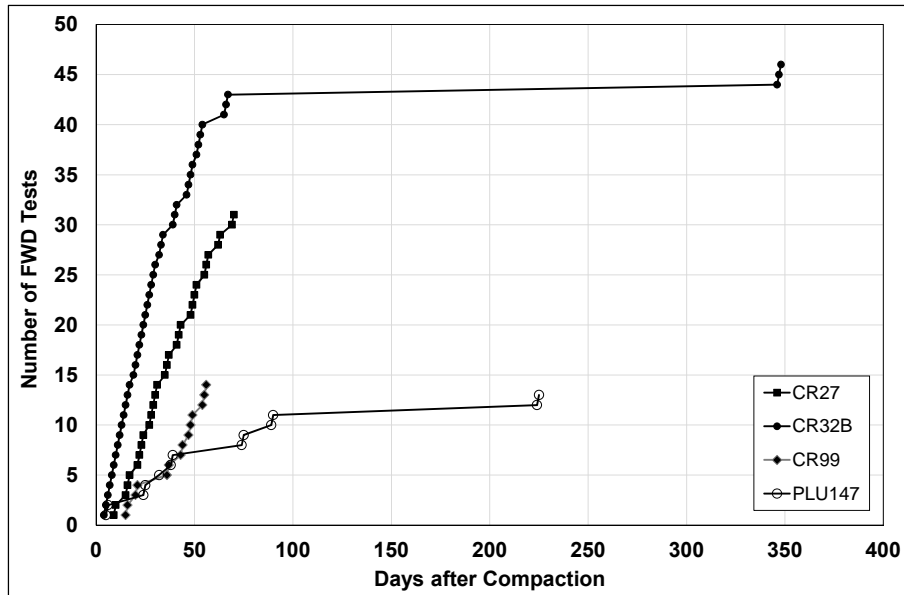


Figure 3.35: FWD testing schedule on each project.

The backcalculated FDR-PC layer stiffnesses measured on August 27, 2015, 350 days after microcracking, are plotted in Figure 3.38 to show the effect of temperature. The average surface temperatures measured during testing were 23°C and 53°C for the low- and high-temperature tests, respectively. Figure 3.38 shows that increasing temperature resulted in a decrease in base stiffness, and this was attributed primarily to the confining effects of the 125 mm asphalt concrete surface layer. The old asphalt surface that was recycled into the FDR-PC base layer probably also had a small impact on the drop in stiffness due to its temperature-sensitive, viscoelastic properties.

3.8.2 FDR Layer Stiffness Change on CR27

The FWD testing plan on CR27 focused on capturing initial stiffness gain characteristics, in-project variability, and the effect of traffic over time. FWD test stations were selected in both the eastbound (EB) and westbound (WB) directions, and in both the right wheelpath (RWP) and between the wheelpaths (BWP) (see Table A.2 in Appendix A). Figure 3.39 shows the backcalculated stiffness variation along the project on November 10, 2015, 62 days after microcracking. Figure 3.40 shows the average increase in the backcalculated stiffnesses of each construction section. The standard deviation in backcalculated stiffness for each construction section over time is shown in Figure 3.41. The data in Figure 3.40 and Figure 3.41

are limited to the eastbound / between-wheelpath dataset, which was chosen to represent longitudinal variability with no traffic effects. Both figures show that Construction Sections #1, #9, and #10 had significantly lower base stiffnesses compared to the other sections. This is likely due to the observation made in Section 3.4.2, that the in-situ material at both ends of the project had a finer grading compared to those on the rest of the project.

Figure 3.42 shows a subset of the data collected between the wheelpaths and in the right wheelpath in both directions at corresponding stations 62 days after microcracking. Direction and wheelpath location are both identified. The wheelpath stiffnesses were generally lower than those measured between the wheelpaths, indicating that traffic is causing permanent damage to the base.

3.8.3 FDR Layer Stiffness Change on CR99

Due to limited opportunities for closures on CR99, the FWD testing plan focused only on capturing initial stiffness gain characteristics. Testing was conducted in both the northbound (NB) and southbound (SB) directions, between the wheelpaths as well as in the right wheelpath (see Table A.3 in Appendix A).

The mean backcalculated stiffness for each construction section over time is shown in Figure 3.43. The test results revealed a significant reduction in stiffness measured 48 days after microcracking compared to that measured 36 days after microcracking (Figure 3.44). The minimum, maximum, and mean temperatures for the time period during which CR99 was tested is plotted in Figure 3.45. The reduction in stiffness after October 29, 2015 corresponds to the notable drop in ambient temperature recorded over the same time period, and differs from the observations with regard to temperature on CR32B (i.e., stiffness decreased with increasing temperature due to lowering of confinement of the asphalt concrete). This suggests that the stiffness decrease was likely the result of some structural effect: most likely shrinkage cracking due to increased tensile stresses as the temperature of the base layer decreased.

3.8.4 FDR Layer Stiffness Change on PLU147

The test plan for FWD testing on PLU147 focused on the effects of temperature, traffic, and the high cement contents that accumulated at the ends of the construction sections, as discussed in Section 3.4.4. FWD testing was performed in the following sequence (see Table A.4 in Appendix A):

1. Northbound lane, between wheelpaths (NB_BWP)
2. Southbound lane, between wheelpaths (SB_BWP)
3. Northbound lane, right wheelpath (NB_RWP)
4. Southbound lane, right wheelpath (SB_RWP)
5. Northbound lane, between wheelpaths (NB_BWP2)

The right wheelpath stations were 1.0 m (3.28 ft.) to the right of the between-wheelpath stations. The between-wheelpath stations in both lanes were selected to monitor the effect of high cement contents at the end of the construction sections, and for determining a mean modulus of the FDR-PC layer. The right-wheelpath stations were in the same transverse line as the between-wheelpath stations, but the number of tests was reduced to fit the time available for testing. These tests were used to monitor the effect of traffic. The second set of between-wheelpath tests in the northbound lane overlapped the stations for the first set of between-wheelpath tests in the northbound lane, and were used to measure the effect of temperature. The number of testing locations was limited to 12 to fit the time available for testing. A complete set of test results was not obtained on a number of the visits due to the very cold temperatures that were below the effective operating range of the FWD. Testing was also limited by the number of road closure opportunities.

Average backcalculated stiffnesses over time are plotted in Figure 3.46 with standard deviations to show variability plotted in Figure 3.47. Variability was relatively high as expected, given the inconsistencies observed during construction. The average pavement surface temperatures for the testing periods for each wheelpath are provided in Figure 3.48. The ambient air temperatures for the town of Chester, located 16 km (10 miles) west of the project, are shown in Figure 3.49 to provide an indication of temperature change during testing. The temperatures during the first set of tests between wheelpaths (Sequence #1 and Sequence #2) were consistently lower than the temperatures measured during testing in the right wheelpath (Sequence #3 and Sequence #4), and during the second pass between wheelpaths (Sequence #5).

The effects of traffic and temperature were evaluated using a subset of the data (northbound between wheelpaths and northbound right wheelpath), 25, 39, 90, and 225 days after compaction. Data was collected between wheelpaths twice on the same day (cold and warm), which allowed stiffnesses to be normalized to the mean temperature of each day (Table 3.15). The between-wheelpath test results were used to develop a log-linear relationship between temperature and stiffness for each day to assess the effects of traffic. The normalized stiffnesses are shown in Figure 3.50. The difference between the right wheelpath and the between-wheelpath measurements was also determined to compare the change in stiffnesses in trafficked and untrafficked areas over time (Figure 3.51). After 225 days, the stiffness in the wheelpath was 28 percent lower than that measured in the adjacent untrafficked area.

Table 3.15: PLU147: Normalization Temperature for Each Day

Date	Days after Compaction	Temperature (°C)
10/12/2015	25	27
10/26/2015	39	14
12/16/2015	90	3
04/29/2016	225	27

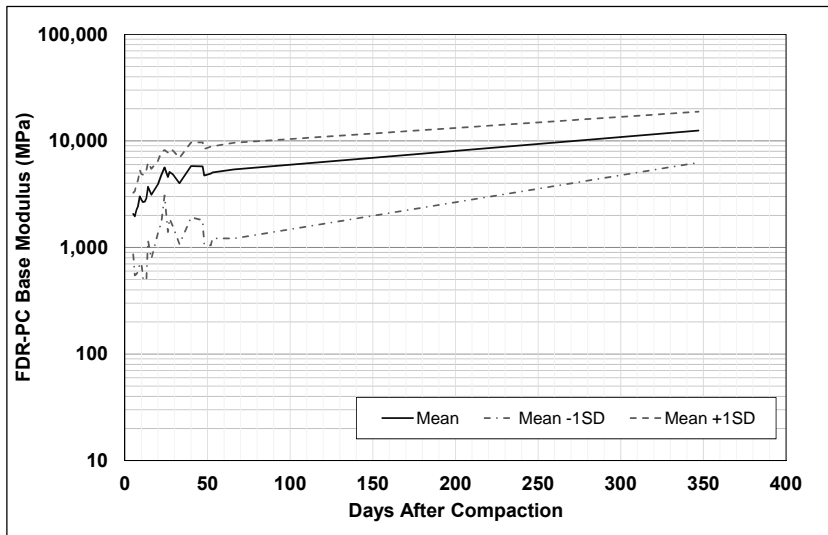


Figure 3.36: CR32B: Change in FDR-PC base moduli over time.

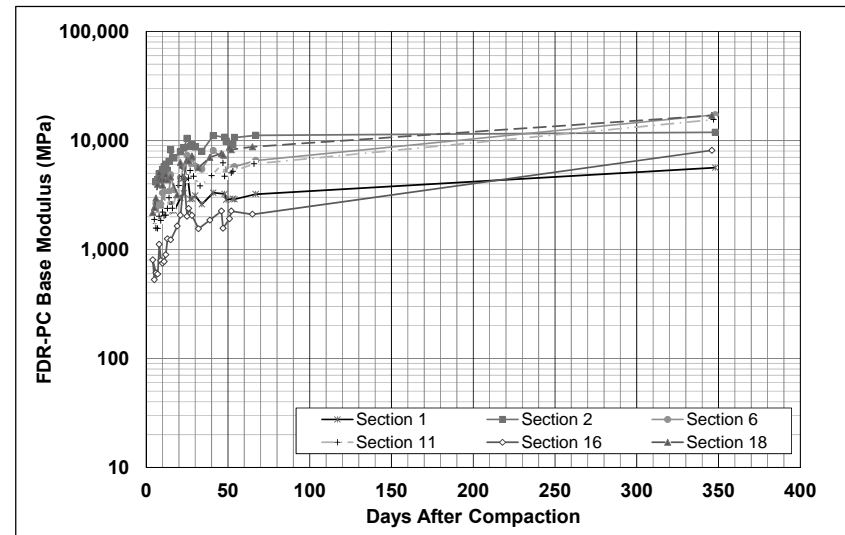


Figure 3.37: CR32B: Average base moduli for selected construction sections over time.

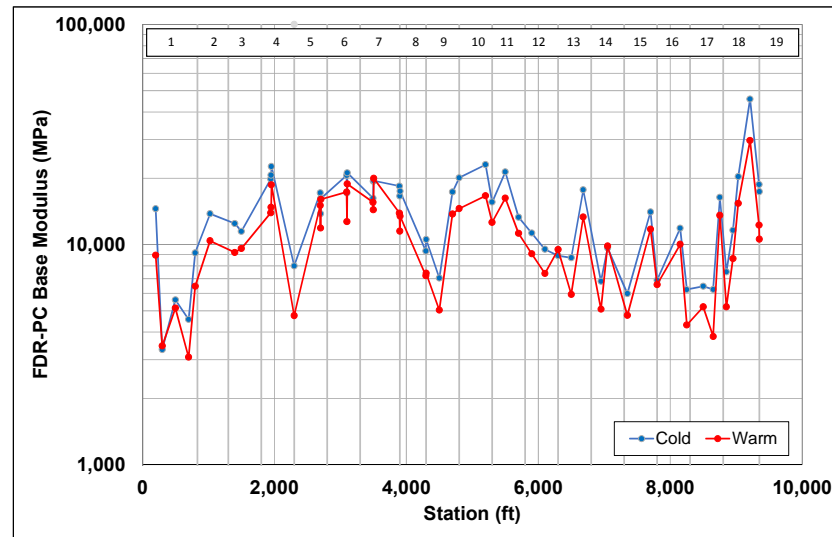


Figure 3.38: CR32B: FDR-PC base moduli at two temperatures (350 days after microcracking).

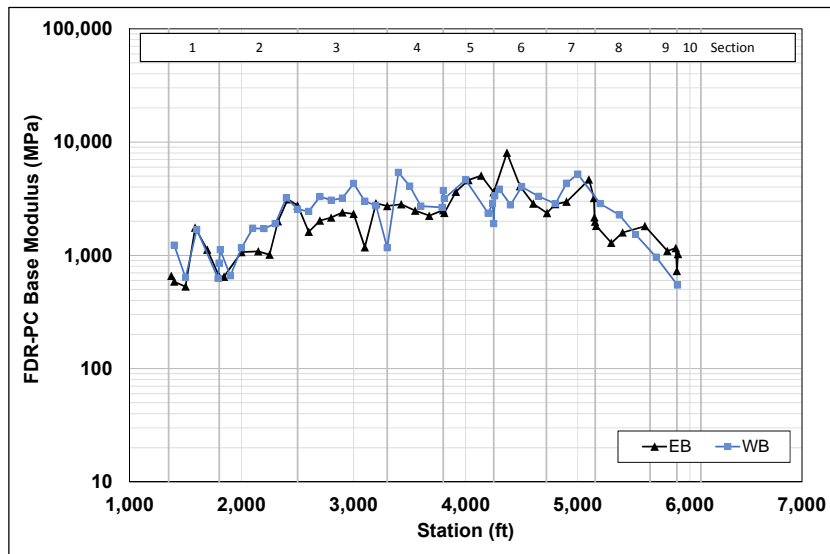


Figure 3.39: CR27: Mean FDR-PC base moduli 62 days after compaction.

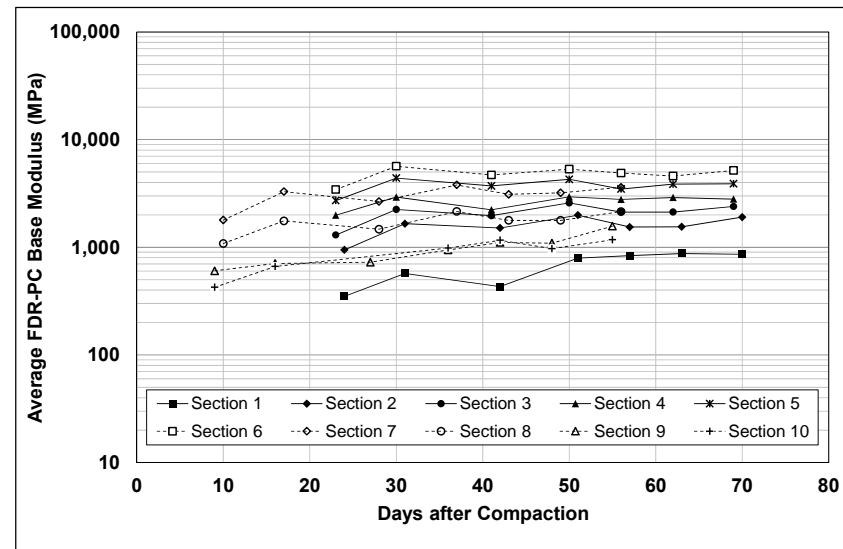


Figure 3.40: CR27: Mean FDR-PC base moduli for each construction section over time.

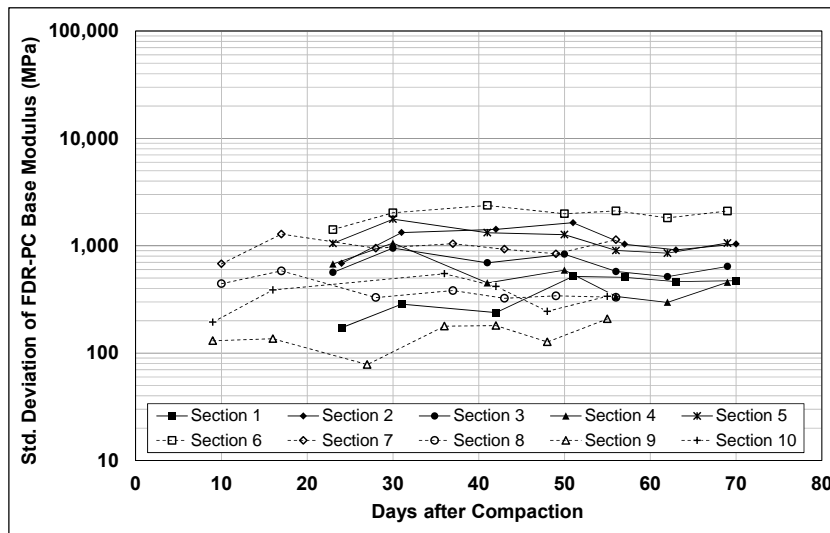


Figure 3.41: CR27: Standard deviation of FDR-PC base moduli for each construction section.

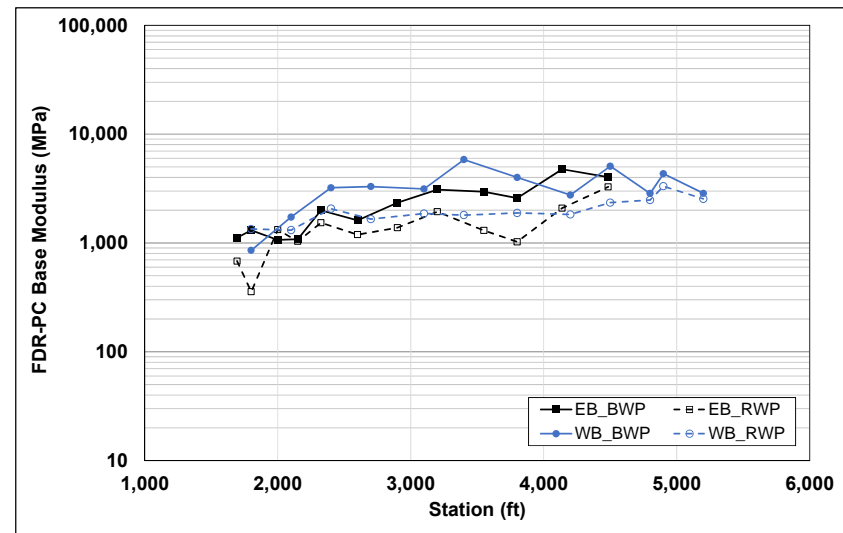


Figure 3.42: CR27: FDR-PC base moduli in the wheelpath and between wheelpaths after 62 days.

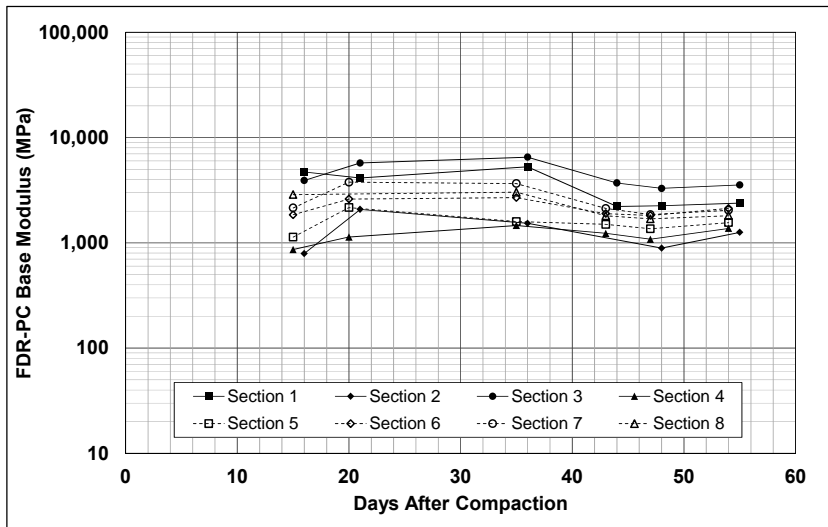


Figure 3.43: CR99: Mean FDR-PC base moduli per construction section over time.

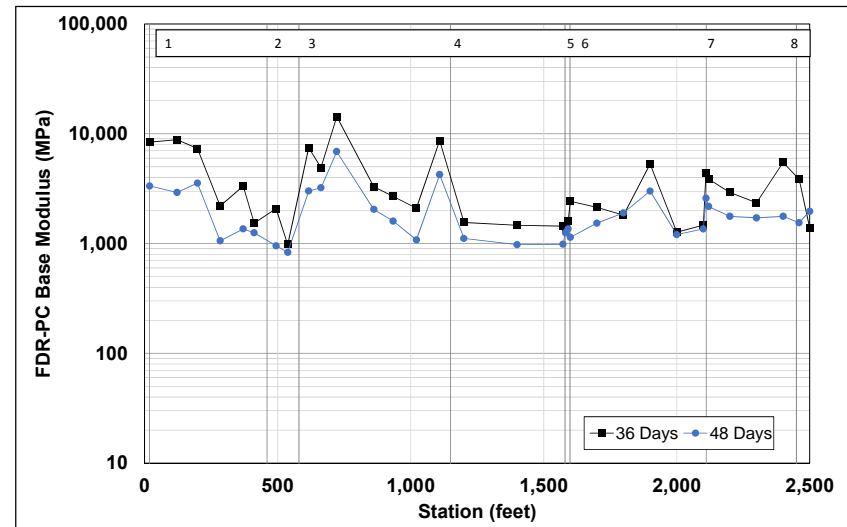


Figure 3.44: CR99: FDR-PC base moduli results for 36 days and 48 days after compaction.

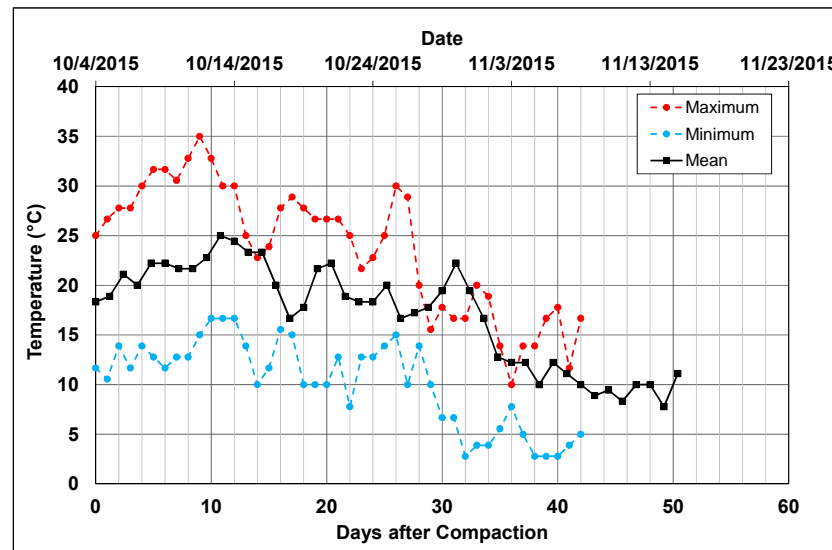


Figure 3.45: CR99: Ambient temperature variation over time of FWD measurements.

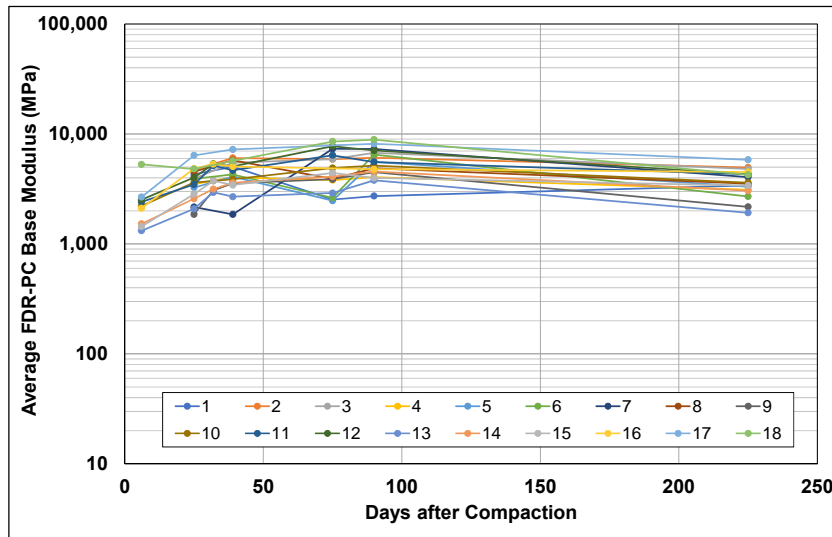


Figure 3.46: PLU147: Average backcalculated stiffnesses for each section.

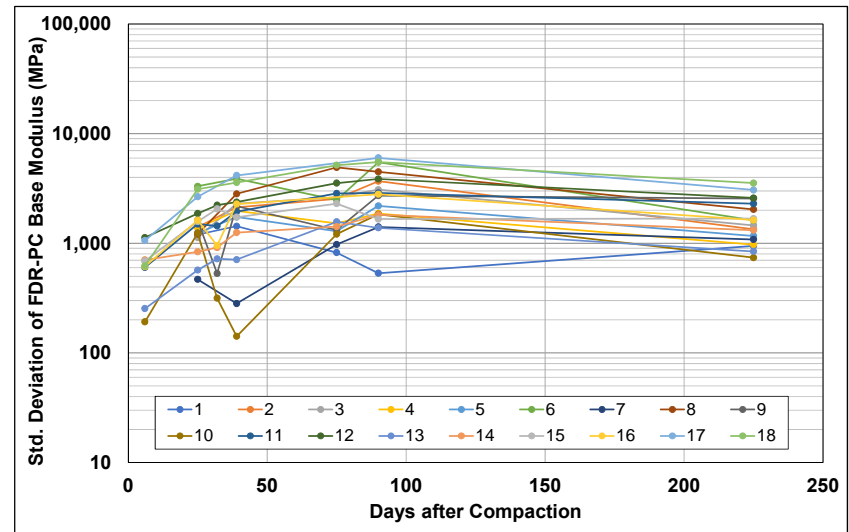


Figure 3.47: PLU147: Standard deviation of backcalculated stiffnesses for each section.

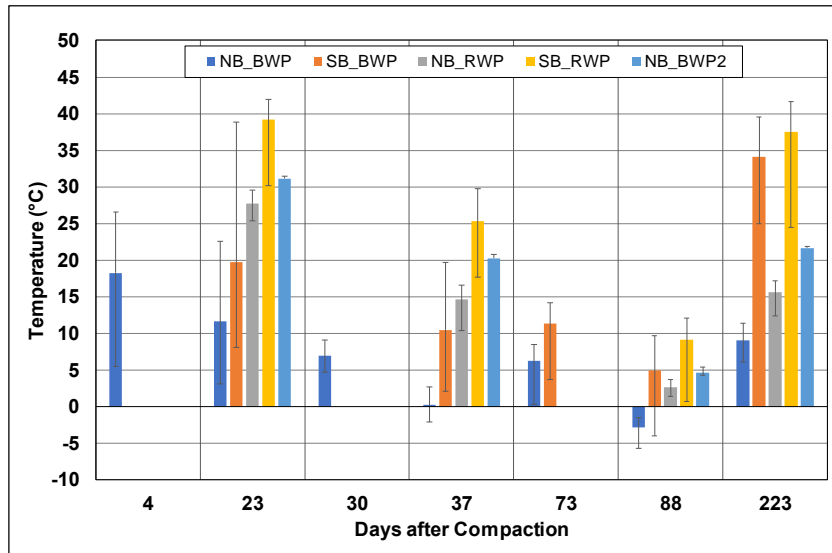


Figure 3.48: PLU147: Surface temperatures in each wheelpath during testing.

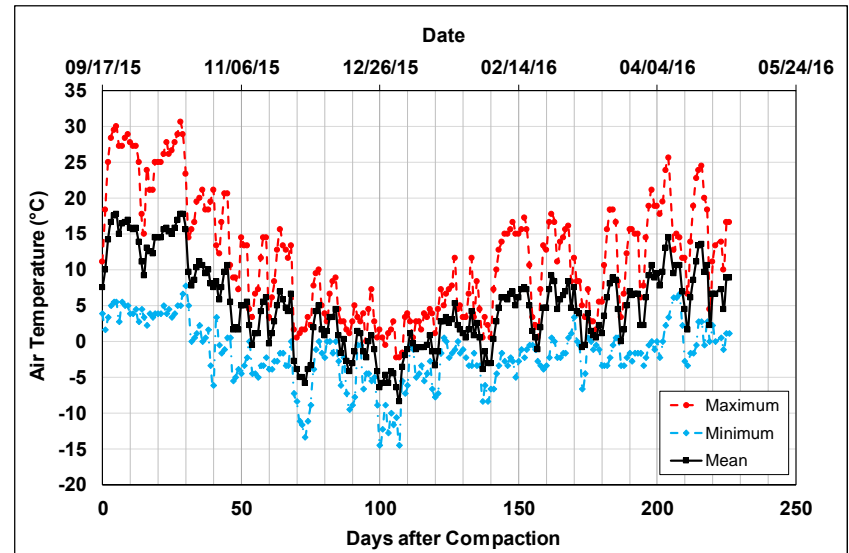


Figure 3.49: PLU147: Air temperatures during FWD testing.

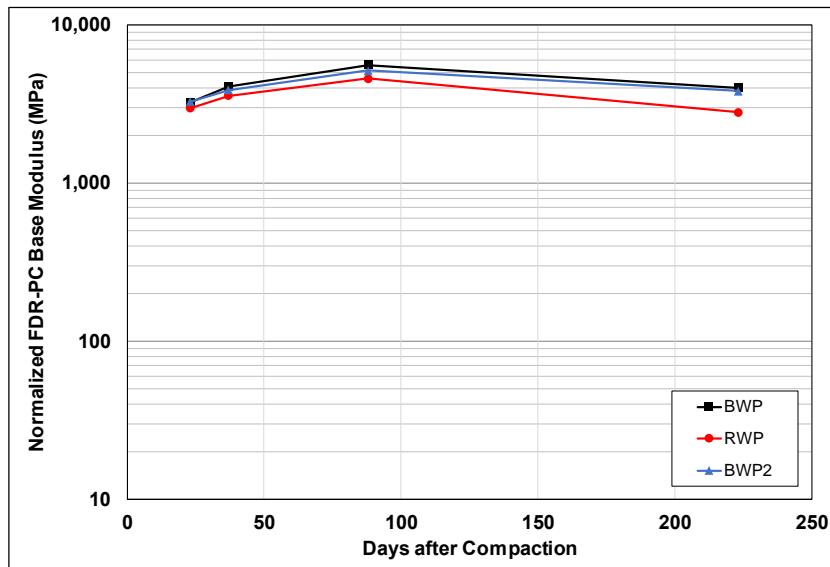


Figure 3.50: PLU147: Normalized FDR-PC base moduli comparison between test locations.

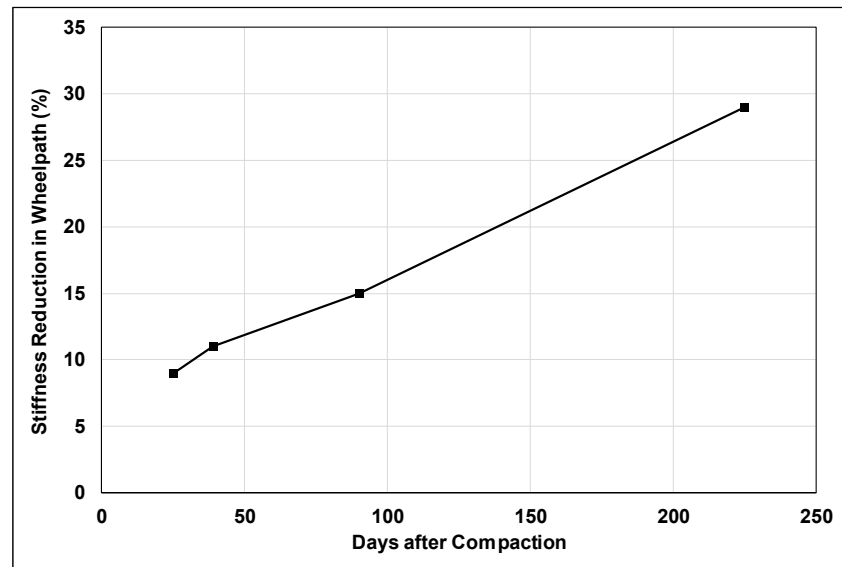


Figure 3.51: PLU147: Stiffness reduction in the wheelpath compared to between the wheelpaths.

The reduction in the base modulus after 75 days (Figure 3.50) cannot be fully explained due to the limited number of tests undertaken (all FWD tests after 225 days were unsuccessful due to equipment problems at the very low temperatures or to the unavailability of road closures), but one possible explanation would be the same as that discussed for CR99, namely that shrinkage cracks occurred as a result of the increased tensile stresses associated with the low temperatures.

The mean FDR-PC layer moduli over the testing period between September 23, 2015 (25 days) and April 29, 2016 (225 days) for the first set of between-wheelpath tests is shown in Figure 3.52. Results for both the 2.5 percent and 4.0 percent design cement contents are shown. The results show that there was an initial increase in stiffness followed by a reduction in stiffness after December 16, 2015 (39 days).

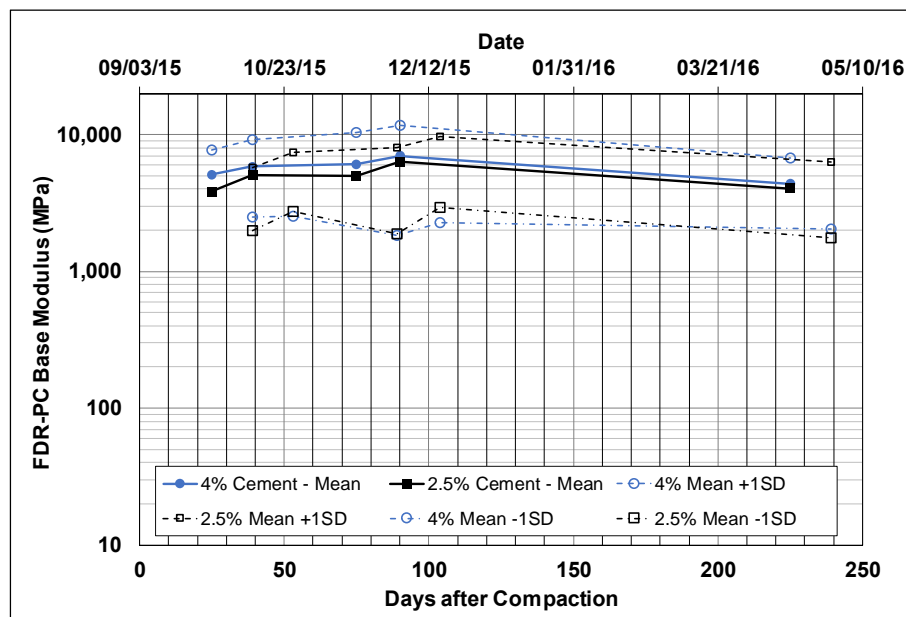


Figure 3.52: PLU147: Mean FDR-PC base moduli for different cement contents over time.

The mean modulus for the 2.5 percent cement content section was on average 800 MPa lower than that measured on the 4.0 percent cement section. The difference between the two sections decreased with time, however. Taking the large overall variation in measured stiffness on the project into consideration, the small differences in mean stiffness on the two sections illustrated the advantages of completing a thorough project assessment prior to construction; this allowed identification of the differences in the pavement structure and subgrade materials, and directed mix design testing to determine cement contents that would result in a consistent pavement structure over the length of the project.

The stiffnesses across two construction section interfaces are plotted in Figure 3.53. FWD measurements were taken at five test stations, spaced at 1.5 m (5 ft.) intervals across the interface. The effect of the high

cement contents is clear at the three interfaces shown (between Section #1 and Section #4). A difference of 4,000 MPa was measured over a distance of 7.5 m (25 ft.) in the interface between Section #1 and Section #2.

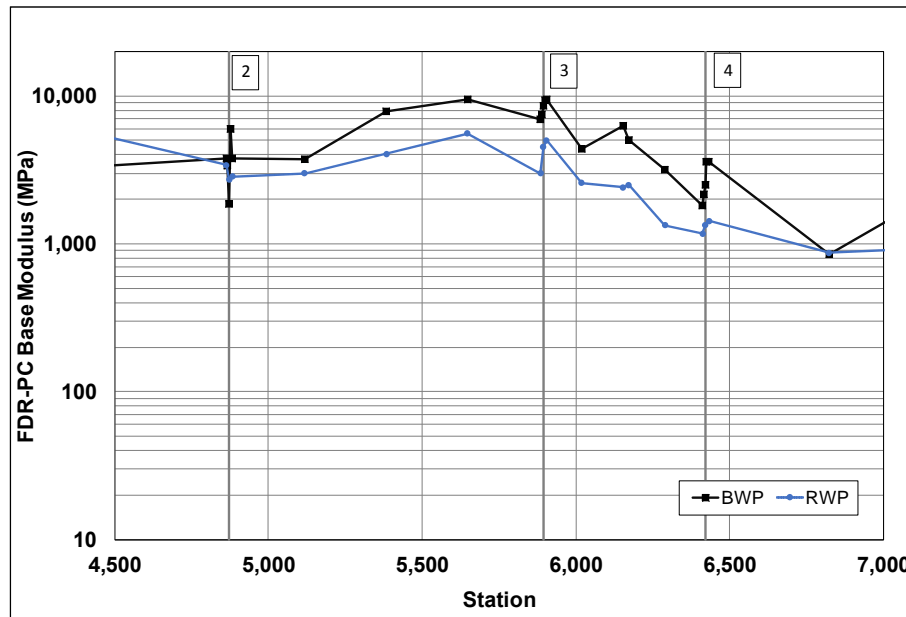


Figure 3.53: PLU147: Construction section interface variability due to high cement contents.

3.9 Field Testing Conclusions

The following conclusions with regard to field testing on four FDR-PC projects in California were made based on a series of observations during construction and statistical analyses of soil stiffness gauge (SSG) and falling weight deflectometer (FWD) data:

- There was a wide variation in pavement materials and in pavement construction quality across the four projects. On the county road projects, where minimal sampling and testing appears to have been carried out in the project assessment phase, the mix designs did not necessarily accommodate the variation in materials and pavement conditions.
- Specifications are not always being followed to the fullest extent by contractors and they are not being fully enforced by agency engineers.
- In addition to being useful for assessing unbound layer thicknesses and the subgrade conditions of the existing road prior to FDR, DCP tests can also provide a quick indication of weak areas on the project after final compaction.
- The SSG is useful for measuring/checking stiffness gain over time on the days between final compaction and microcracking, for determining the number of roller passes used to achieve a satisfactory level of stiffness reduction by microcracking, and for checking that a satisfactory drop in stiffness was achieved after microcracking. It can also be used to check areas suspected of having too little or too much cement, especially those areas at the beginning and end of construction sections, and in lane overlap areas. However, the rate at which SSG testing can be conducted is slower than

the pace of construction activities and more than one SSG may be required on site on the day of microcracking to keep up with the equipment.

- FWD testing provided useful insights into stiffness change in FDR-PC layers over time and how this change is affected by material variability, the distribution of cement during construction, and the effectiveness of the microcracking process.
- FWD and SSG results both indicate that microcracking does result in an immediate and notable drop in stiffness in the FDR-PC layer after the procedure has been completed. However, much of the stiffness is recovered by recementation in the days after microcracking, after which stiffness appears to plateau. Stiffness change over time appears to be influenced by temperature; however, insufficient data has been collected to date to draw any firm conclusions about longer-term performance.

4. PHASE 1: LABORATORY EXPERIMENT DESIGN

4.1 Introduction

The Phase 1 laboratory study focused on understanding the microcracking mechanism in cement-treated materials, and identifying criteria for modeling the effects of microcracking. Testing included the following two subphases:

- Phase 1a: Simulating microcracking in the laboratory using different methods with available equipment
- Phase 1b: Conducting different stiffness/modulus tests to determine the sensitivity of the tests to the microcracking effort

Issues considered in the testing included the following:

- Assessment of the effect of microcracking on stiffness on different days after compaction
- Determination of the effectiveness and repeatability with which microcracking can be conducted in the laboratory
- Determination of whether cement-treated materials continue to hydrate and increase in stiffness after microcracking

4.2 Experiment Plan Factors

In the Phase 1a study, the methods evaluated for laboratory simulation of microcracking included a handheld vibrating hammer, a vibrating table, and a small dual steel wheel vibrating roller. Factors considered in the experimental plan included cement content, the intervals between final compaction and microcracking, and the vibration settings on the roller.

Various factors were considered in the Phase 1b study based on actual practice observed on field projects. Factors included cement content, number of days that passed between compaction of the specimens and when they were microcracked, the method used to measure stiffness of the specimens before and after microcracking, and the intervals between repeated stiffness tests on the specimens.

4.3 Materials Used for Testing

The material used for this study was sampled during pre-pulverization on a pavement recycling project on State Route 88 in Amador County, California. The pulverization depth was approximately 0.7 ft. (200 mm), consisting of between 0.5 ft. and 0.58 ft. (150 mm to 175 mm) of cracked asphalt pavement, and between 0.08 ft. and 0.16 ft. (25 mm and 50 mm) of the underlying aggregate base. The aggregates in the reclaimed asphalt pavement (RAP) and underlying base materials were of granitic origin.

The material grading was determined with a wet and dry sieve analysis following AASHTO T 11 and AASHTO T 27. The results of the sieve analysis are provided in Figure 4.1. The percentage of material passing the #200 (0.075 mm) sieve was seven percent.

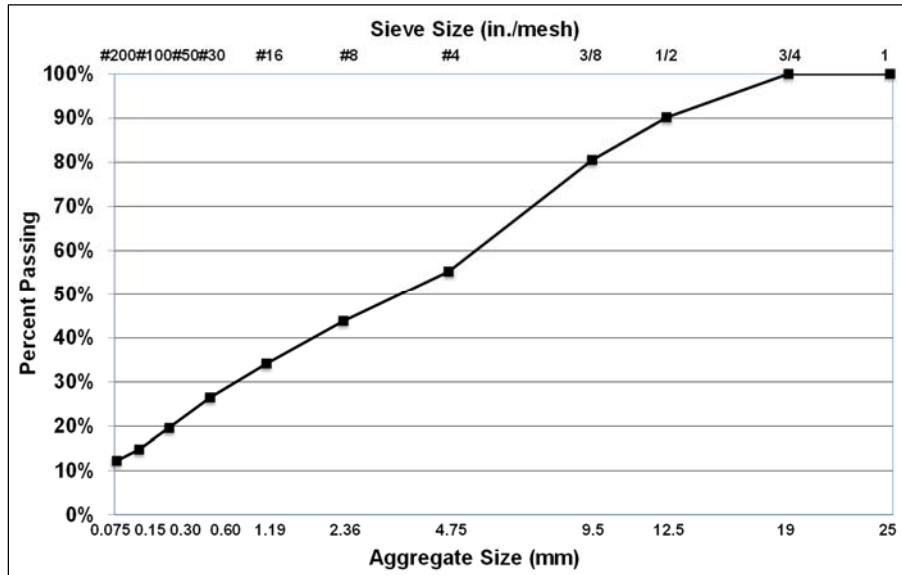


Figure 4.1: Sieve analysis of SR88 material.

An Atterberg Limit test (AASHTO T 89 and AASHTO T 90) indicated that the material was non-plastic.

The maximum dry density (MDD) and optimum compaction moisture content (OMC) were determined according to AASHTO T 180. An MDD of 2,190 kg/m³ was achieved at a moisture content of five percent.

5. PHASE 1a: LABORATORY MICROCRACKING METHODS

5.1 Introduction

The methods that were considered to microcrack compacted specimens in the laboratory were based on the use of equipment commonly used to compact 6 in. by 12 in. (150 mm by 300 mm) cylindrical specimens. These methods included vibrating hammer compaction, a vibrating table, and a modified setup used to compact asphalt ingots with a small dual steel wheel vibrating roller. Each method is discussed below.

5.2 Vibrating Hammer

A Hilti™ TE 70 vibrating hammer was used for this study and was selected based on its ability to impart repeated percussive blows to the face of the sample to induce microcracking. Microcracking was attempted on both confined and unconfined specimens, with the operator placing the compaction attachment onto the face of the sample and applying vibration energy for a set period of time (Figure 5.1). Despite experimenting with a range of vibration times and a range of applied pressures, the shock imparted by the drill in all instances caused stabilized material to break off of the specimen (Figure 5.2) rendering it unsuitable for triaxial testing. This method in its current form was therefore not considered suitable for laboratory microcracking given that the lateral movement of the compaction attachment and the pressure applied by the operator were uncontrolled and likely to have a significant impact on the repeatability and reproducibility of the method, and that the impact force of the compaction attachment damaged the specimen to the extent that confined triaxial testing could not be performed on it. However, the method was still considered as being potentially suitable if the following modifications could be made:

- The impact hammer drill was installed in a frame in which load, time, and the position of the compaction attachment could be strictly controlled, thereby eliminating operator variability.
- The specimen was confined in a mold to represent conditions in the pavement under a 12-ton roller.

Since completion of this part of the study, a prototype compaction hammer meeting the above requirements was developed by *Wirtgen* that produces large (6 in. by 12 in. [150 mm by 300 mm]) triaxial specimens that are representative of recycled pavement layers. One of these prototypes was loaned to the UCPRC and the results of testing with it will be discussed in a subsequent report. Assuming that the new compaction hammer setup can be used for microcracking laboratory-prepared specimens, the approach would have the following advantages:

- Microcracking can be performed with the same equipment used for specimen compaction.
- The equipment is commercially available, relatively inexpensive, and operator independent.



Figure 5.1: Using the vibrating hammer to microcrack a compacted specimen.



Figure 5.2: Result of microcracking effort with vibrating hammer.

5.3 Vibrating Table

A vibrating table commonly used for consolidating concrete specimens (Figure 5.3) was used in this part of the study. This method worked on the same principle as the vibrating compaction hammer discussed above, except that the energy applied could be better controlled through amplitude settings on the vibrating table and the weight of the surcharge load placed on top of the specimen.

After some experimentation to determine appropriate equipment settings and surcharge rates, the procedure adopted entailed the following:

- Determine the stiffness of the compacted specimen according to AASHTO T 307.
- Place the specimen on the vibrating table with the long axis perpendicular to the table, position a 14 kg weight on top of the specimen, and then run the vibrating table at maximum amplitude for 15 seconds.
- Determine the stiffness of the specimen immediately after microcracking to assess the change in stiffness as a result of the microcracking.

Based on the results obtained, the vibrating table method was considered to be ineffective in reducing the elastic modulus of the specimens to a similar extent to that measured on full-scale field projects. Although test duration was extended and the surcharge weight was incrementally increased to the point that the

vibrating table would not actuate, no significant microcracking effect was induced. The option of placing the specimen with the axis of the cylinder parallel to the vibrating table was also considered, but this resulted in the specimens failing in a similar manner to that in an indirect tensile test. Further experimentation using a more powerful vibrating table was not considered worthwhile in this phase of the study given that such equipment is typically not standard in pavement engineering laboratories.



Figure 5.3: Vibrating table.

5.4 Steel Wheel Vibrating Roller

A small steel wheel vibrating roller running over previously compacted cylindrical specimens confined in plastic tubes was the third option considered for this study (Figure 5.4 through Figure 5.6). This approach was thought to be potentially the closest simulation to actual field conditions. The method required the construction of a rectangular concrete pit in which the compacted specimens could be placed to allow the roller to pass over them and apply dynamic stresses similar to microcracking procedures on full-scale projects. The concrete test pit was 32 in. wide by 32 in. long by 12 in. deep (800 mm by 800 mm by 305 mm) and designed to accommodate 25 specimens. The total length of the structure was 8.5 ft. (2.6 m) to accommodate on- and off-ramps for the roller to access the pit. The wall and slab thickness of the structure was 6 in. (150 mm), reinforced with 0.5 in. (12 mm) diameter steel bars at 6 in. (150 mm) spacing.



Figure 5.4: Steel wheel vibrating roller.



Figure 5.5: Test pit preparation.



Figure 5.6: Final setup before microcracking.

In the method, three of the 25 specimens were first tested to determine initial stiffness prior to placement. The 25 specimens were then placed with the three selected specimens placed in the middle three locations in the middle row. Sand was then spread over the pit and lightly vibrated with a plate compactor to fill the gaps between the cylinders. A thin layer of sand was retained to cover the specimens to provide a level

surface for the roller and prevent damage to the specimens by the roller as it passed. After rolling, the three selected specimens were removed and retested to assess any change in stiffness after microcracking.

The steel wheel vibrating roller method used for subsequent testing in Phase 1b is summarized as follows:

1. Prepare the microcracking pit by inserting 22 canisters, each containing a compacted specimen of similar strength to those being tested, leaving the middle three spaces open.
2. Remove the three prepared specimens from the curing chamber and determine the resilient modulus of each specimen following AASHTO T 307.
3. Insert the specimens into plastic canisters.
4. Insert the three canisters containing the test specimens in the center three spots.
5. Insert wooden keys between the selected specimens to simplify later extraction.
6. Pack moist sand between the canisters and gently vibrate with a tamper or plate compactor.
7. Spread a 20 mm layer of moist sand across the top of the pit.
8. Place a steel plate across the pit and apply one roller pass to compact the top sand layer.
9. Remove the steel plate.
10. Apply six roller passes (three back and forth actions) at maximum vibration.
11. Using a steel rod and an industrial vacuum, remove the compacted sand from around the three test specimens. Remove the wooden keys located between the selected canisters.
12. Remove the loosened canisters until the test specimens can be easily removed without applying any side or point loading with the pry bars. Save the remaining specimens for future testing.
13. Remove the three test specimens from their canisters.
14. Determine the resilient modulus of each microcracked specimen.

This microcracking method was considered to be the most appropriate of the three approaches tested, and although some minor surface distortion was observed, the specimens were still considered suitable for subsequent testing. However, the equipment used is not typically available in pavement testing laboratories, and the need to construct a dedicated pit to accommodate the specimens was considered to be an unrealistic expectation for routine testing.

5.5 Summary of Laboratory Microcracking Methods

Three laboratory-scale microcracking methods were considered in this phase of the study. Based on observations of the specimens before and after microcracking, the method that uses a dual steel wheel vibrating roller to microcrack specimens in a specially constructed pit appeared to provide the best results of the three approaches. However, given that the equipment and set up used is not standard in most laboratories, further experimentation using a frame-mounted vibration hammer and the same dynamic testing apparatus used for triaxial testing are recommended for further evaluation in Phase 2 of this study.

Blank page

6. PHASE 1b: LABORATORY TESTING

6.1 Introduction

Phase 1b of the study included different modulus tests on laboratory-prepared specimens to determine the sensitivity of the tests to any microcracking effort on the specimen. Work included a mix design to determine optimal cement contents, specimen preparation and curing, and testing according to two different stiffness test methods (resilient modulus [AASHTO T 307] and indirect tensile modulus [AASHTO TP9]).

6.2 Mix Design

A mix design was performed on the reclaimed material to determine an appropriate cement content. A total of five different cement contents were considered in the mix design. Specimens were compacted according to ASTM D1557 and tested following ASTM D1633, after modified curing according to Section 30 of the Caltrans specifications (samples wrapped in plastic and cured in an oven at 38°C [100°F]). The unconfined compressive strength (UCS) test results are shown in Figure 6.1.

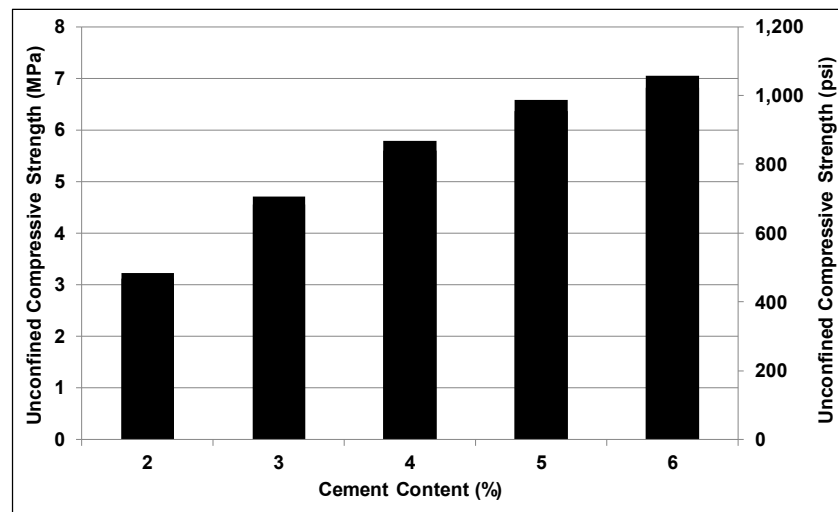


Figure 6.1: FDR-PC mix design.

The UCS results from standard curing and testing were higher than expected, with two percent cement resulting in a UCS in excess of 3.0 MPa (430 psi). This was attributed to the good quality of the RAP/aggregate base blend, to the small quantity of fines (percent passing the 0.075 mm [#200] sieve) in the sample, and to the absence of any clay in those fines (the material tested nonplastic), which would have reacted with the cement and reduced the amount of cement available for strength increase. Given that the aim of the study focused primarily on the effects of microcracking, a decision was made to use three percent and four percent cement, by dry weight of aggregate, because these were representative of the cement

contents used on the projects discussed in Chapter 3, and because the stiffness of high RAP content specimens stabilized with two percent cement would likely not reduce sufficiently after microcracking to be statistically significant.

6.3 Test Method

The AASHTO T 307 test method was selected for this study given that it is the most widely used method of determining the resilient modulus of stabilized materials.

6.4 Test Factorial

The testing factorial is shown in Table 6.1. Control specimens that were not subjected to any microcracking were included for comparison purposes. Microcracked specimens were tested before and after microcracking.

Table 6.1: Phase 1b Testing Factorial

Factor	Number	Values
Water content (%)	1	6
Cement content (%)	2	3 and 4
Days between compaction and microcracking	3	1, 2, and 3
Testing intervals (time after compaction)	8	1, 24, 48, and 72 hrs, 7, 14, 21, and 28 days
Modulus tests	1	Resilient modulus
Replicates	3	

6.5 Specimen Preparation and Conditioning

Specimens were prepared according to AASHTO T 307. The material was scalped at 19 mm (3/4 in.) to remove any oversize aggregates. The predetermined quantities of cement and water were mixed with a measured mass of pulverized material in a pug mill mixer (Figure 6.2) that replicates the mixing action of recycling equipment used on FDR projects.



Figure 6.2: Pug mill mixer.

The test sequence for AASHTO T 307 is provided in Table 6.2. The standard method was followed without adjustment. Stress and strain data are collected during each load cycle to describe the elastic and permanent strains and deviatoric stress. The load sequence is graphically represented in Figure 6.3.

Table 6.2: Load Sequence for AASHTO T 307

Sequence No.	Confining Pressure		Max. Axial Stress		Cyclic Stress		Constant Stress		No. of Load Applications
	kPa	psi	kPa	psi	kPa	psi	kPa	psi	
0	103.4	15	103.4	15	93.1	13.5	10.3	1.5	500 – 1,000
1	20.7	3	20.7	3	18.6	2.7	2.1	0.3	100
2	20.7	3	41.4	6	37.3	5.4	4.1	0.6	100
3	20.7	3	62.1	9	55.9	8.1	6.2	0.9	100
4	34.5	5	34.5	5	31.0	4.5	3.5	0.5	100
5	34.5	5	68.9	10	62.0	9.0	6.9	1.0	100
6	34.5	5	103.4	15	93.1	13.5	10.3	1.5	100
7	68.9	10	68.9	10	62.0	9.0	6.9	1.0	100
8	68.9	10	137.9	20	124.1	18.0	13.8	2.0	100
9	68.9	10	206.8	30	186.1	27.0	20.7	3.0	100
10	103.4	15	68.9	10	62.0	9.0	6.9	1.0	100
11	103.4	15	103.4	15	93.1	13.5	10.3	1.5	100
12	103.4	15	206.8	30	186.1	27.0	20.7	3.0	100
13	137.9	20	103.4	15	93.1	13.5	10.3	1.5	100
14	137.9	20	137.8	20	124.1	18.0	13.8	2.0	100
15	137.9	20	275.8	40	248.2	36.0	27.6	4.0	100

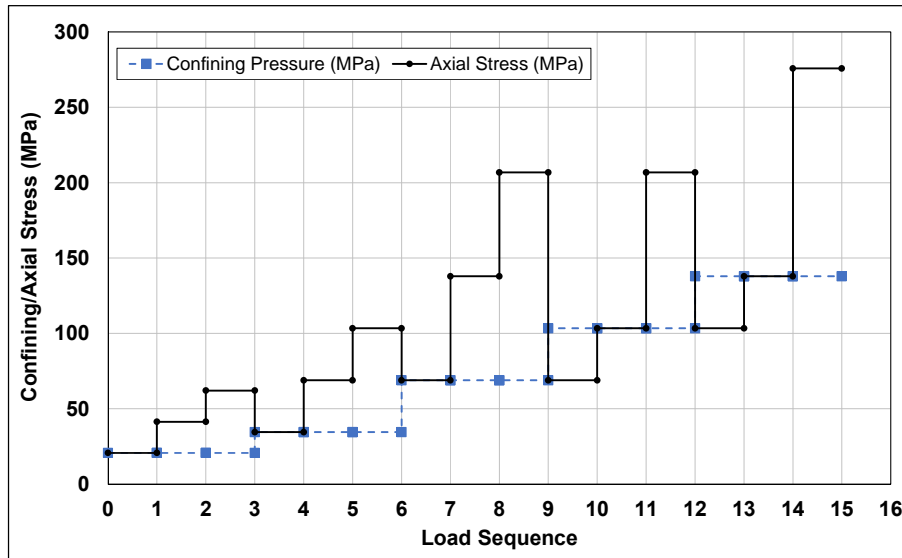


Figure 6.3: Load sequence for AASHTO T 307.

The mixed material was compacted in 25 mm (1.0 in.) lifts to prepare indirect tensile modulus specimens 152 mm (6.0 in.) in diameter and 63 mm (2.5 in.) high, and resilient modulus specimens 152 mm (6.0 in.) in diameter and 304 mm (12 in.) high (specifically three lifts for indirect tensile modulus specimens and 12 lifts for resilient modulus specimens). Compaction was achieved with a vibrating hammer (Figure 6.4) fitted with a 148 mm compaction head. A scouring tool was used to roughen the compacted face after each lift to ensure complete bonding between consecutive lifts (Figure 6.5). Specimens were extracted

immediately after compaction, and placed in a curing chamber for the predetermined delay times between compaction and microcracking. The curing chamber was maintained at a temperature of 25°C (77°F) and 100 percent humidity for the duration of the study. Individual specimens were removed from the chamber when scheduled for testing, tested, and then replaced in the humidity chamber until the next testing cycle.



Figure 6.4: Vibrating compaction hammer with 148 mm compaction attachment.



Figure 6.5: Scouring tool: general view and bottom view.

6.6 Microcracking

Microcracking of the specimens was carried out following the method described in Section 5.4 at the intervals listed in Table 6.1, which span the current Caltrans specification requirements that microcracking be completed between 48 and 72 hours after completion of compaction on FDR projects.

6.7 Assessment of Stiffness

A universal testing machine was used to evaluate the following parameters for specimens conditioned and microcracked according to the testing factorial in Table 6.1:

- Resilient modulus
- The effect of bulk stress
- The effect of shear stress
- The effect of cement content on stiffness gain
- Stiffness before and after microcracking
- The effect of curing age

6.7.1 Resilient Modulus

The average resilient modulus of specimens tested at the same curing age, with respect to the load sequence number, is plotted in Figure 6.6 for specimens with three and four percent cement with no microcracking. An initial assessment of the data indicates that the magnitude of the measured resilient modulus was in the region of 1,000 MPa and lower than expected. The material used to prepare the specimens was collected from an FDR-FA project (23) where the backcalculated stiffness of the material in the field was calculated to be about 3,000 MPa. Backcalculated stiffnesses on the FDR-PC projects discussed in Chapter 3 ranged between 3,000 MPa and 10,000 MPa, which is considerably higher than the stiffnesses measured in the laboratory.

6.7.2 Effect of Bulk Stress

The resilient moduli of the control specimens (no microcracking) measured at different curing times and stress states are plotted in Figure 6.7 with respect to the bulk stress ($\theta = 3\sigma_0 + \sigma_d$, where σ_0 is the confining stress and σ_d is the deviatoric stress). The results indicate that the resilient modulus is positively correlated with bulk stress. This is consistent with results from Puppala (28), Potturi (29), and Amini (53). The significant stress dependency of the resilient modulus implies that cement-stabilized mixes behave similarly to weakly bound granular materials.

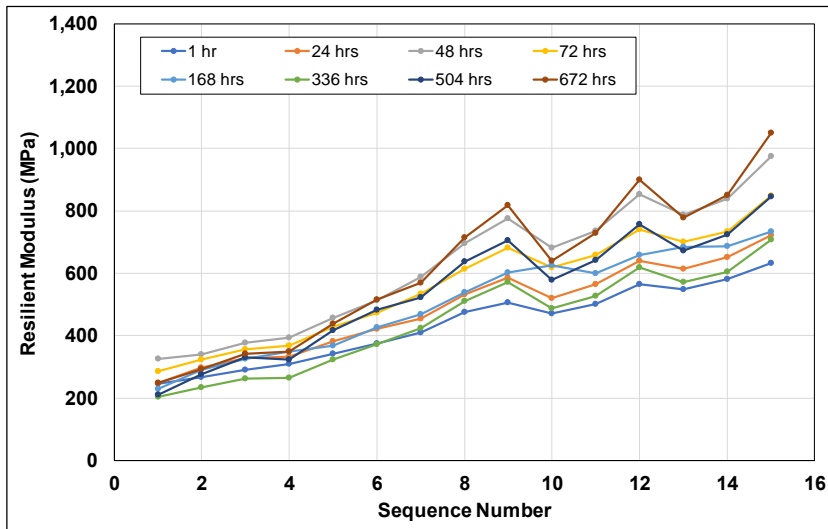
No consistent trends between resilient modulus and curing age were apparent in Figure 6.6 and Figure 6.7. This suggests that the test setup used was not able to measure the expected increase in stiffness of cement-stabilized materials over time, nor was it able to replicate stiffness-change trends measured on field projects with an FWD (see Section 3.8).

6.7.3 Effect of Shear Stress

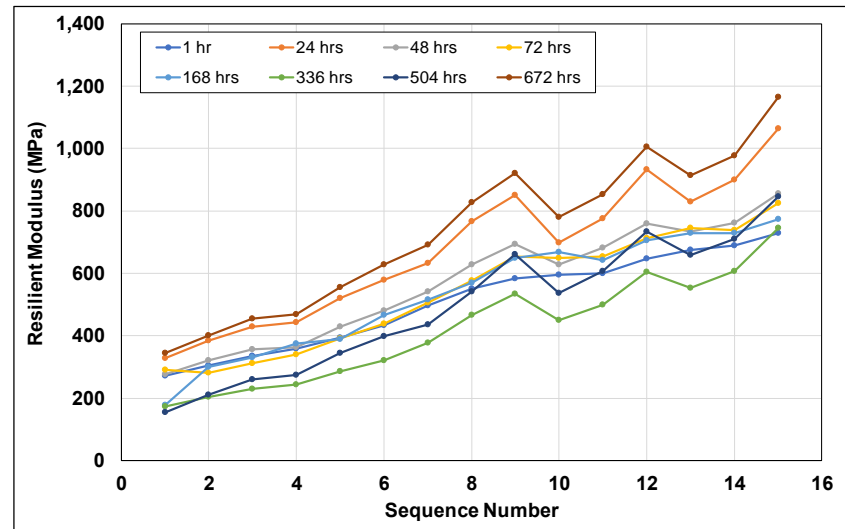
The effect of changes in shear stress is shown Figure 6.8. The sensitivity of the resilient modulus to changes in the octahedral shear stress ($\tau_{oct} = \sqrt{2}\sigma_d/3$), which is a function of the deviatoric stress, in the triaxial stress state are clearly apparent, with a trend of increasing resilient modulus with increasing deviatoric stress, indicating that the material is stress hardening.

6.7.4 Effect of Cement Content

Increasing the cement content from 3 percent to 4 percent did not have a significant effect on the resilient modulus in these tests, as shown in Figure 6.9; this was an unexpected result given the sensitivity of the unconfined compressive strengths to the two cement contents.

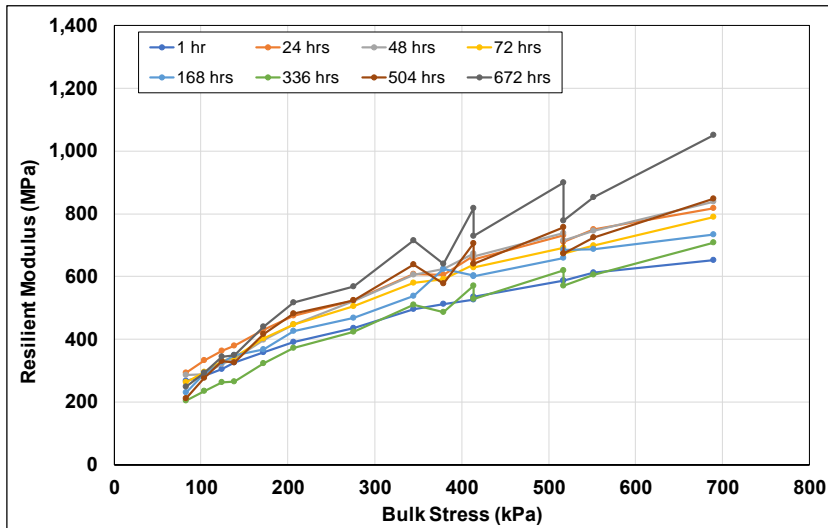


3% cement, no microcracking

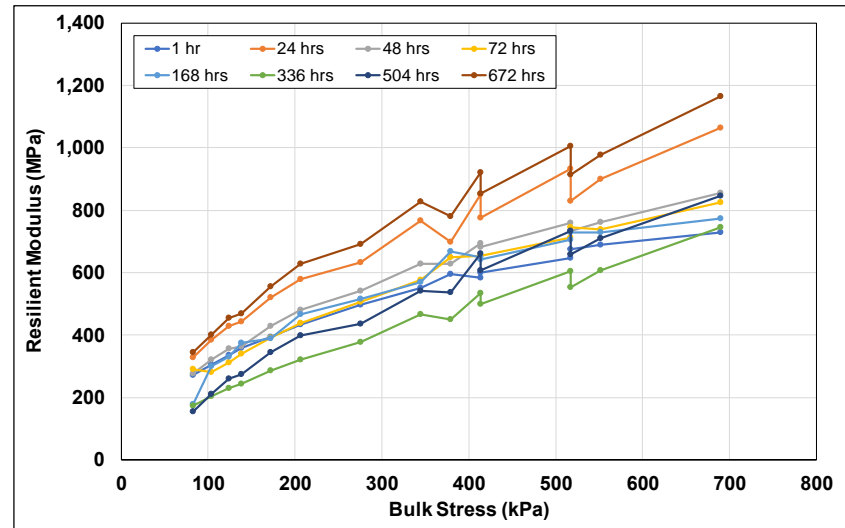


4% cement, no microcracking

Figure 6.6: Resilient modulus vs. curing time (3% and 4% cement, no microcracking).

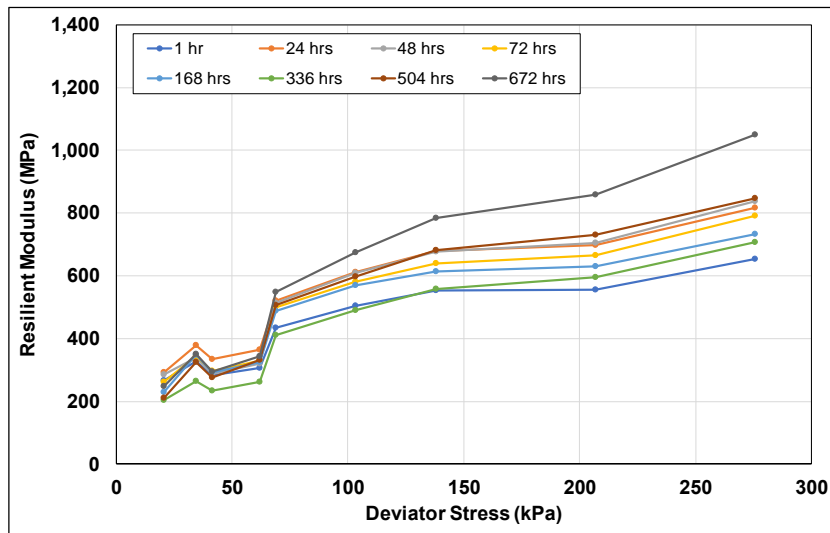


3% cement, no microcracking

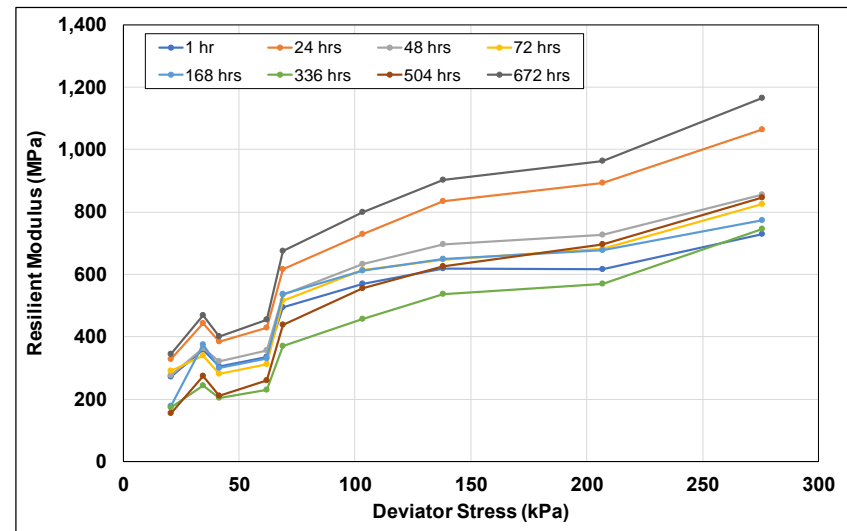


4% cement, no microcracking

Figure 6.7: Resilient modulus vs. bulk stress (3% and 4% cement, no microcracking).



3% cement, no microcracking



4% cement, no microcracking

Figure 6.8: Resilient modulus vs. deviatoric shear stress (3% and 4% cement, no microcracking).

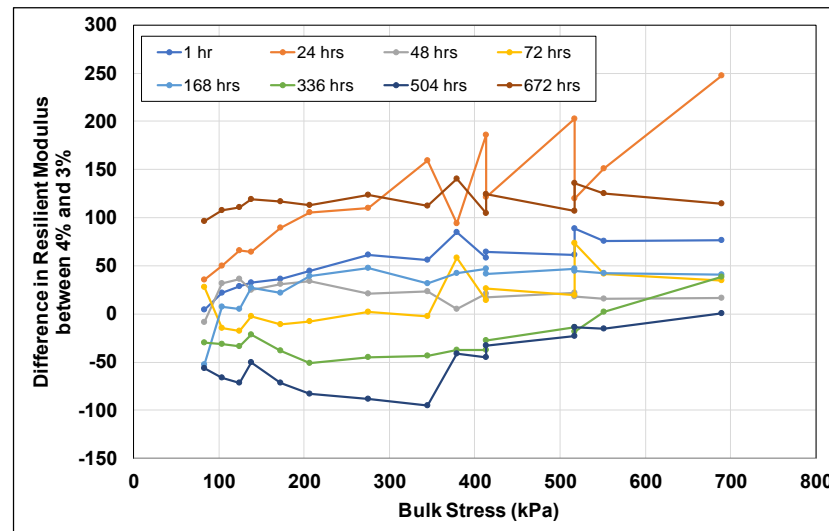


Figure 6.9: Difference in resilient modulus between 3% and 4% cement content.

6.7.5 Stiffness Before and After Microcracking

Microcracking was applied to specimens after 24, 48, and 72 hours. Resilient modulus tests were performed before and after microcracking. The effects of microcracking on the mean resilient modulus of specimens prepared at both cement contents is shown in Figure 6.10 through Figure 6.12. The specimens prepared with 3 percent cement and microcracked after 24 hours failed during microcracking and therefore a resilient modulus for them after microcracking could not be determined.

Figure 6.10 and Figure 6.11 show that the microcracking process had little to no effect on the specimens prepared with 4 percent cement and microcracked after 24 and 48 hours, respectively. Microcracking effectively reduced the stiffness of the specimens prepared with 3 percent cement and cured for 48 and 72 hours.

6.7.6 Effect of Curing Age

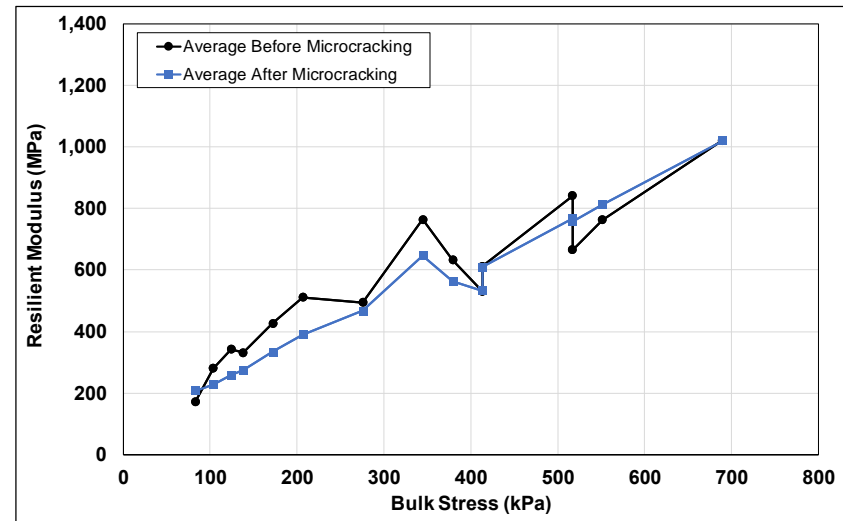
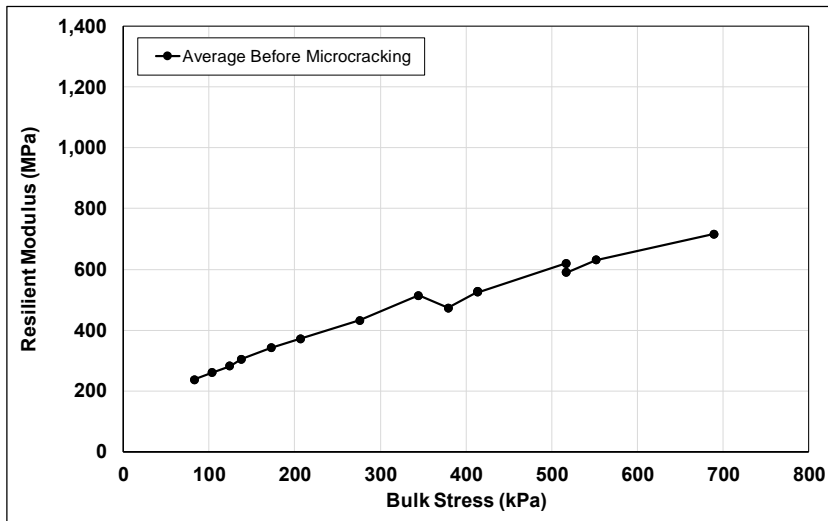
The average resilient modulus before and after microcracking for each loading sequence is plotted with respect to curing age in Figure 6.13. The resilient modulus generally increased with curing age, but some results were inconsistent with this trend, which could not be explained given that the testing procedures were consistent for all the specimens.

6.7.7 Discussion

Several inconsistencies in the results discussed in the previous sections point to the resilient modulus data not being representative of the stiffnesses backcalculated from FWD measurements on FDR-PC field projects, and behavior that is not representative of lightly cemented materials. Based on these observations, a thorough evaluation of the procedures followed and the test setup used was initiated, primarily focused on why the resilient modulus did not increase with increasing cement content and increasing curing time, why changes in stiffness were inconsistent over time, and what effect confining stress had on the results.

The AASHTO T 307 method was originally developed for unstabilized materials. Consequently, results from tests on stabilized materials need to be interpreted with care given these materials typically have higher stiffnesses than most unbound materials. After some preliminary study, the following conclusions were drawn:

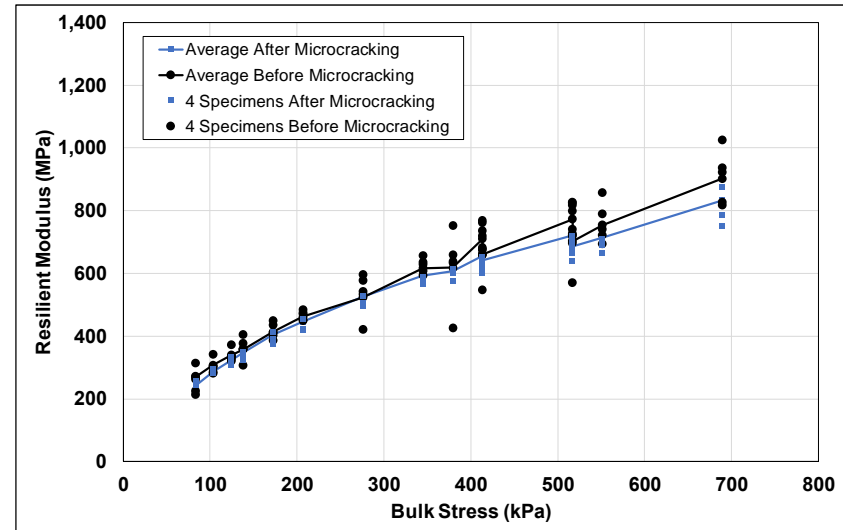
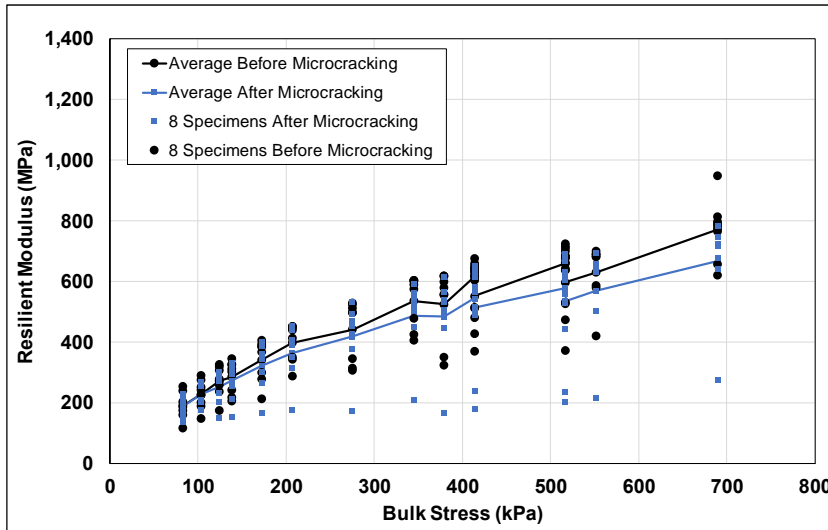
- Laboratory-determined stiffnesses are highly dependent on how the linear variable displacement transducers (LVDTs) are mounted. In particular, LVDTs mounted on specimens recorded much higher and more representative stiffnesses than the external LVDT mounting setups prescribed in AASHTO T 307.



3% cement

4% cement

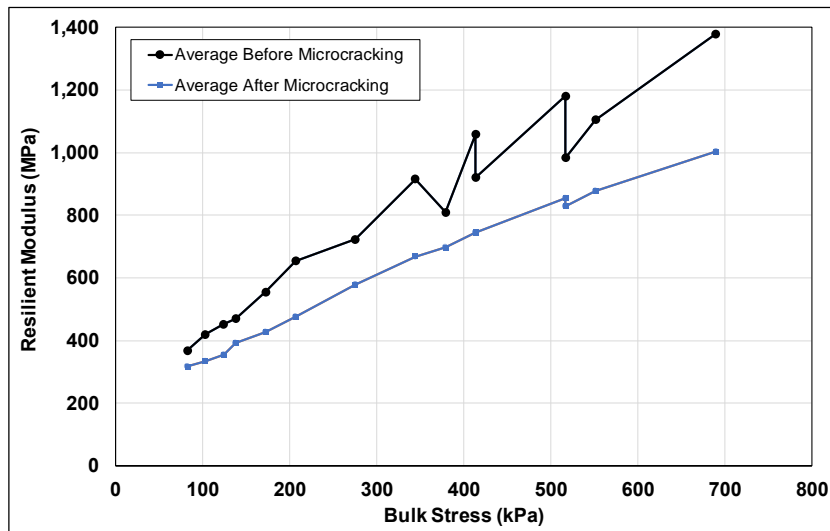
Figure 6.10: Resilient modulus before and after microcracking after 24 hours.



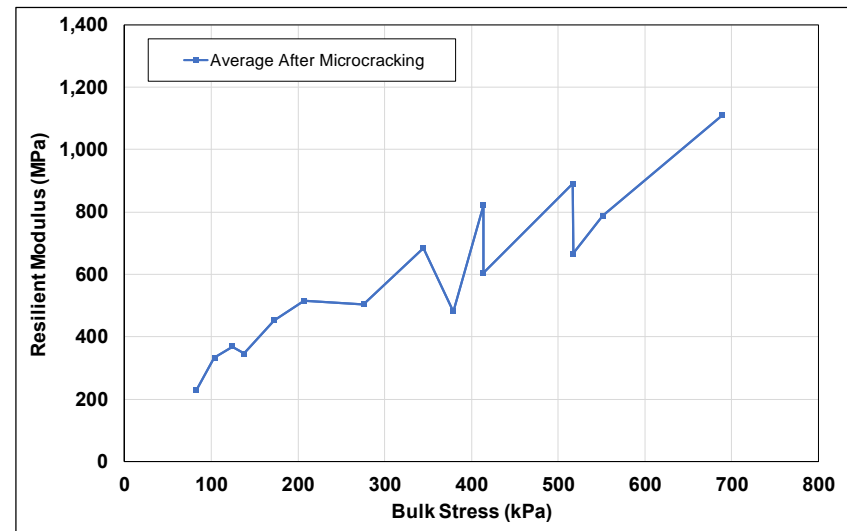
3% cement

4% cement

Figure 6.11: Resilient modulus before and after microcracking after 48 hours.

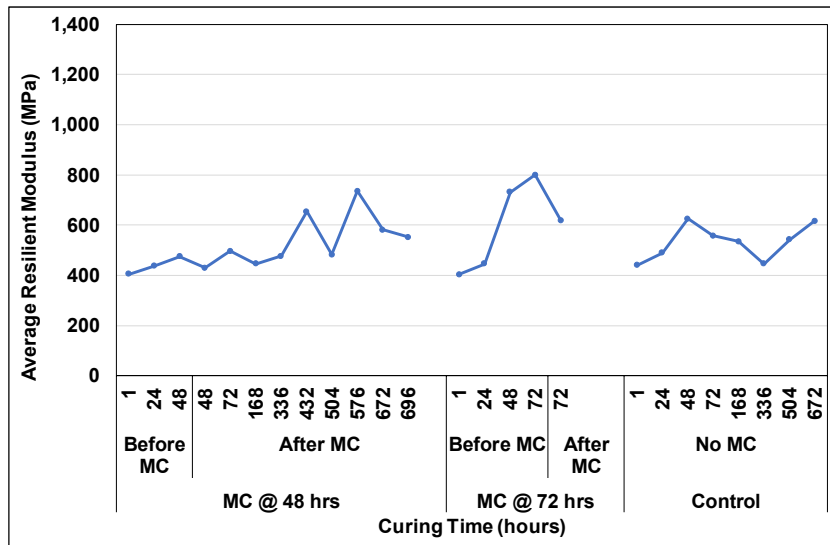


3% cement

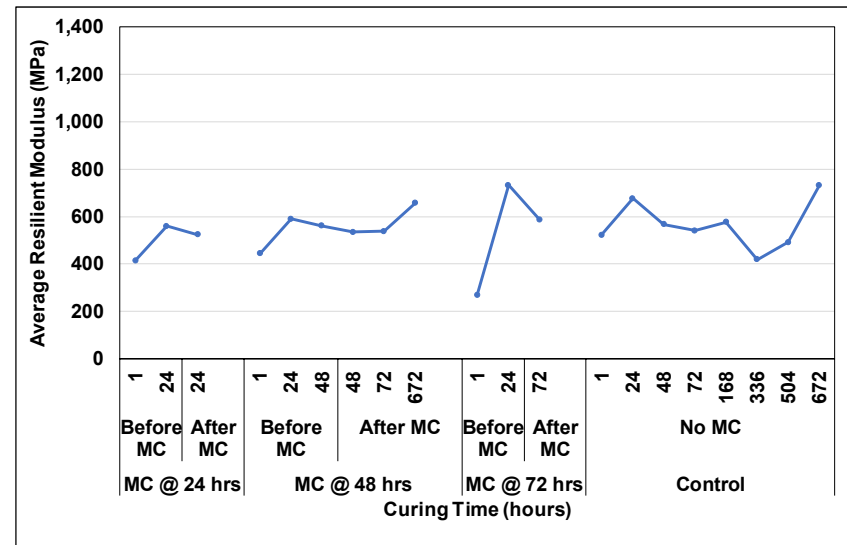


4% cement

Figure 6.12: Resilient modulus before and after microcracking after 72 hours.



3% cement



4% cement

Figure 6.13: Average resilient modulus vs. curing age before and after microcracking.

- Specimen preparation might also have a significant impact on the results since cement-stabilized specimens often have inconsistent end faces as a result of the difficulty in trimming them after compaction and because of damage done to them during extrusion from the mold and subsequent handling. In both cases, this can be attributed to the stabilized material being more brittle than unbound materials (Figure 6.14). These irregularities do not conform to the loading platens, which leads to poor contact between the platens and the specimen (Figure 6.15), which in turn leads to nonuniform stress and strain distributions that influence the axial deflection across the length of the specimen. Increasing the confinement pressure stepwise improves the contact between the specimen ends and the loading platens, and this would explain the more consistent results at higher confinement.



Figure 6.14: Broken edges caused by brittle nature of stabilized material.



Figure 6.15: Irregular specimen ends leading to poor contact.

Based on these observations, and since no conclusive information on optimal gauge location on stabilized specimens was found in the literature, a study was initiated to investigate the sensitivity of different test setups and to determine which setup provided results most consistent with the stiffnesses backcalculated from FWD testing on FDR projects. A refined specimen preparation procedure, discussed in Section 6.8 below, was also developed to address the testing inconsistencies associated with irregular specimen ends and with mounting of LVDTs.

6.8 Resilient Modulus Test Method Revision

6.8.1 Specimen Setup Procedure

Two gauge-point attachment jigs were developed for this study. The jig provided by *IPC Global* for attaching gauge-points to AMPT specimens was modified to attach gauge-points at quarter-point locations with 120° offsets on 200 mm × 100 mm specimens (i.e., cores sampled from FDR projects). The jig is shown in Figure 6.16. A second custom-built jig (Figure 6.17) was designed and built for attaching gauge-points at the same locations on 300 mm × 150 mm laboratory-prepared specimens. The jigs allow the

operator to consistently and easily locate and prepare the gauge point locations using cyanoacrylate glue, which provides a bonded surface for precisely attaching the gauge-points with epoxy.



Figure 6.16: Modified jig for mounting LVDTs on 200 mm × 100 mm specimens.



Figure 6.17: Fabricated jig for mounting LVDTs on 300 mm × 150 mm specimens.

The poor contact between the platen and the specimen as a result of compaction irregularities was addressed by capping the specimen ends with a thin layer of gypsum using a vertical cylinder capper to ensure a flat, square face for full contact with the platens. A strip of tape was applied around the top and bottom edges of the specimen prior to capping to prevent any gypsum overflow from adhering to the sides of the specimen. Excess gypsum was carefully removed from the tape before the tape itself was removed to achieve a smooth, constant-diameter specimen without dislodging any material. The gypsum had a stiffness of 15,000 MPa and a break stress of 15.3 MPa, based on testing a 200 mm × 100 mm specimen after a one-day cure at 25°C. This was higher than the stiffnesses of the specimens being tested. Comparative testing with and without gypsum caps was done on an FDR-FA specimen. The gypsum caps resulted in an increase in resilient modulus of approximately 400 MPa at low contact stresses and 100 MPa at high contact stresses.

It is believed that the slightly higher stiffnesses measured with the gypsum capping better represent the actual material properties due to better alignment of the specimen.

6.8.2 Test Setup Evaluation Parameters

A series of tests were performed to determine if the improved setup and specimen preparation procedures would overcome the identified problems. Test parameters included the following:

- Mounting LVDTs at different locations on the specimen to confirm the effect of non-uniform stress distribution along the length of the specimen
- Measuring the signal-to-noise ratio at low stresses to ensure the transducers were capable of accurately measuring the deflection of the stiff specimens
- Increasing the contact stresses during cyclic testing to simulate the effect that confining pressures have on the top loading platen (i.e., overcoming poor contact between the specimen and loading platen)
- Increasing cyclic axial stresses to assess the stress sensitivity of the stabilized material

Specimens

The testing was carried out on FDR-PC and FDR-FA specimens cored from the full-depth reclamation test track at the UCPRC facility. The FDR-FA specimens were included to assess test sensitivity given that they would have a significantly lower stiffness than FDR-PC specimens. FWD measurements on the test track prior to coring were backcalculated to determine a stiffness range for the cores. Mean stiffnesses of approximately 16,000 MPa and 5,000 MPa were determined for the FDR-PC and FDR-FA sections, respectively. It is acknowledged that the conditions between field and laboratory are not the same and that backcalculated results include the confinement effect of the 60 mm of asphalt concrete over the FDR layer, potentially different moisture contents, and capillary suction. The unconfined compressive strengths (UCS) of cores removed from the track were 75 MPa and 25 MPa for the FDR-PC and FDR-FA sections, respectively.

LVDT Configurations

Five different LVDT test setups (TS) on 200 mm × 100 mm specimens were investigated (Figure 6.18). Each of the test setups used three equally-spaced LVDTs, and all the tests included porous stone plates and filter paper between the specimen and the top and bottom platens (i.e., frictional specimen ends).

1. TS-1: ±0.1 mm LVDTs with a gauge length of 70 mm attached at approximately third-points over the center of the specimen (this gauge length is 4 mm longer than the gauge length required to measure at exactly third-points)
2. TS-2: ±0.1 mm LVDTs with a gauge length of 100 mm attached at quarter-points over the center of the specimen
3. TS-3: ±0.1 mm LVDTs with a gauge length of 185 mm attached near the ends of the specimen

4. TS-4: ± 1 mm LVDTs measuring the deflection between the top of the specimen and the bottom platen
5. TS-5: ± 1 mm LVDTs measuring the deflection between the top and bottom caps. This is the setup prescribed in AASHTO T 307.

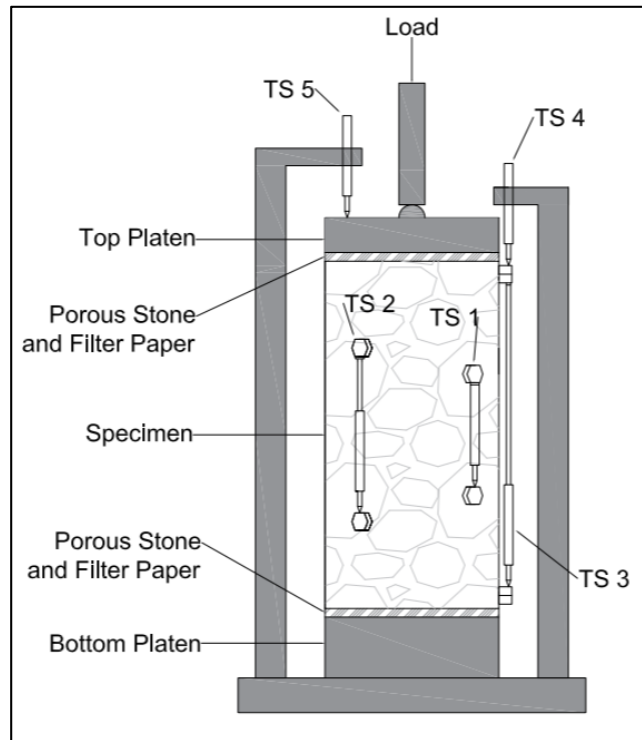


Figure 6.18: LVDT configurations for the different test setups.

TS-1, TS-2, and TS-3 focused on assessing the effects of gauge length and gauge mounting position on non-uniformity in vertical strain measurements. TS-4 and TS-5 focused on addressing the effects of cap-to-specimen interface movements. TS-1, TS-2, and TS-3 required the use of on-specimen, high-sensitivity LVDTs with a range of ± 0.1 mm. The externally mounted LVDTs used in TS-4 and TS-5 required less sensitive LVDTs with a range of ± 1 mm.

Cyclic Stress Sequences

The five test setups were evaluated by measuring the resilient modulus of FDR-PC and FDR-FA field cores under repeated loading through a range of contact and cyclic stresses as well as monotonic loading at a rate of 0.1 kN/s up to 5 kN, and unloading at a rate of 0.1 kN/s down to 0.1 kN.

The FDR-PC and FDR-FA specimens had unconfined compressive strengths (UCSs) of 75 MPa and 25 MPa, respectively. The contact stresses used for each cyclic stress were 20 kPa, 100 kPa, 180 kPa, 260 kPa, and 340 kPa (the minimum and maximum contact stresses in AASHTO T 307 are 3 kPa and 28 kPa, which correspond to UCSs typical of unbound materials). Different cyclic stresses were selected for

the FDR-PC and FDR-FA specimens to correspond with the different UCSs of each material. Cyclic stresses were based on a comparison of the mean and coefficient of variation of the resilient modulus for the different test setups and stress states to determine which test setup required the lowest stress state to measure the representative strain for stiffness calculations without breaking the specimen. The cyclic stresses selected for FDR-PC tests were 93 kPa, 138 kPa, and 300 kPa, and those for FDR-FA tests were 62 kPa and 93 kPa (the cyclic stresses in AASHTO T 307 range between 18 kPa and 248 kPa). The tests were performed in the test setup sequence (i.e., TS-1 through TS-5), with TS-1 repeated at 300 kPa after TS-5 to determine the extent of permanent damage in the specimen as a result of the repeated load tests.

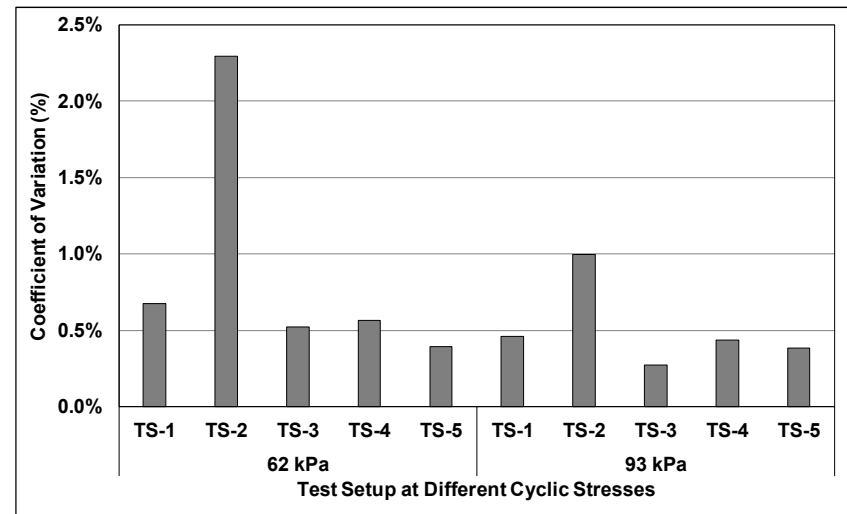
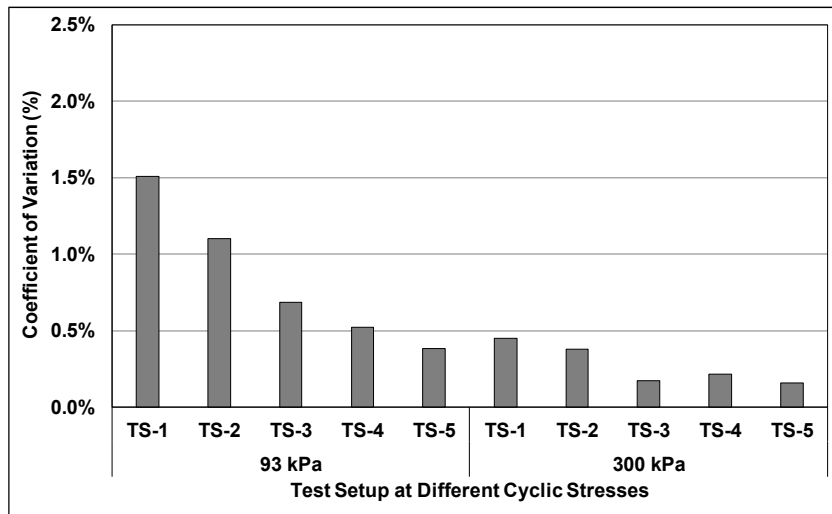
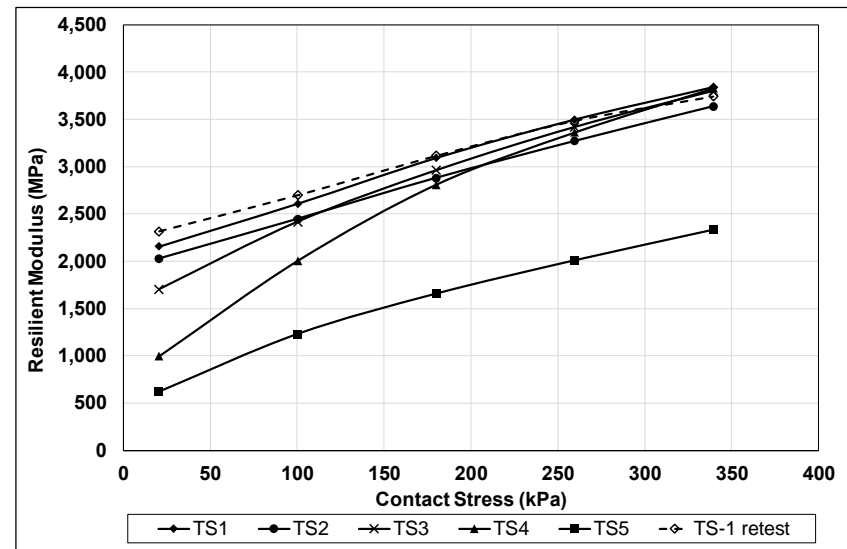
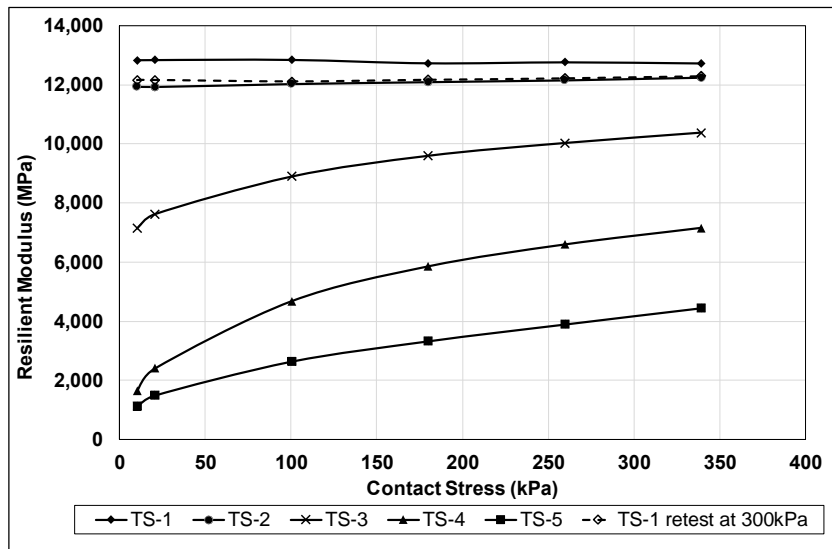
6.8.3 Resilient Modulus Test Results

The average resilient modulus test results for the five different test setups on FDR-PC and FDR-FA specimens, and the corresponding coefficients of variation, are shown in Figure 6.19. Test results for each of the cyclic stresses on the FDR-PC specimens are shown in Figure 6.20.

Discussion of FDR-PC Test Results

The following observations were made from the FDR-PC test results:

- Specimens tested using TS-1 and TS-2 had similar calculated resilient moduli consistent with backcalculated FWD results. The moduli were significantly different from those determined with TS-3, which implies that the vertical strain is approximately the same from the center to the quarter-points of a specimen, but that it changes considerably toward the ends.
- The resilient moduli determined using TS-4 and TS-5 were significantly lower than those determined using TS-3, which indicates that there was significant movement in the top and bottom cap-to-specimen interfaces.
- The difference between resilient moduli determined using TS-1 and TS-3 decreased with increasing contact stress, which suggests that the vertical strain became increasingly uniform with the overall stress increase. However, the difference between the TS-3 and TS-5 results remained relatively constant with increasing contact stress, indicating that cap-to-specimen interface movements are not sensitive to contact stress.
- The FDR-PC material appeared to be stress sensitive under the TS-3, TS-4, and TS-5 setups, implying that the material was stress hardened, which would disagree with Loveday's theoretical model (49) but would agree with the observations by Taylor (37), Shockley et al. (38), and Peng (39). However, when the measured area is at third- or quarter-points (TS-1 or TS-2, respectively) around the specimen center, the specimen's response is largely insensitive to stress change.
- There was minimal difference recorded in modulus for each of the cyclic stresses recorded for TS-2, attributable to the longer gauge length, which would produce a higher signal-to-noise ratio compared to TS-1 (discussed below).
- The coefficient of variation decreased with increasing cyclic load, as expected, due to larger resilient deflections and lower signal-to-noise ratios of the transducers at higher stresses. The coefficients of variation for all the test setups and stress levels were less than 1.5 percent, which is considered to be acceptable for this test.



FDR-PC

FDR-FA

Figure 6.19: Average resilient modulus test results for FDR-PC and FDR-FA specimens.

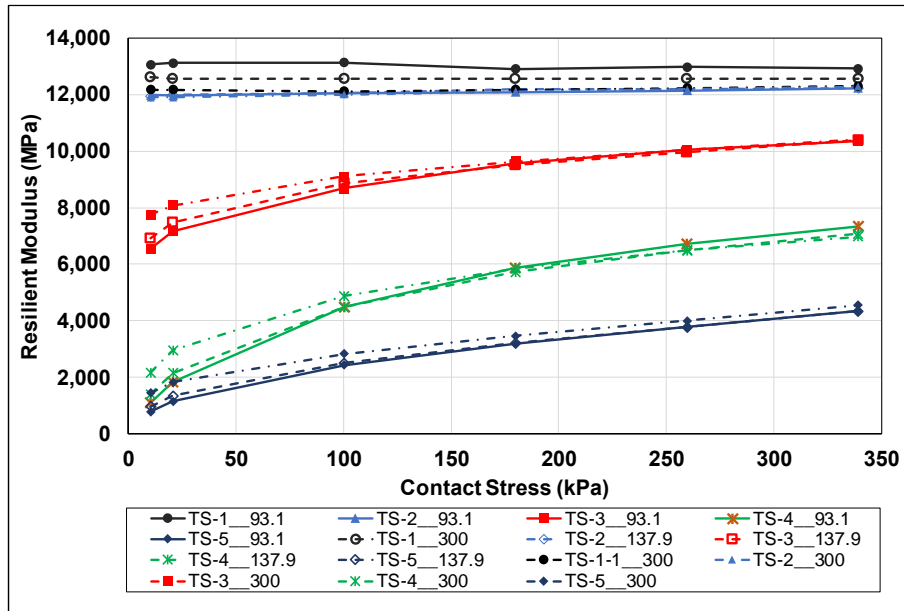


Figure 6.20: Resilient modulus test results at each cyclic stress for FDR-PC specimens.

- The laboratory test setup shown in Figure 2.17 corresponds with TS-5, which measured very low contact stress levels on the specimens. By using a different test setup, the laboratory-determined stiffness of an FDR-PC specimen increased from 1,000 MPa determined using TS-5, to 12,000 MPa determined using TS-2, and 13,500 MPa determined using TS-1.
- There was a decrease of about 1,500 MPa (~11.5 percent) in stiffness between the initial TS-1 test and the final TS-1 retest. This decrease in stiffness over the course of the six tests was considered to be too small to have had an impact on the observations discussed above.

Discussion of FDR-FA Test Results

The following observations were made from the FDR-FA test results:

- The resilient moduli calculated for FDR-FA specimens tested using TS-1 and TS-2 were similar and also consistent with backcalculated FWD stiffnesses.
- The TS-3 results were significantly lower at the lower contact stress, but they increased significantly to within the same range as TS-1 and TS-2 when the contact stress was increased. This indicates that the vertical strain distribution was relatively consistent from the center to the quarter-points of the specimen, and that vertical strain distribution became more consistent over the specimen as the contact stress increased.
- The resilient moduli determined using TS-4 and TS-5 were significantly lower than those determined using TS-3, which is consistent with the FDR-PC results and indicates significant movement in the top and bottom cap-to-specimen interfaces. Changes in contact stress had little effect, indicating that the cap-to-specimen interface movements were not sensitive to this stress.
- The coefficients of variation measured were small for all the test setups and within an acceptable range, except for TS-2, which was likely caused by a poor connection between the LVDT and the gauge-point.

- The difference between the resilient moduli determined using TS-1 at 62 kPa and 93 kPa cyclic stresses was on average 57 MPa. TS-2 had a similar mean difference of 42 MPa. The mean calculated resilient modulus difference for specimens tested with TS-1 and TS-2 was 180 MPa, with resilient moduli determined using TS-1 higher than TS-2.
- There was a slight increase of about 160 MPa in stiffness between the initial TS-1 test and the final TS-1 retest, at the lower contact stress, and a decrease of 100 MPa at the higher contact stress. This difference was likely caused by a small temperature change in the specimen, and was also considered too small to have altered the observations discussed above.

6.8.4 Monotonic Test Results

The stress-strain results from monotonic tests on the FDR-PC and FDR-FA specimens are summarized in Figure 6.21. The results for each test setup ranked similar to those recorded in the resilient modulus tests, with the highest stiffness (i.e., slope) recorded when using TS-1 and the lowest recorded when using TS-5. The large difference in measured strain between those for TS-1, TS-2, and TS-3 and those recorded for TS-4 and TS-5 is believed to correspond to the cap-to-specimen interface movement.

6.8.5 Signal-to-Noise Ratio

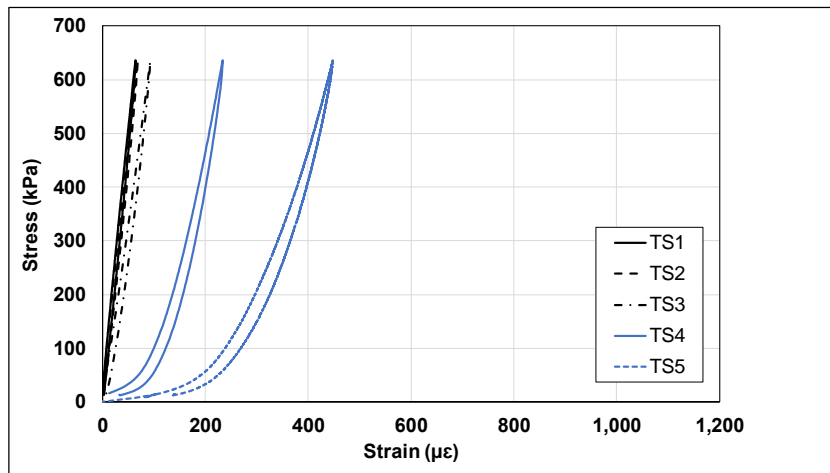
The level of noise in analog and digital instrumentation can be evaluated with the signal-to-noise ratio (SNR), which is a measure of the signal strength relative to the background noise. The SNR for this study was defined as the ratio of the minimum peak signal response during the 0.1 second haversine cyclic stress, to the absolute maximum error from the linear signal response during the last 0.85 seconds of the 0.9 second rest period, for the 100 cycles applied during the resilient modulus testing (Figure 6.22). Since the resilient strain is calculated without a smoothing function on the strain signal, the effects of the noise are included in the resilient strain. Yeo (54) recommended an SNR above 10 for resilient modulus tests on stabilized materials. The SNR for Hilbrich's tests (44), discussed above, was below four.

The difference in the results from the five test setups was attributed in part to different signal-to-noise ratios resulting from the different LVDT configurations. The signal-to-noise ratio for each cyclic and loading stress combination was calculated according to Figure 6.22. The possible error was calculated using Equation 6.1:

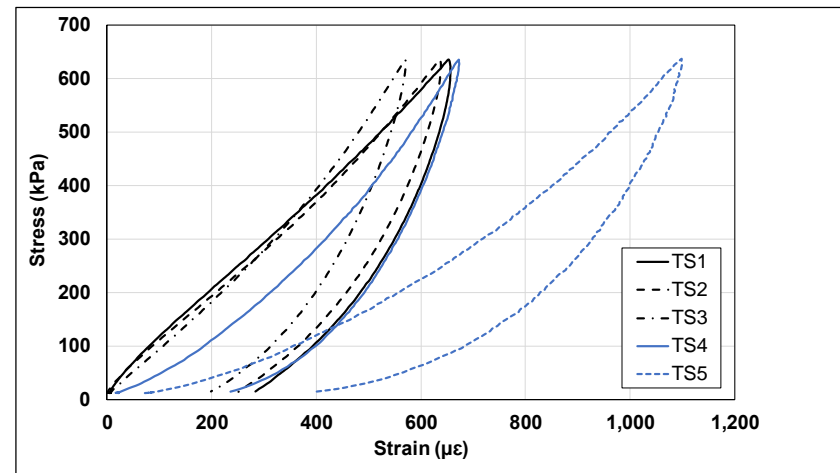
$$\frac{1}{SNR} * M_R \tag{6.1}$$

where M_R is the average resilient modulus calculated for each sequence.

Results for TS-1 and TS-2 are shown in Table 6.3. The possible error in the calculation of the resilient modulus was relatively large for TS-1 compared to TS-2 for each of the cyclic stresses.



FDR-PC



FDR-FA

Figure 6.21: Monotonic test results.

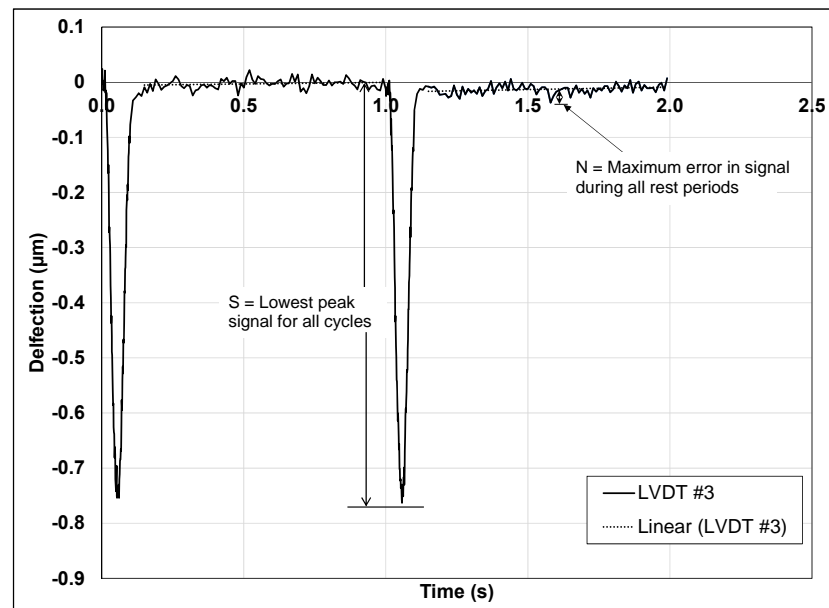


Figure 6.22: Schematic of signal-to-noise ratio.

Table 6.3: Signal-to-Noise Ratio and Potential Error for TS-1 and TS-2.

Contact Stress (kPa)	SNR					Potential Error (MPa)				
	TS-1		TS-2			TS-1		TS-2		
	93.1 ¹	300	93.1	137.9	300	93.1	300	93.1	137.9	300
20	21.0	67.7	31.3	46.5	87.4	624.2	185.7	382.2	257.9	136.0
100	21.7	67.8	31.6	45.3	83.8	606.3	185.2	382.0	265.9	143.2
180	21.3	66.8	31.8	45.7	84.5	606.3	188.1	379.5	266.5	143.5
260	21.2	66.2	31.8	44.2	86.5	612.7	189.8	381.8	276.0	140.8
340	21.4	66.5	29.6	40.0	89.1	603.9	188.5	413.5	306.1	137.8

¹ Cyclic stress (kPa)

Mean signal-to-noise ratios measured on an FDR-PC specimen with TS-1 through TS-5 at a cyclic stress of 93 kPa were 14, 21, 57, 86, and 123, respectively, all well above the minimum recommended SNR of 10. The mean ratios recorded on TS-1 through TS-5 on FDR-FA specimens with a contact stress of 20 kPa and cyclic stress of 62 kPa were 23, 27, 30, 42, and 44, respectively. TS-1 was expected to have the lowest ratio due to the short gauge length of the LVDTs and the relatively high stiffness of the specimen. Signal-to-noise ratios also increased with increasing cyclic stress, as expected. The raw deflection data recorded by the LVDTs on an FDR-PC specimen using TS-1 at 93 kPa and 300 kPa cyclic stresses at a contact stress of 20 kPa are provided in Figure 6.23.

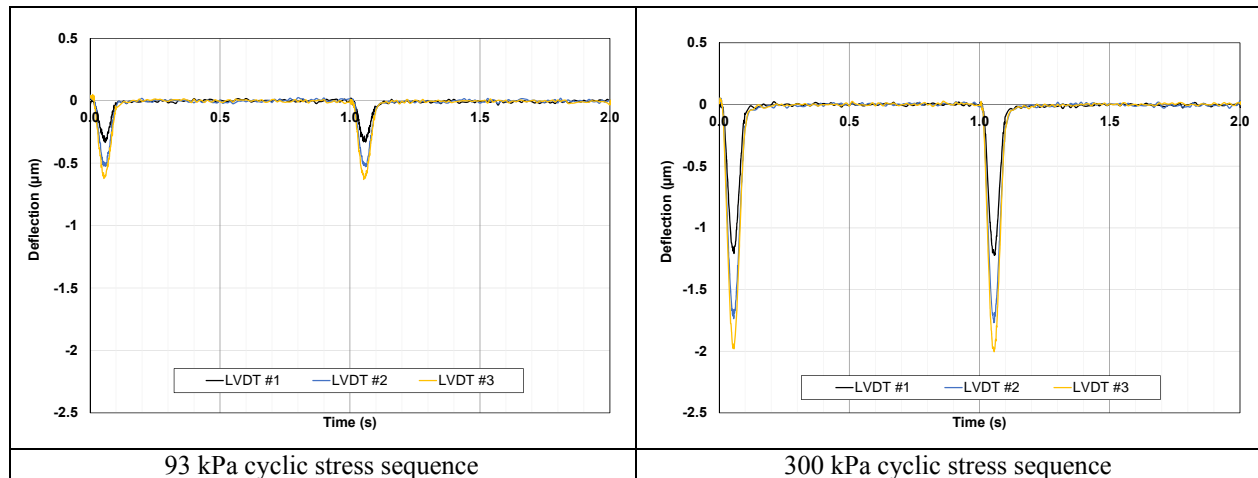
**Figure 6.23: LVDT responses measured using TS-1.**

Figure 6.23 also shows that the specimen did not deflect uniformly during the test. The signal-to-noise ratio for the 93 kPa cyclic stress was 9 for LVDT #1 and 17 for LVDT #3, increasing with increasing cyclic stress to 33 and 50, respectively, at 300 kPa. This trend was routinely observed over the course of resilient modulus testing for the project and was attributed to non-uniform contact with the end platens and the known inherent non-homogeneity of laboratory-compacted and field-cored specimens. The use of at least three LVDTs is considered essential to better accommodate this variability and to better capture the representative average response of the specimen to stress.

6.8.6 Discussion

Both TS-1 and TS-2 provided resilient moduli within the expected range of backcalculated FWD stiffnesses on the same materials. Both of these setups also produced results that conform to the theory that cemented materials are not sensitive to stress changes until the cemented bonds break down (49). However, TS-1 had a higher than desirable signal-to-noise ratio when testing very stiff materials such as FDR-PC. The high ratio introduces possible errors in the calculation of the resilient modulus that are difficult to quantify and could produce results that incorrectly imply that the material is stress sensitive. The cyclic stresses prescribed in AASHTO T 307 are within the lower range of vertical stresses induced in the field by traffic; however, the upper stress (248.2 kPa) may induce permanent damage during the test, and consequently incorrect stiffness values.

TS-2 also has minor drawbacks in that it includes the effect of non-uniform stress distribution. This effect is small compared to the results obtained using TS-1 at high cyclic stress levels. The results for TS-2 also show a slight stress sensitivity with increased contact stresses, but this is considered negligible compared to the magnitude of the average resilient modulus and the consistency of the results for each cyclic stress.

Although TS-1 is considered to be the most appropriate for resilient modulus testing, the LVDTs that are currently available for this configuration are insufficiently sensitive and lead to high signal-to-noise ratios (testing with a cyclic stress of 93.1 kPa requires an LVDT range of 0.3 μm , which is 0.2 percent of the range of the LVDTs used [range of $\pm 0.1 \text{ mm}$]). TS-2 was therefore selected for all future testing until LVDTs with a shorter gauge length and a higher resolution are available for TS-1.

6.9 Phase 1b Conclusions and Recommendations

The results from the Phase 1b laboratory experiment were considered to be unrepresentative of field conditions. Factors contributing to this include the following:

- The laboratory-determined resilient moduli using the conventional AASHTO T 307 setup were too low compared to backcalculated FWD stiffnesses.
- The sensitivity to confining stress of the resilient modulus of FDR-PC materials determined using the conventional AASHTO T 307 setup suggests that the material behaves more like an unbound material, which is unlikely given the cemented nature of the material.
- Testing with the conventional AASHTO T 307 setup could not effectively differentiate between the different cement contents of different curing intervals.

A new test setup is proposed for future testing. This setup produced results that matched backcalculated FWD stiffness and showed that cement-stabilized material is not sensitive to confining pressure. This method will be used for Phase 2 testing. Other recommendations for Phase 2 testing include the following:

- Develop a more consistent method of specimen compaction that reduces or eliminates operator bias. The compaction frame developed by *Wirtgen* is proposed for further evaluation.
- Develop a more appropriate method to induce microcracking in compacted specimens. The method must simulate microcracking on FDR projects. Two approaches are proposed for further study:
 - + Use the *Wirtgen* compaction frame to induce microcracking in the previously compacted specimens. Specimens will need to be placed back into the compaction mold after preliminary curing and subjected to a controlled period of vibration under load. Testing will need to determine whether microcracking can be satisfactorily induced throughout the specimen or whether only the surface of the specimen is damaged.
 - + Use a universal testing machine to simulate the vibration and stress of a steel wheel vibrating roller. The method should be a cyclic and stress controlled to reduce the stiffness of the confined specimen to a set percentage.

7. CONCLUSIONS AND RECOMMENDATIONS

7.1 Summary

The California Department of Transportation (Caltrans) has been using full-depth reclamation (FDR) as a rehabilitation strategy since 2001. Most projects to date have used a combination of foamed asphalt and portland cement as a stabilizing agent. Recently though, the increasing cost of asphalt binder coupled with the relatively complex mix-design procedure for foamed asphalt has generated interest in the use of portland cement (FDR-PC) alone as an alternative stabilizing agent, where appropriate. However, the high initial stiffness and shrinkage cracking associated with the hydration and curing of the cement-treated layers remains a concern, especially with regard to crack reflection through asphalt concrete surfacings and the related problems caused by water ingress.

Considerable research has been undertaken on crack mitigation on FDR-PC projects, and a range of measures related to improved mix designs and construction practices have been implemented by road agencies. One of the most promising measures, used in conjunction with appropriate mix designs, is that of microcracking the cement-treated layer between 24 and 72 hours after construction. In theory, this action creates a fine network of cracks in the layer that limits or prevents the wider and more severe block cracks typical of cement-treated layers. Limited research to assess microcracking as a crack mitigation measure has been completed on a number of projects in Texas, Utah, and New Hampshire. Recommendations from these studies were first implemented by the Texas Department of Transportation and later by other state departments of transportation. However, longer-term monitoring on a range of projects in Texas and other states has revealed that microcracking has not always been successful in preventing cracking, with some projects showing reflected transverse and block cracks in a relatively short time period.

Discussions with researchers in Texas indicated that additional research was necessary to better understand the microcracking mechanism, and to identify the key factors influencing performance, including but not limited to aggregate properties, cement content, the time period before microcracking starts, layer moisture contents, roller weights and vibration settings, the number of roller passes applied, the field test methods and criteria used to assess the degree of microcracking, the time period before opening the road to traffic, and the time period before placing the surfacing. A project was therefore initiated at the University of California Pavement Research Center (UCPRC) to investigate these outstanding issues. The first phase of this study is discussed in this report, which covers the literature review, preliminary laboratory testing, and early results from field testing on four projects where microcracking was implemented.

7.2 Conclusions

7.2.1 Literature Review

A review of the literature on shrinkage crack mitigation revealed that microcracking in combination with selecting an appropriate cement content to achieve a target seven-day unconfined compressive strength of 300 psi (≈ 2.0 MPa) is likely the most appropriate approach to be implemented in California at this time given the research already conducted. The literature review also identified a range of devices that could be used for measuring the effect of microcracking on the stiffness of cement-treated layers. Each device has limitations that have not been fully quantified in terms of either their suitability for verifying whether microcracking has resulted in satisfactory stiffness reduction and/or their applicability as a microcracking quality control procedure on construction projects.

7.2.2 Field Testing

The following conclusions with regard to field testing on four FDR-PC projects in California were made based on a series of observations during construction and statistical analyses of soil stiffness gauge (SSG) and falling weight deflectometer (FWD) data:

- There was a wide variation in pavement materials and in pavement construction quality across the four projects. On the county road projects, where minimal sampling and testing appears to have been carried out in the project assessment phase, the mix designs did not necessarily accommodate the variation in materials and pavement conditions.
- Specifications are not always being followed to the fullest extent by contractors and they are not being fully enforced by agency engineers.
- In addition to being useful for assessing unbound layer thicknesses and the subgrade conditions of the existing road prior to FDR, DCP tests can also provide a quick indication of weak areas on the project after final compaction.
- The SSG can provide repeatable and reproducible results provided that the testing method is strictly adhered to and that operators are suitably trained and experienced. The variability between consecutive measurements by an experienced operator on the four projects were discussed with the SSG manufacturer.
- The SSG is useful for measuring/checking stiffness gain over time on the days between final compaction and microcracking, for dictating the number of roller passes used to achieve a satisfactory level of stiffness reduction by microcracking, and for checking that a satisfactory drop in stiffness was achieved after microcracking. It can also be used to check areas suspected of having too little or too much cement, especially those areas at the beginning and end of construction sections, and in lane overlap areas. However, the rate at which SSG testing can be conducted is slower than the pace of construction activities and more than one SSG may be required on site on the day of microcracking to keep up with the equipment.
- FWD testing provided useful insights into the stiffness change in FDR-PC layers over time and how this change is affected by material variability, the distribution of cement during construction, and the effectiveness of the microcracking process.

- FWD and SSG results both indicate that microcracking does result in an immediate and notable drop in stiffness in the FDR-PC layer after the procedure has been completed. However, much of the stiffness is recovered by recementation in the days after microcracking, after which stiffness appears to plateau. Stiffness change over time appears to be influenced by temperature; however, insufficient data has been collected to date to draw any firm conclusions about longer-term performance.

7.2.3 Phase 1a: Laboratory Microcracking Methods

Three laboratory-scale microcracking methods were considered. The method using a dual steel wheel vibrating roller to microcrack specimens in a specially constructed pit appeared to provide the best results of the three approaches, based on observations of the specimen before and after microcracking. However, given that the equipment and set up used is not standard, further experimentation using a frame-mounted vibration hammer and the same dynamic testing apparatus used for triaxial testing are recommended for further evaluation in Phase 2 of this study.

7.2.4 Phase 1b: Preliminary Laboratory Testing

The results from the preliminary laboratory testing experiment were considered to be inconclusive. Factors contributing to this include the following:

- The laboratory-determined resilient moduli using the conventional AASHTO T 307 setup were too low compared to the backcalculated FWD stiffnesses on the same material.
- The sensitivity to confining stress of the resilient modulus of FDR-PC materials determined using the conventional AASHTO T 307 setup suggested that the material behaves more like an unbound material, which is unlikely given the cemented nature of the material.
- Testing with the conventional AASHTO T 307 setup could not effectively differentiate between the different cement contents of different curing intervals.
- The resilient modulus test results did not accurately reflect the expected effects of microcracking (i.e., they were not similar to those measured on field projects with a stiffness gauge), cement content, and curing time of the laboratory-compacted specimens. The primary reason for this was attributed to the laboratory microcracking procedures developed in Phase 1a not being representative of actual microcracking procedures on FDR-PC construction projects. The approach did not appear to reduce the stiffness of the samples in a repeatable and consistent manner, and in many instances it resulted in cracking and disintegration of the specimens.
- The large variability in the resilient modulus results from tests on both the control and microcracked specimens points to the compaction method that was followed. Based on previous findings from earlier UCPRC research on FDR with foamed asphalt, the sample preparation (quartering and batching) and mixing method were considered to be consistent and unlikely to have contributed much to the variability. However, the compaction method used, although consistent with the AASHTO T 307 method, was considered to be too operator dependent and probably a significant contributor to the variability.
- The brittleness of the laboratory-compacted FDR-PC samples caused the edges of the specimens to chip during handling and testing, which in turn led to tears in the latex membrane used for confining

the specimen during testing. These tears led to a loss of confinement, which might also have contributed to the wide variation in the test results.

7.3 Recommendations

Based on the above observations, the following recommendations are made for Phase 2:

- Develop a more consistent method of laboratory specimen compaction that reduces or eliminates operator bias. The vibrating hammer compaction frame developed by *Wirtgen* is proposed for further evaluation.
- Develop a more appropriate method to induce microcracking in compacted specimens. The method must simulate microcracking on FDR projects. Two approaches are proposed for further study in Phase 2:
 - + Use the *Wirtgen* compaction frame to induce microcracking in the previously compacted specimens. Specimens will need to be placed back into the compaction mold after preliminary curing and subjected to a controlled period of vibration under load. Testing will need to determine whether microcracking can be satisfactorily induced throughout the specimen or whether only the surface of the specimen is simply damaged.
 - + Use a universal testing machine to simulate the vibration and stress of a steel wheel vibrating roller. The method should be cyclic and stress controlled to reduce the stiffness of the confined specimen to a set percentage.
- Use a new test setup for future resilient modulus testing. Preliminary testing with this setup produced results that matched backcalculated FWD stiffness closely and showed that the cement-stabilized material is not sensitive to confining pressure.
- Consider the construction and monitoring of a test road to assess outstanding construction and microcracking issues that cannot be assessed on typical FDR-PC projects on state and county roads. Key factors that need to be investigated include the effect of design strength (i.e., cement content), the time between final compaction and microcracking, roller type, roller settings, and stiffness change over time. Control sections that are not microcracked should be included for performance comparison purposes. The proposed test plan for test road construction and monitoring is discussed in Chapter 8.

8. PROPOSED PHASE 2 TEST ROAD WORKPLAN

8.1 Introduction

During the original planning of this project, it was anticipated that the literature review, the findings from Phase 1 laboratory testing, and the initial monitoring of field experiments would provide sufficient information to decide whether accelerated wheel-load testing to develop mechanistic analysis criteria was justified, and if it was justified, to design the test track. However, the findings from the literature review, discussions with other researchers working on the topic, observations and measurements during the construction of a number of FDR-PC projects on Caltrans and county roads, and early results from Phase 1 laboratory testing revealed that there were numerous fundamental questions about microcracking and its effectiveness in mitigating shrinkage cracking that have not been answered and cannot be answered with the data and experience currently available.

The most appropriate approach for answering these questions is considered to be through the construction of a full-scale test road, implementing various crack mitigation strategies, and then evaluating the stiffness behavior resulting from these strategies over time. This test road should carry only very light traffic to understand the crack mitigation process and its effectiveness without the influence to traffic loading, which could mask some of the environmental parameters that influence the crack mitigation process. The test road approach was considered to be the most appropriate to understand both the fundamentals of the microcracking mechanism, and the effects of environment (primarily climate) on the performance of pavement with the stabilized layer.

A proposal to proceed with the design and construction of a test track was presented to Caltrans at a project progress meeting on June 25, 2015. The meeting participants agreed that the test road approach was appropriate and that the workplan should be revised to accommodate this phase ahead of the originally proposed accelerated wheel-load testing phase. The revised workplan is summarized below (55).

8.2 Revised Phase 2 Test Plan

8.2.1 Task 7: Test Road Design

Test Road Identification

Numerous locations for the test road were considered. Key requirements for this test road included the following:

- The road should be as close to the UCPRC as possible to facilitate regular stiffness testing and visual assessments.

- The road should have a sufficiently long uniform section to accommodate the test factorial (i.e., approximately 1 mile [1.6 km] long).
- The road should carry very light volumes of traffic so that key crack mitigation behavior mechanisms could be assessed. A secondary advantage of having very light traffic volumes is that evaluations can be safely carried out with minimum disruption to traffic.
- The road should be surfaced with a thin surfacing (i.e., maximum 0.08 ft. [25 mm] of asphalt concrete, chip seal, cape seal, or microsurfacing) to facilitate the observation of any cracking that does occur and to optimize the usefulness of stiffness measurements recorded on the pavement structure.
- The road owner should accept that early cracking may occur on some of the test sections.

These requirements essentially excluded constructing the test road on a Caltrans or county road. This prompted the consideration of using a road on the University of California, Davis campus (considered a state road). Discussions were held with the university and a suitable road meeting the above requirements was located. Agreement was obtained from Caltrans at the June 25 meeting to use this road as the test road.

The identified roads, Brooks Road and Levee Road, are on the UC Davis West Campus (Figure 8.1) and carry very light traffic volumes. The current pavement structure consists of 0.17 ft. (50 mm) of asphalt concrete on a thin (~ 0.25 ft. [75 mm]) fine gravel layer on top of silty clay subgrade.



Figure 8.1: Proposed test road location.

Test Road Pavement Design and Construction

A 7 in. (175 mm) layer of recycled asphalt pavement will be spread on top of the existing road, shaped, and lightly compacted. This will create a structure similar to rural Caltrans routes that are typically considered

for rehabilitation with FDR. The imported RAP, the existing asphalt concrete layer, and the subgrade will be pulverized to produce a ratio of approximately 90 percent RAP to 10 percent subgrade, consistent with typical Caltrans FDR projects. Design cement contents will be determined in the laboratory to meet typical lower and upper Caltrans strength ranges (i.e., 300 and 500 psi [2.0 and 3.5 MPa]). The ratio of RAP to subgrade material will be adjusted to ensure that a minimum cement content of 2.5 percent by weight of the aggregate is required to achieve the 300 psi target strength (higher fines content and higher plasticity in the subgrade will require more cement to meet the target strength). Cement contents lower than 2.0 percent are unlikely to lead to shrinkage cracks. The same ratio will be used for the higher-strength design. Cement will be spread on top of the imported RAP material and mixed in using a reclaimer. This will be followed by primary compaction, shaping, and final compaction. Microcracking will be undertaken at the design intervals, after which the road will be surfaced with a thin surfacing.

Test Sections

The proposed factors that will be considered in the test road factorial design are summarized in Table 8.1.

Table 8.1: Factors Considered in Test Road Design

Design Strength	Parameter	Details
300 psi (~2 MPa)	Control section Roller weights Vibration amplitude	No microcracking 12 ton and >15 ton High and low (low to simulate traffic)
500 psi (~3.5 MPa)	Microcracking timing Stiffness reduction (from SSG)	48 hrs, 72 hrs, 48+72 hrs after construction 20%, 40%, 60%, 80%

The proposed test road factorial of 36 test sections, each 50 m (~ 150 ft.) long is shown in Table 8.2. Although the different microcracking actions will be applied across the full width of the road, only the eastbound lane will be evaluated (Figure 8.2). The westbound lane will be used to maneuver the roller so that the behavior on one test section will not be affected by the microcracking activities on an adjacent section. To further minimize actions on one section influencing another section, only the middle 40 m of each test section will be evaluated, with the 5 m on either end of each section being considered as a transition zone between sections.

Instrumentation

Thermocouples, moisture sensors, and strain gauges will be installed in selected sections.

Test Road Evaluation

The following evaluations will be undertaken:

- Pre-construction
 - + Visual assessment
 - + FWD measurements to determine subgrade stiffness

- + Dynamic cone penetrometer tests to determine subgrade shear strength
- + Asphalt thickness measurements
- + Material sampling for cement content and pulverizing depth determination

Table 8.2: Proposed Test Road Factorial

Cell	Design	Test Parameter	Comment
1	300 psi	Control	No microcracking
2		12 ton, low amp., 48 hrs, 3 passes	Check effect of traffic
3		12 ton, low amp., 72 hrs, 3 passes	
4		12 ton, high amp., 48 hrs, 20% reduction	Count number of roller passes
5		12 ton, high amp., 48 hrs, 40% reduction	
6		12 ton, high amp., 48 hrs, 60% reduction	
7		12 ton, high amp., 72 hrs, 20% reduction	
8		12 ton, high amp., 72 hrs, 40% reduction	
9		12 ton, high amp., 72 hrs, 60% reduction	
10		12 ton, high amp., 48 + 72 hrs, 3 pass	Assess effect of two microcracking actions
11		>15 ton, high amp., 48 hrs, 3 pass	Check effect of roller weight
12		>15 ton, high amp., 72 hrs, 3 pass	
13		>15 ton, high amp., 48 hrs, 40% reduction	
14		Spare	
15		Spare	
16		Spare	
17		Instrument calibration section	
18		Control	
19	500 psi	Control	No microcracking
20		12 ton, low amp., 48 hrs, 3 passes	
21		12 ton, low amp., 72 hrs, 3 passes	
22		12 ton, high amp., 48 hrs, 20% reduction	Count number of roller passes
23		12 ton, high amp., 48 hrs, 40% reduction	
24		12 ton, high amp., 48 hrs, 60% reduction	
25		12 ton, high amp., 72 hrs, 20% reduction	
26		12 ton, high amp., 72 hrs, 40% reduction	
27		12 ton, high amp., 72 hrs, 60% reduction	
28		12 ton, high amp., 48 + 72 hrs, 3 passes	Assess effect of two microcracking actions
29		>15 ton, high amp., 48 hrs, 3 passes	Check effect of roller weight
30		>15 ton, high amp., 72 hrs, 3 passes	
31		>15 ton, high amp., 48 hrs, 40% reduction	
32		Spare	
33		Spare	
34		Spare	
35		Calibration section	
36		Control	

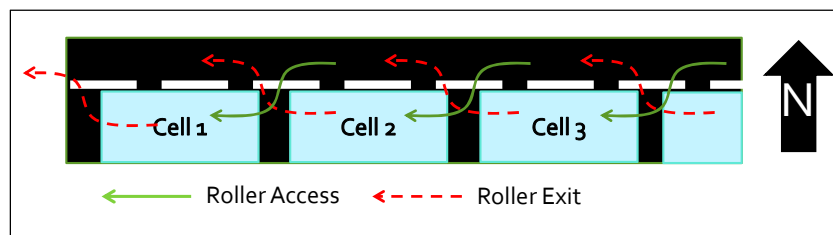


Figure 8.2: Test section planning.

- Construction
 - + Written and photographic log of all construction activities, including water curing, spraying of the prime coat and placing of the microsurfacing. Any deviations from the Caltrans specifications will be noted.
 - + Recycling depth
 - + Cement content determination
 - + Material sampling to determine moisture content, as-built gradation, and density, and to prepare specimens for as-built strength determination and for later performance testing
 - + Compaction density and moisture content
 - + Instrument installation
 - + Pre-microcracking stiffness measurements (stiffness gauge and light weight deflectometer)
 - + Post-microcracking stiffness measurements
 - + Baseline instrumentation measurements
- Post-construction
 - + Visual assessment
 - + Crack monitoring and measurement
 - + Stiffness measurements to determine stiffness gain/change (stiffness gauge and light weight deflectometer until the surfacing has been placed and/or until the equipment's measuring limits have been reached. Thereafter, FWD testing will be conducted daily for one week, every second day for the following two weeks, twice a week for the following five weeks, once a week for the following four weeks, and then twice a month until all visual observations are completed. Measurements will be taken twice on each test day to obtain a temperature range.
 - + Instrumentation measurements
 - + Weather conditions

Task 7 Deliverables

- Test road design
- Summary of observations and measurements during construction
- Summary of observations during trafficking of the test road

8.2.2 Task 8: Phase 2 Laboratory Testing

Materials and specimens sampled from the test road and other field projects will be tested in the laboratory to determine key mechanistic properties and to compare laboratory test results with results measured in the field with the stiffness gauge and FWD. Testing will focus on triaxial testing to measure stiffness change and distresses under repeated loading with the goal of identifying suitable criteria for refining mechanistic-empirical design procedures and performance models for pavements with cement-treated layers. Key test variables will be identified that can be used to refine mix designs that incorporate crack mitigation. Microscope studies will be undertaken to assess and understand the effects of crack mitigation on the cement-stabilization mechanism.

Task 8 Deliverables

- Laboratory testing factorial
- Summary of laboratory test results

8.2.3 Task 9: Phase 2 Research Report and Interim Guidelines

A research report summarizing Phase 2 testing will be prepared in this task. Results from field and laboratory testing will be used to prepare interim guidelines on crack mitigation of cement-treated layers and to prepare recommendations for revisions to specification language if considered appropriate. Recommendations for Phase 3 accelerated wheel-load testing, if considered appropriate, will also be prepared in this task.

Task 9 Deliverables

- Research report summarizing Phase 2 activities
- Draft guidelines for crack mitigation on cement-treated layers
- Recommended revisions to specification language, if considered appropriate
- Recommendations for Phase 3 accelerated wheel-load testing, if considered appropriate

REFERENCES

1. LEOCI, R. 2014. **Animal By-Products (ABPs): Origins, Uses, and European Regulations**. Mantova, Italy: Universitas Studiorum.
2. GEORGE, K.P. 2002. **Minimizing Cracking in Cement-treated Materials for Improved Performance**. Skokie, IL: Portland Cement Association.
3. ADASKA, W.S. and Luhr, D.R. 2004. Control of Reflective Cracking in Cement Stabilized Pavements. **Cracking in Pavements: Mitigation, Risk Assessment and Prevention**. Proceedings of the 5th International RILEM Conference. Bagneux, France: RILEM Publications.
4. SEBESTA, S. 2005. **Continued Evaluation of Microcracking in Texas**. College Station, TX: Texas Transportation (Report 0-4502-2).
5. ATKINSON, D.J. 1990. Evaluation of Rehabilitation Measures for Cracked Cement-treated Pavements. **Proceedings 6th Road Engineering Association of Asia and Australasia (REAAA), Conference**. Kuala Lumpur, Malaysia.
6. CHEN, D.H. 2007. Field and Laboratory Investigations of Prematurely Cracking Pavements. **Journal of Performance of Constructed Facilities, Vol. 21, 9**.
7. ZUBE, E., Gates, C.G., Shirley, E.C. and Munday, H.A. 1969. Service Performance of Cement-treated Bases as Used in Composite Pavements. **Highway Research Record, No. 13**. Washington DC: Transportation Research Board.
8. WEN, H., Muhuntham, B., Wang, J., Li, X., Edil, T. and Tinjum, J.M. 2014. **Characterization of Cementitiously Stabilized Layers for Use in Pavement Design and Analysis**. Washington, DC: Transportation Research Board (NCHRP Report 789).
9. SCULLION, T., Guthrie, S. and Sebesta, S. 2003. **Field Performance and Design Recommendations for Full-depth Recycling in Texas**. College Station, TX: Texas Transportation Institute, Texas A&M University (FHWA/TX-03/4182-1).
10. **Guide for Mechanistic-Empirical Design of New and Rehabilitated Pavement Structures**. 2004. Washington, DC: Transportation Research Board (NCHRP 1-37).
11. SCULLION, T. 2002. Field Investigation: Pre-Cracking of Soil-cement Bases to Reduce Reflection Cracking. **Transportation Research Record: Journal of the Transportation Research Board, No. 1787**. Washington, DC: Transportation Research Board.
12. NETTERBERG, F. and De Beer, M. 2012. Weak Interlayers in Flexible and Semi-Flexible Road Pavements: Part 1. **Journal of the South African Institution of Civil Engineers, Vol. 54**.
13. LUHR, D.R., Adaska, W.S. and Halsted, G.E. 2005. **Guide to Full-depth Reclamation (FDR) with Cement**. Skokie, IL: Portland Cement Association.

14. LITZKA, J. and Haslehner, W. 1995. Cold In-Place Recycling on Low-Volume Roads in Austria. **Proceedings 6th International Conference on Low Volume Roads**. Minneapolis, MN. Washington, DC: Transportation Research Board.
15. BRANDL, H., Barends, F.B.J., Lindenberg, J., Luger, H.J., de Quelerij, L. and Verruit, V. 1999. Mixed in Place Stabilization of Pavement Structures with Cement and Additives. **Proceedings Twelfth European Conference on Soil Mechanics and Geotechnical Engineering**. Amsterdam, Netherlands: Balkema.
16. SCULLION, T. 2014. **Personal Communication**. College Station, TX: Texas Transportation Institute, The Texas A&M University.
17. SEBASTA, S. and Scullion, T. 2004. **Effectiveness of Minimizing Reflective Cracking in Cement-treated Bases by Microcracking**. College Station, TX: Texas Transportation Institute, The Texas A&M University, FHWA/TX-05/0-4502-1.
18. SEBESTA, S. 2005. Use of Microcracking to Reduce Shrinkage Cracking in Cement-treated Bases. **Transportation Research Record: Journal of the Transportation Research Board, No. 1936**. Washington, DC: Transportation Research Board.
19. MILLER, H.J., Guthrie, W.S., Crane, R.A. and Smith, B. 2012. **Evaluation of Cement-stabilized Full-Depth-Recycled Base Materials for Frost and Early Traffic Conditions**. Dartmouth, MA: University of Massachusetts Dartmouth.
20. SYED, I.M. and Scullion, T. 1998. **In-Place Engineering Properties of Recycled and Stabilized Pavement Layers**. College Station, TX: Texas Transportation Institute, The Texas A&M University, TX-00/3903-S.
21. SYED, I.M. 2007. **Full-depth Reclamation with Portland Cement: A Study of Long-Term Performance**. Skokie, IL: Portland Cement Association.
22. STEYN, W. and Jones, D. 2005. **Technical Memorandum: HVS Testing of N12-19 East Section 2**. Pretoria, South Africa: Council for Scientific and Industrial Research (Contract Report CR-2005/51).
23. JONES, D., Fu, P., Harvey, J. and Halles, F. 2008. **Full-depth Recycling with Foamed Asphalt: Final Report**. Davis and Berkeley, CA: University of California Pavement Research Center (UCPRC-RR-2008-07).
24. GUTHRIE, W.S., Young, T.B., Blankenagel, B.J. and Cooley, D.A. 2005. Early-age Strength Assessment of Cement-treated Base Material. **Transportation Research Record: Journal of the Transportation Research Board, No. 1936**. Washington, DC: Transportation Research Board.
25. HOPE, C.A. 2011. **Evaluation of Portable Devices for Monitoring Microcracking of Cement-treated Base Layers**. Master of Science Thesis and Dissertation, Brigham Young University.
26. CO, H.M. 2007. **GeoGauge User Guide, Model H-4140**. Elgin, IL: Humboldt Manufacturing Company.

27. FU, P. 2009. **Micromechanics for Foamed Asphalt Stabilized Materials**. Doctor of Philosophy Thesis. University of California, Davis.
28. PUPPALA, A.J., Hoyos, L.R. and Potturi, A.K. 2011. Resilient Moduli Response of Moderately Cement-Treated Reclaimed Asphalt Pavement Aggregates. **Journal of Materials in Civil Engineering, Vol. 23, No. 7.** (pp.990-998).
29. POTTURI, A.K. 2006. **Evaluation of Resilient Modulus of Cement and Cement-Fiber Treated Reclaimed Asphalt Pavement (RAP) Aggregates using Repeated Load Triaxial Test**. Master of Science in Civil Engineering, The University of Texas at Arlington.
30. ALABASTER, D., Patrick, J., Arampamoorthy, H. and Gonzalez, A. 2013. **The Design of Stabilised Pavements in New Zealand**. New Zealand Transport Agency (Research Report No 498).
31. ARNOLD, G. 2009. Reducing the Risk of Pavement Failure and Utilisation of Local Materials in New Zealand through Repeated Load Triaxial and Beam Fatigue Tests. **Proceedings 13th International Flexible Pavements Conference, Vol. 12.** Surfers Paradise, Queensland, Australia.
32. ARNOLD, G., Werkmeister, S. and Morkel, C. 2010. **Development of a Basecourse/Sub-Base Design Criterion**. New Zealand Transport Agency. (Research Report No 498).
33. GONZALEZ, A. 2009. **An Experimental Study of the Deformational and Performance Characteristics of Foamed Bitumen Stabilised Pavements**. University of Canterbury. Ph.D. Thesis.
34. ARULRAJAH, A., Disfani, M.M., Haghighi, H., Mohammadinia, A. and Horpibulsuk, S. 2015. Modulus of Rupture Evaluation of Cement Stabilized Recycled Glass/Recycled Concrete Aggregate Blends. **Construction and Building Materials, Vol. 84.** (pp.146-155).
35. GNANENDRAN, C.T. and Woodburn, L.J. 2003. **Recycled Aggregate for Pavement Construction and the Influence of Stabilization**. Melbourne, Australia: Australian Road Research Board.
36. OLSON, R.E. and Jiunnren, L. 2004. **Apparatus Details for Triaxial Testing**. Chaoyang University of Technology, Department of Construction Engineering, Advanced Geotechnical Laboratory.
37. TAYLOR, D.W. 1940. **Soil Mechanics Research Program on Cylindrical Compression Testing in Cooperation with US Engineering Department**. Massachusetts Institute of Technology 3rd Report.
38. SHOCKLEY, W.G. and Ahlvin, R.G. 1960. Nonuniform Conditions in Triaxial Test Specimens. In **ASCE Research Conference on Shear Strength of Cohesive Soils.** (pp. 341-357).
39. PENG, S.D. 1971. Stresses Within Elastic Circular Cylinders Loaded Uniaxially and Triaxially. In **International Journal of Rock Mechanics and Mining Sciences and Geomechanics Abstracts** (Vol. 8, No. 5, pp. 399-432). Pergamon.
40. CHIU, H.K., Johnston, I.W. and Donald, I.B. 1983. Appropriate Techniques for Triaxial Testing of Saturated Soft Rock. In **International Journal of Rock Mechanics and Mining Sciences and Geomechanics Abstracts** (Vol. 20, No. 3, pp. 107-120). Pergamon.
41. BROWN, E.T. 1981. **Rock Characterization, Testing and Monitoring: ISRM Suggested Methods**.

42. BURLAND, J.B., and Symes, M.J.P.R.. 1982. A Simple Axial Displacement Gauge for use in the Triaxial Apparatus. **Geotechnique**, Vol.32, No.1.
43. Transportation Research Board (TRB). 1997. **Laboratory Determination of Resilient Modulus for Flexible Pavement Design: Final Report**. Washington, DC: The National Academies Press. NCHRP Web Document 14. <https://doi.org/10.17226/6353>.
44. HILBRICH, S.L. and Scullion, T. 2007. Rapid Alternative for Laboratory Determination of Resilient Modulus Input Values on Stabilized Materials for AASHTO Mechanistic-Empirical Design Guide. **Transportation Research Record, Journal of the Transportation Research Board No 2026**.
45. ARAYA, A.A., Molenaar, A. and Houben, L. 2010. Characterization of Unbound Granular Materials Using Repeated Load CBR and Triaxial Testing. **Proceedings GeoShanghai International Conference 2010**. Shanghai, China.
46. LOUW, S. 2014. **Characterizing Cement Stabilized Base Material Containing Reclaimed Asphalt Pavement**. Master's Thesis, Civil and Environmental Engineering. University of California, Davis.
47. GROEGER, J.L., Rada, G.R. and Lopez, A., 2003. AASHTO T 307 - Background and Discussion. **Resilient Modulus Testing for Pavement Components, ASTM STP 1437**. G.N. Durham, W.A. Marr, and W.L. De Groff, Eds. West Conshohocken, PA: ASTM International.
48. WERKMEISTER, S. 2004. **Permanent Deformation Behaviour of Unbound Granular Materials in Pavement Construction**. Doctor of Philosophy Thesis, Technical University of Dresden, Germany.
49. LOVELADY, P.L. and Picornell, M. 1990. Sample Coupling in Resonant Column Testing of Cemented Soils. **Dynamic Elastic Modulus Measurements in Materials**. ASTM International.
50. RICHART, F.E., Brandtzaeg, A. and Brown, R.L. 1928. **A Study of the Failure of Concrete under Combined Compressive Stresses**. University of Illinois at Urbana Champaign, College of Engineering. Engineering Experiment Station.
51. CAPDEVILLA, J.A. and Rinaldi, V.A. 2015. Stress-Strain Behavior of a Heterogeneous and Lightly Cemented Soil under Triaxial Compression Test. **Electronic Journal of Geotechnical Engineering, Vol. 20, No. 6**. (pp.6745-6760).
52. VINSON, T.S., Wilson, C.R. and Bolander, P. 1983. Dynamic Properties of Naturally Frozen Silt. **Proceedings Fourth International Conference on Permafrost**. Washington, DC: National Academy Press.
53. AMINI, Y. and HAMIDI, A., 2014. Triaxial Shear Behavior of a Cement-Treated Sand–Gravel Mixture. **Journal of Rock Mechanics and Geotechnical Engineering, Vol. 6, No. 5**, pp.455-465.
54. YEO, R. 2008. **The Development and Evaluation of Protocols for the Laboratory Characterisation of Cemented Materials** (No. AP-T101/08).

55. JONES, D and Harvey, J. 2014. **Pavement Recycling: Workplan for Developing Guidelines for Shrinkage Crack Mitigation in Cement-Treated Layers.** Davis and Berkeley, CA: University of California Pavement Research Center. (UCPRC-WP-2014-08.4).

Blank page

APPENDIX°A: FIELD TESTING LOCATIONS

This appendix provides the locations of the four projects where field testing, discussed in Chapter 3, was conducted. Locations of the falling weight deflectometer (FWD) test drop point stations are also listed.

A.1 Road CR32B



Figure A.1: CR32B: Project location.

Table A.1: CR32B: FWD Testing Stations (distance in feet from start of project)

Eastbound		Westbound	
Between Wheelpaths		Between Wheelpaths	
200.00	3,505.00	300.00	5,300.00
300.00	3,895.00	500.00	5,700.00
700.00	3,900.00	700.00	6,100.00
800.00	3,905.00	1,025.00	6,500.00
1,100.00	4,300.00	1,400.00	6,950.00
1,500.00	4,700.00	1,950.00	7,350.00
1,945.00	5,200.00	2,300.00	7,700.00
1,950.00	5,500.00	2,700.00	8,150.00
1,955.00	5,900.00	3,100.00	8,500.00
2,295.00	6,300.00	3,500.00	8,752.00
2,300.00	6,680.36	3,900.00	8,950.00
2,305.00	7,050.00	4,295.00	9,345.00
2,695.00	7,450.00	4,300.00	9,350.00
2,700.00	7,800.00	4,500.00	
2,705.00	8,250.00	4,800.00	
3,095.00	8,650.00		
3,100.00	8,850.00		
3,105.00	9,030.00		
3,495.00	9,209.00		
3,500.00			

A.2 Road CR27



Figure A.2: CR27: Project location.

Table A.2: CR27: FWD Testing Stations (distance in feet from start of project)

Eastbound		Westbound		Eastbound		Westbound
Between Wheelpaths				Right Wheelpath		
1,374.00	3,800.00	1,400.00	3,790.00	1,374.00	3,800.00	1,800.00
1,400.00	3,810.00	1,500.00	3,800.00	1,400.00	3,810.00	2,100.00
1,500.00	3,913.00	1,600.00	3,810.00	1,500.00	3,913.00	2,400.00
1,586.00	4,025.00	1,700.00	4,000.00	1,586.00	4,025.00	2,700.00
1,694.00	4,138.00	1,790.00	4,200.00	1,694.00	4,138.00	3,100.00
1,747.00	4,250.00	1,800.00	4,240.00	1,747.00	4,250.00	3,200.00
1,800.00	4,368.00	1,810.00	4,250.00	1,800.00	4,368.00	3,400.00
1,844.00	4,485.00	1,900.00	4,260.00	1,844.00	4,485.00	3,800.00
2,000.00	4,603.00	2,000.00	4,300.00	2,000.00	4,603.00	4,200.00
2,150.00	4,726.00	2,100.00	4,400.00	2,150.00	4,726.00	4,500.00
2,250.00	4,746.00	2,200.00	4,500.00	2,250.00	4,746.00	4,800.00
2,325.00	4,800.00	2,300.00	4,650.00	2,325.00	4,800.00	4,900.00
2,413.00	4,900.00	2,400.00	4,800.00	2,413.00	4,900.00	5,200.00
2,500.00	5,100.00	2,500.00	4,900.00	2,500.00	5,100.00	
2,600.00	5,145.00	2,600.00	5,000.00	2,600.00	5,145.00	
2,700.00	5,150.00	2,700.00	5,200.00	2,700.00	5,150.00	
2,800.00	5,155.00	2,800.00	5,372.00	2,800.00	5,155.00	
2,900.00	5,165.00	2,900.00	5,516.30	2,900.00	5,165.00	
3,000.00	5,300.00	3,000.00	5,700.00	3,000.00	5,300.00	
3,100.00	5,400.00	3,100.00	5,890.00	3,100.00	5,400.00	
3,200.00	5,600.00	3,200.00	5,990.00	3,200.00	5,600.00	
3,300.00	5,800.00	3,300.00		3,300.00	5,800.00	
3,425.00	5,875.00	3,400.00		3,425.00	5,875.00	
3,550.00	5,885.00	3,500.00		3,550.00	5,885.00	
3,675.00	5,895.00	3,600.00		3,675.00	5,895.00	

A.3 Road CR99

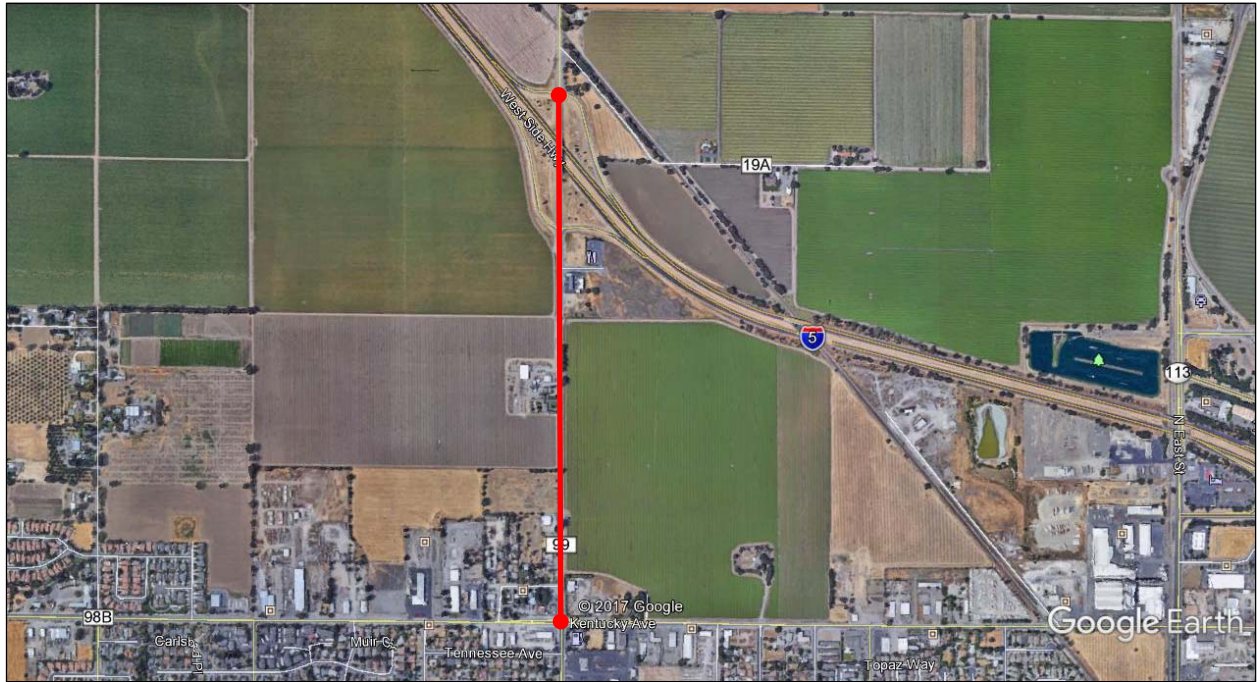


Figure A.3: CR99: Project location.

Table A.3: CR99: FWD Testing Stations (distance in feet from start of project)

Northbound	Southbound	Northbound	Southbound
Between Wheelpaths		Right Wheelpath	
19.00	146.50	100.00	121.70
121.70	284.10	121.70	370.30
198.40	411.40	198.40	494.00
370.30	538.00	370.30	721.90
494.00	662.70	494.00	933.90
616.70	861.40	721.90	1,109.10
721.90	1,109.10	933.90	1,592.00
933.90	1,200.00	1,109.10	1,600.00
1,021.50	1,572.00	1,592.00	1,800.00
1,109.10	1,582.00	1,600.00	2,000.00
1,400.00	1,592.00	1,800.00	2,200.00
1,592.00	1,700.00	2,000.00	2,460.00
1,600.00	1,900.00	2,200.00	
1,800.00	2,100.00	2,460.00	
2,000.00	2,110.00		
2,200.00	2,120.00		
2,460.00	2,300.00		
	2,400.00		
	2,500.00		

A.4 Road PLU147

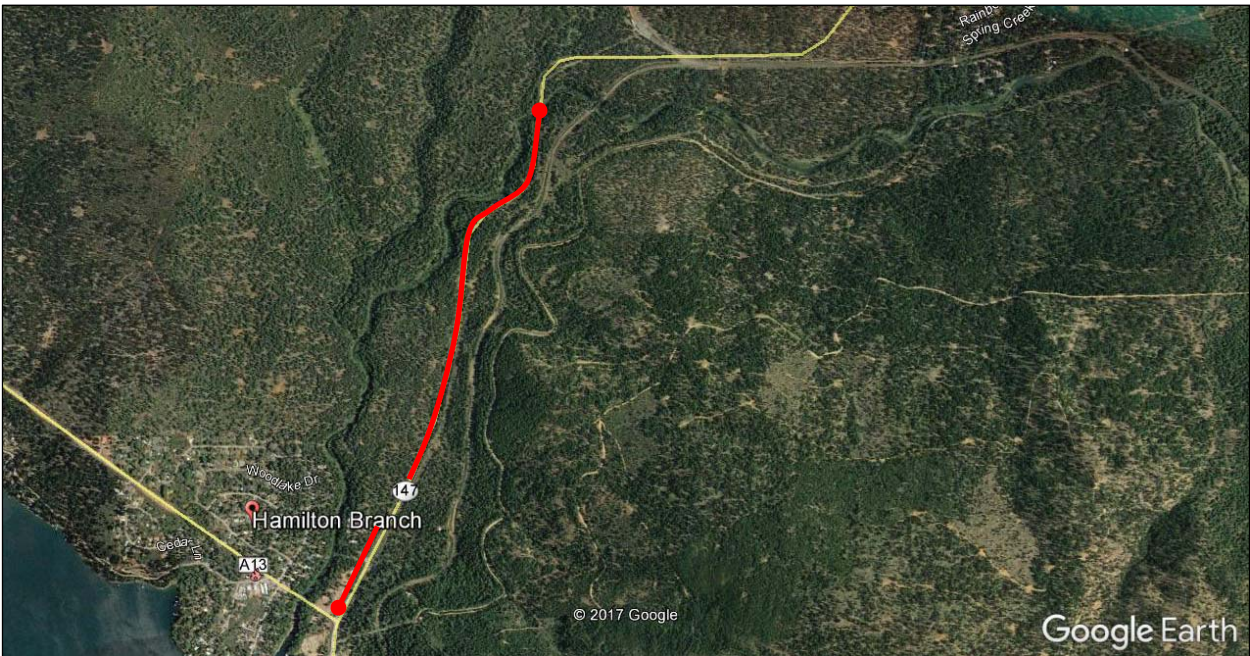


Figure A.4: PLU147: Project location.

Table A.4: PLU147: FWD Testing Stations (distance in feet from start of project)

Northbound		Southbound		Northbound		Southbound		Northbound
Between Wheelpaths				Right Wheelpath				Between Wheelpaths-2
3,670.00	8,664.50	4,459.00	8,223.20	3,670.00	9,216.30	4,459.00	9,436.40	3,670.00
4,267.50	8,669.80	4,464.30	8,228.00	4,267.50	9,227.50	4,470.10	9,447.10	4,872.00
4,863.70	8,674.70	4,470.10	8,234.40	4,863.70	9,237.70	4,480.40	9,837.40	5,383.50
4,867.20	8,680.50	4,475.00	8,546.00	4,872.00	9,464.00	4,739.30	10,224.80	5,894.50
4,872.00	8,685.40	4,480.40	8,600.00	4,882.70	9,691.80	4,910.10	10,611.70	6,152.90
4,876.90	8,701.50	4,739.30	8,634.00	5,082.00	9,701.50	5,176.80	10,990.00	6,421.00
4,882.70	8,769.60	4,910.10	8,650.50	5,117.80	9,712.20	5,339.80	11,000.00	7,250.80
5,117.80	8,950.10	5,176.80	8,847.60	5,383.50	9,818.80	5,350.00		8,006.00
5,383.50	9,043.60	5,339.80	9,147.80	5,647.70	9,931.00	5,360.20		8,318.50
5,647.70	9,216.30	5,345.10	9,426.20	5,884.70	10,000.00	5,582.60		8,674.70
5,884.70	9,221.20	5,350.00	9,431.50	5,894.50	10,154.00	5,730.60		8,950.10
5,889.10	9,227.50	5,354.40	9,436.40	5,903.70	10,163.00	5,960.30		9,227.50
5,894.50	9,232.40	5,360.20	9,441.80	6,018.10	10,173.00	6,141.30		
5,898.90	9,237.70	5,582.60	9,447.10	6,152.90	10,342.00	6,152.00		
5,903.70	9,464.00	5,730.60	9,837.40	6,172.20	10,607.00	6,160.80		
6,018.10	9,691.80	5,960.30	10,224.80	6,290.10	10,841.30	6,462.00		
6,152.90	9,696.70	6,141.30	10,611.70	6,411.30	11,046.60	6,791.00		
6,172.20	9,701.50	6,146.70	10,990.00	6,421.00	11,056.40	7,088.00		
6,290.10	9,707.90	6,152.00	10,995.00	6,432.20		7,361.80		
6,411.30	9,712.20	6,156.90	11,000.00	6,822.50		7,371.50		
6,416.60	9,818.80	6,160.80		7,250.80		7,381.80		
6,421.00	9,931.00	6,462.00		7,617.20		7,610.50		
6,424.90	10,000.00	6,791.00		7,995.80		7,796.00		
6,432.20	10,154.00	7,088.00		8,006.00		8,033.40		
6,822.50	10,159.00	7,361.80		8,017.20		8,213.90		
7,250.80	10,163.00	7,366.70		8,168.10		8,218.00		
7,617.20	10,169.00	7,371.50		8,318.50		8,223.20		
7,995.80	10,173.00	7,376.40		8,478.10		8,234.40		
8,000.20	10,342.00	7,381.80		8,664.50		8,546.00		
8,006.00	10,607.00	7,610.50		8,669.80		8,600.00		
8,011.40	10,841.30	7,796.00		8,674.70		8,634.00		
8,017.20	11,046.60	8,033.40		8,680.50		8,650.50		
8,168.10	11,051.50	8,213.90		8,769.60		8,847.60		
8,318.50	11,056.40	8,218.00		8,950.10		9,147.80		
8,478.10				9,043.60		9,426.20		